UNIVERSITY OF PORTO

Faculty of Sciences

Numerical Methods to Study Crystal Field Effects in 4f Magnetic Systems.

André Miguel Trindade Pereira

Thesis submitted in partial fulfillment of the requirements

for the degree of

Master

Supervisor: Prof. João Pedro Araújo

23 de Fevereiro de 2006

Acknowledgments

This work was realized on the ambit of Master degree and was performed in the group of transport properties (IFIMUP-A) on Science Faculty Physics department, with the orientation of Dr. João Pedro Esteves Araújo, who I want to thank very much for his teaching, motivation and for believing in me even in the hard moments during this thesis. Also I want to thank for his friendship and companionship in these last 3 years and for accepting to be my PhD guide and work with me 4 years more. Finally I want to thank for the accomplishment of a child's dream which was to know the CERN institute and for the magnific days in Switzerland.

Also I want to thank Dr. João Bessa Sousa for the special friendship, teaching, motivation, for the precious help always very important and also for the fruitful discussions in this work. Thank you for believing in me as an investigator and giving me the chance to work in IFIMUP Linha A. I have to tell that for me it is a great pleasure working with a "mitic"and a learned world physician.

A special and biggest thank for the magnificent team (João Ventura and José Miguel) and for the "francesinhas", "copos"and "borga".

A special word to Prof. José M. Moreira, Dr^{a}. Elina, Dr^{a}. Rafaela Pinto and Dr^{a}. Manuela Amado for being always available to help me.

Thanks for all the people from Zaragoza (Dr. Cesar Magen and Dr. Pedro Algarabel) for giving me the sample here studied.

A big thank you for my fathers, my sister and all my family.

For my love (Clarinha) I want to tell her: "Thank you very much and also sorry". Thank you for all the availability, motivation, dedication and help in

the hardest days and sorry for the days that I promised that I would be with you and did not go.

Thank you for anybody that I forgot to thank and gave me some contribution on this thesis.

Thank you ...

List of symbols

Roman characters

A_l^m	Crystal field parameters
B	Induced magnetic field
$\mathcal{B}$	Brillouin function
B_l^m	Crystal field parameters
C	Curie constant
C_m	Specific heat
$C's$	Clebsch-Gordan coefficients
E_F	Energy Fermi
E_n	Energy
e	Electron charge
F	Free energy
g	Landé factor
H	Applied magnetic field
H_M	Magnetic hamiltonian
H_{CF}	Crystal field hamiltonian
H_{ani}	Anisotropy hamiltonian
J	Total magnetic momentum
$\mathcal{J}$	Exchange coefficient
k_B	Boltzmann constant
$K's$	Coefficient of anisotropy
L	Orbital magnetic momentum
M	Magnetization

O_m^n	Stevens operator
S	Thermoelectrical power
S	Spin magnetic momentum
T_{SR1}	Spin reorientation transition
T_S	Structural transition
V_cf	Energy potential of crystal field
x	Silicon concentration
Y_l^m	Spherical harmonic

Greek characters

χ	Susceptibility
μ_B	Magnetum Bohr
λ	molecular-field
θ_C	Curie temperature
ψ_l^m	wave function
ρ	Electrical resistivity

Abreviations

AFM	Antiferromagnetism
$CF - interaction$	Crystal field interaction
FM	Ferromagnetic
M	Monoclinic structural phase
MCE	Magneto caloric effect
MR	Magnetoresistance
$O(I)$	orthorhombic structural phase
PM	Paramagnetic
S	Thermoelectrical power
R	Rare earth element
$RKKY$	Rudermann-Kittel-Kasuya-Yosida magnetic interaction

Abstract

The investigation of new magnetic compounds of the $R_5(Si_xGe_{1-x})_4$ family (where R represents a rare-earth) is promoting an increasing interest for their scientific and technological applications, due to their great potentialities as magnetic sensors or materials for magnetorefrigeration. The compounds with $x \sim 0.5$ display a combination of giant magnetocaloric, magnetostrictive and magnetoresistivity effects, because of the strong interplay between the crystal lattice, magnetic moments and electronic fluid.

Here we study the $Tb_5Si_2Ge_2$ compound that presents an incomplete magneto-structural coupling responsible for its magnetocaloric effect, with the magnetic transition occurring first (at 105 K), followed by the structural transition (at 100 K) upon cooling. This compound also exhibits a second-order spin reorientation transition between 40 and 65 K, which originates important magnetocrystalline anisotropy effects.

In this Thesis, it was studied the microscopic origin of the magnetocrystalline anisotropy of the $Tb_5Si_2Ge_2$ compound, its crystalline and magnetic structures and the indirect-exchange interaction responsible for the appearance of ferromagnetism using the mean-field approximation. To study the magnetic anisotropy it was necessary to introduce the crystal field interaction. We studied its effects in two limiting cases: weak and strong interactions. Our numerical results show that magnetic and thermodynamic properties dependent largely on crystal field parameters. Also our numerical results shows that we can predicted the easy direction of magnetization and described the evolution of the crystal field interaction with change on temperature.

Detailed transport and magnetic measurements were performed and compared with the numerical results. The interconnection between microscopic and

macroscopic properties (namely the free energy) is also performed, based on a simple phenomenological treatment, based on an approximate model of the magnetic structure of $Tb_5Si_2Ge_2$ at low temperatures.

The obtained results gave a satisfactory description of the main features oh the spin reorientation process.

Resumo

A investigação de novos compostos magnéticos da família $R_5(Si_xGe_{1-x})_4$ (onde R representa um terra-rara), tem suscitado um interesse crescente pelas suas aplicações científicas e tecnológicas, devido às suas grandes potencialidades como por exemplo em sensores magnéticos e materiais para magnetorefrigeração. Os compostos com $x \sim 0.5$ apresentam uma combinação de efeitos magnetocalóricos, magnetostrictivos e magnetorresistivos gigantes, devidos às fortes interacções da rede cristalina, dos momentos magnéticos e do fluido electrónico.

O composto em estudo é o $Tb_5Si_2Ge_2$, que apresenta um acoplamento magneto-estrutural incompleto responsável pelo efeito magnetocalórico, ocorrendo primeiro a transição magnética (a 105 K) seguida da transição estrutural (a 100 K), em arrefecimento. Este composto apresenta também uma transição magnética do tipo reorientação de spin de segunda ordem entre 40 e 65 K, que origina importantes efeitos de anisotropia magnetocristalina.

Nesta tese de dissertação estudou-se a origem microscópica da anisotropia magnetocristalina do $Tb_5Si_2Ge_2$ descrevendo-se a sua estrutura cristalina e magnética, assim como a interacção de troca indirecta responsável pelo aparecimento do ferromagnetismo usando uma aproximação de campo médio. Para o estudo da anisotropia magnética foi necessário introduzir a interacção do campo de cristal. Nós estudamos o seu efeito em dois casos limites: interacção fraca e interacção forte. Os nossos resultados numéricos mostram que as propriedades magnéticas e termodinâmicas dependem largamente dos parâmetros do campo de cristal. Os resultados numéricos podem também prever a direcção do eixo fácil da magnetização e descrever a evolução da interacção do campo de cristal com a alteração da temperatura.

Um estudo detalhado das propriedades magnéticas e de transporte foi tam-

bém realizado comparando-se posteriormente com os resultados numéricos. A interconexão entre propriedades microscópicas e macroscópicas foram feitas, baseado num tratamento fenómenologico onde se construí um modelo aproximado da estrutura magnética do $Tb_5Si_2Ge_2$.

Os resultados obtidos dão-nos uma satisfactória descrição dos principais processos das transições de reorientação de spin.

Table of Contents

List of Tables

List of Figures

Chapter 1

Introduction

The magnetocaloric effect (MCE) emerges as a competitive technology for refrigeration down to helium liquefaction temperature, offering the prospect of an energy-efficient and environment friendly alternative to common vapour-cycle technology. The MCE consists in a temperature variation (cooling or heating) of a magnetic material due to the application/removal of a external magnetic field ($\vec{H}$) [1, 2, 3]. This effect was discovered in 1881, in an iron sample [4]. The origin of this effect was investigated independently by Debye and Giauque who suggested a first technological application - *adiabatic demagnetization*, which is used to obtain temperatures lower than those of liquid helium (4.2 K). The $R_5(Si_xGe_{1-x})_4$ compounds with R = Gd, Tb, Nd, Er have shown promising MCE results, specially for R = Gd, Tb and for x $\sim$ 0.5 [2, 4, 5, 6, 7, 8, 9]. Besides, these compounds exhibit a number of unique properties due to their layered structure, namely a 1st-order magneto-structural transition (at T=T_S, martensitic-like) driven by the electronic fluid. The stratification results in a sequence of parallel rigid slabs of five atomic layers of Si, Ge and R. At low temperatures, covalent pairs of Si (or Ge) atoms produce strong interslab bonding, but upon heating the 1st-order transition at T_S produces the sliding of neighboring slabs with total or partial breaking of the referred bonds, drastically changing the electronic bands. Under cooling through T_S the reverse effects occur but with thermal hysteresis. The microscopic effects associated to such magneto-structural transition are very sensitive to thermal cycling,

magnetic field, pressure and Si/Ge ratio, producing important effects like giant MCE, colossal magnetostriction and giant magnetoresistance. Our recent work on thermal cycling effects revealed the onset of a new premartensitic phase displaying a universal electrical resistivity behavior near T_S [10]. Intensive research is in progress on these new phenomena, namely using magnetization, X-ray, neutron diffraction, pressure and magnetostriction [11, 12, 13]. Scarce information still exists on the theory of magnetism and anisotropy that will be considered in the present work. Also the transport properties (resistivity, thermopower), which are highly sensitive both to the electronic band features and to electron scattering (lattice and spin) will be considered. A recent innovative approach on $Gd_5(Si_{0.5}Ge_{0.5})_4$ showed that the substitution of a small amount of Ge (5 %) by Fe drastically reduced the hysteretic losses, greatly improving the magnetic refrigeration efficiency [9]. The magnetic entropy peak was also shifted to higher temperatures, which is a desirable feature. Fe-substitution in different compounds, as well as other transition metal substitutions, are still lacking. The $Tb_5(Si_xGe_{1-x})_4$ system similarly displays a large magnetocaloric effect. Compounds with $0.4 \leq x \leq 0.6$ are paramagnetic (PM)- monoclinic (M) at room temperature and ferromagnetic (FM) - orthorhombic (O) at low temperatures [13]. Under cooling from room temperature, cooperative (or granular-like) ferromagnetism seems to occur a few degrees before the structural transition temperature rising the interesting question of the possible decoupling of such transitions [14, 13]. This was inferred from recent neutron diffraction data, magnetization, thermal expansion, as well as thermopower and electrical resistivity. Interestingly, the fully coupled magneto-structural transition may be induced by pressure, revealing a tricritical point at $\sim$ 8.6 kbar with a colossal magnetocaloric effect [11]. At low temperatures, the x=0.5 compound exhibits a spin reorientation transition detected by well defined anomalies in the thermopower and electrical resistivity, and confirmed by neutron diffraction [13, 15].

In this work we will focus on the $Tb_5Si_2Ge_2$ compound which has great importance because of its considerable MCE [16]. The purpose of this study is to investigate the structural and magnetic properties of this compound, in order to understand the physical processes responsible for the MCE and the

magnetocrystalline anisotropy experimentally observed.

This dissertation is divided in seven chapters, that will now be described succinctly.

In chapter 2, an introduction to the structural and magnetic states of the family of $Tb_5(Si_xGe_{1-x})_4$ compounds will be presented. The crystalline and magnetic structures of $Tb_5Si_2Ge_2$ compound will be described in detail, as they constitute an important basis to understand all phenomenological effects observed in these compounds.

In chapter 3, the theoretical principles of magnetism.

Chapter 4 focus in the crystal field theory and also the magnetocrystalline anisotropy both at a microscopic (quantum) and macroscopic systems (phenomelogical).

In the chapter 5 we present experimental results and analysis that shows evidence for the spin reorientation transition in $Tb_5Si_2Ge_2$ compounds.

The chapter 6 the numerical results obtained will be presented and discussed.

Finally some conclusions and perspective of this work will be presented.

Chapter 2

Study of Crystalline of $Tb_5Si_2Ge_2$ Compound

In this chapter the crystalline and magnetic structures of the $Tb_5(Si_xGe_{1-x})_4$ system will be described. The crystalline structure of $Tb_5Si_2Ge_2$ will be analyzed in detail describing its atomic structure and defining its symmetry. The magnetic and structural phase transitions will be studied, showing the modifications in the interatomic distances and the magnetic moment alignment that occur in the compound.

The phase diagram of the $Tb_5(Si_xGe_{1-x})_4$ system has been established, both as a function of composition and temperature as presented in Fig. 2.1. At room temperature, the $Tb_5(Si_xGe_{1-x})_4$ compounds exhibit three structural phases, all of them in the paramagnetic (PM) state [12]. The compounds with $x > 0.65$ have an orthorhombic structure of the Gd_5Si_4-type (O(I); *Pnma*), which persists down to the lowest temperatures. However, under cooling, these compounds become ferromagnetic (FM1) through a 2nd-order phase transition, with a Curie temperature (T_C) linearly increasing with Si concentration. A spin reorientation transition occurs at lower temperatures, from the FM1 into another ferromagnetic phase (FM2), with the corresponding transition temperature (T_{SR}) being almost independent of the Si concentration [13, 15].

For $x < 0.35$, the compounds are orthorhombic (O(II);*Pnma*) at room temperature. Under cooling, they first undergo a 2nd-order magnetic transition

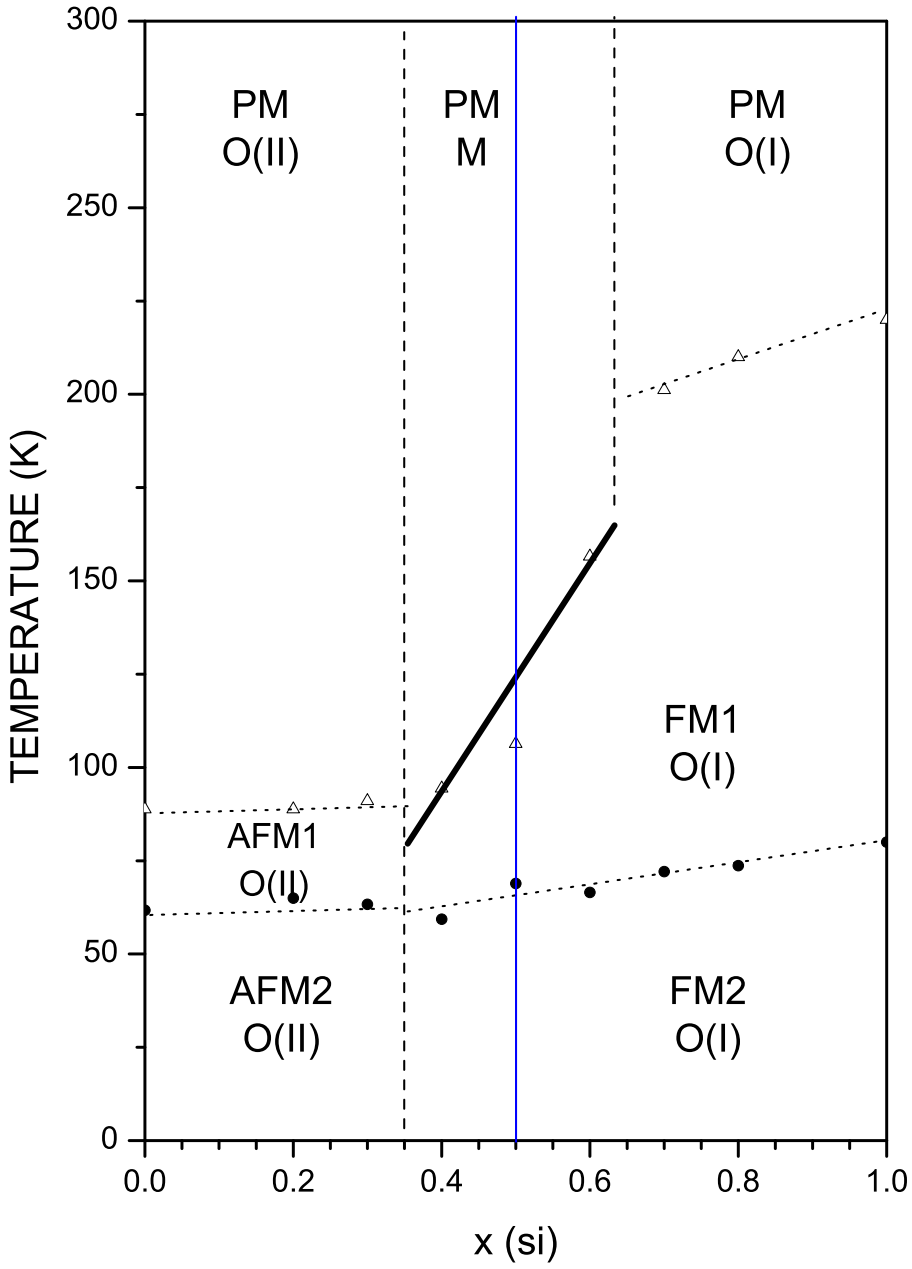

Figure 2.1: Magnetic and crystallographic phase diagram of the $Tb_5(Si_xGe_{1-x})_4$ materials with temperature and Si (x) concentration dependence.

from the PM to an antiferromagnetic phase (AFM1) at the Néel temperature (T_N), followed by a spin reorientation transition of the AFM1 $\longrightarrow$ AFM2 type at lower temperatures.

The compounds with $0.35 < x < 0.65$, which encompasses the particular composition discussed in this work, are monoclinic (M; $P112_1/a$ group) at room temperature but, upon cooling, suffer a 1st-order magneto-structural transition from the [PM, M] into the [FM1, O(I)] phases at a critical temperature T_S [13]. Recent detailed neutron diffraction works [**?**] show that such magnetic and crystallographic changes are not simultaneous as initially considered [13], i.e. the transitions are not fully coupled [**?**, 11]: the magnetic transition precedes by a few degrees the structural one (under cooling). At lower temperatures a spin reorientation transition was also observed in three Tb compounds (x = 0.4, 0.5 and 0.6), from the FM1 into another FM2 phase, occurring between 57 K and 73 K (see Fig. 2.1). In the following we will describe the crystalline structure of the $Tb_5Si_2Ge_2$ compound which is marked in Fig. 2.1 by a blue line.

2.1 Crystalline structure of $Tb_5Si_2Ge_2$ compound

2.1.1 Unit Cell and Symmetry Space Group

In Fig. 2.2 we represent the low temperature orthorhombic phase and the high temperature monoclinic phase of the $Tb_5Si_2Ge_2$ alloy, using crystallographic data obtained by X-ray power diffraction with a Rietveld refinement [13] (see table in appendix A).

These two crystalline structures are complex and contain a total of 36 atoms per unit cell (20 atoms of Tb and 16 atoms of Si(Ge)), distributed among six independent crystallographic sites (Tb1-dark blue, Tb2-violet blue, Tb3-light blue and M1-dark green, M2-light green and M3-red) in the orthorhombic structure (see Fig. 2.2a) and among nine independent crystallographic sites (Tb1-dark blue ,Tb2A-violet blue,Tb2B-violet blue, Tb3A-light blue, Tb3B-light blue and M1-dark green, M2-light green, M3A-red and M3B-red) in the monoclinic crystal system (see Fig. 2.2b).

In Fig. 2.2a) the crystalline system is orthorhombic, meaning that the angles between adjacent sides are right angles (90°) and in Hermann-Mauguin

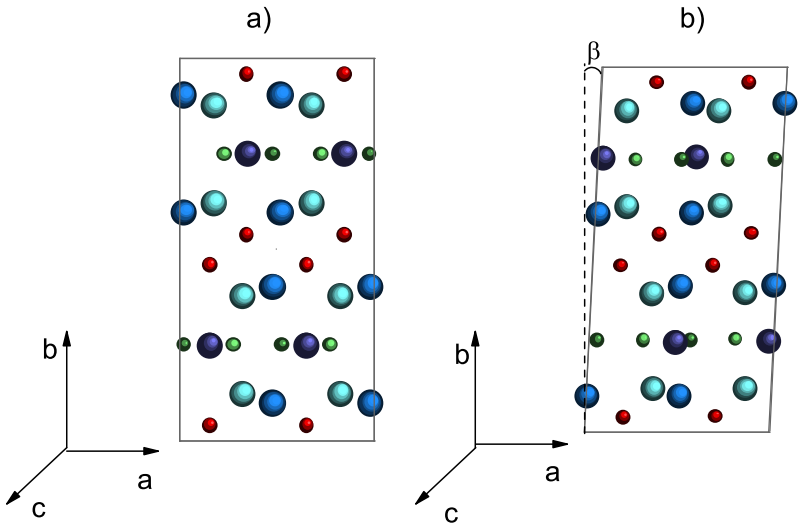

Figure 2.2: Unit Cell of $Tb_5Si_2Ge_2$ compound: a) Orthorhombic phase ($Pnma$) at 100K b) Monoclinic phase ($P112_1/a$) at 250 K.

representation has a $Pnma$ structure [17]. The P symbol means that the unit cell is primitive, that is, only has atoms on the corners in the rectangular cell. The character n is associated with the x-axis (parallel to the lattice a - axis) and is denominated glide-plane - this means that first the atoms are reflected in a symmetry plane and afterwards suffer a diagonal translation ($\vec{a} + \vec{b}$). The letter m designates a mirror plane and is associated with the y-axis (parallel to the lattice b-axis of the unit cell). Finally, the letter a is associated with the z-axis (parallel to the lattice c-axis) and is a glide plane, like letter n, but with a translation parallel to the x-axis. The monoclinic structure differs from the orthorhombic structure only in one angle that has a little deviation from 90° ($\beta = 90° \rightarrow 93.019°$, see Fig. 2.2), causing a small change in the symmetry space group, known as $P112_1/a$ in Hermann-Mauguin representation [17]. The symbol P as the same meaning referred above, the numbers 1 mean that there is only one reflection in the symmetry plane corresponding to the main reflection, and the 2_1/a symbol is a screw axis along the lattice a-axis of the unit cell [17].

These two structural states are both based in two different polyhedra, as

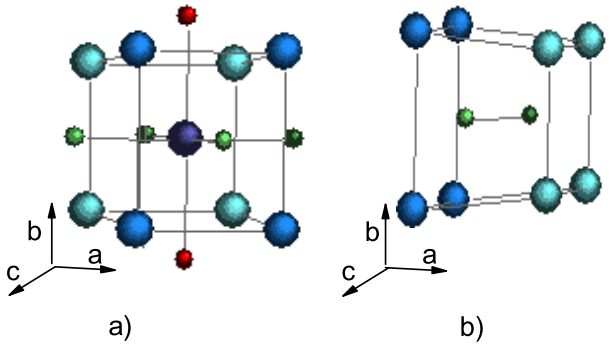

Figure 2.3: Crystalline structure of $Tb_5Si_2Ge_2$ alloy: a) cubo-octahedron $[TbM_6Tb_8]$ b) double trigonal prism $[M_2Tb_8]$.

shown in Fig. 2.3: the cubo-octahedron $[TbM_6Tb_8]$ and the double trigonal prism $[M_2Tb_8]$, where M can be Si and Ge atoms, which are nearly equally distributed among their respective crystallographic sites [18].

Both polyhedra are assembled by tight bonds and are alternatively ordered (cubo-octahedron/double trigonal prism/cubo-octahedron) giving periodic structures, forming rigid slabs, which are shown in Fig. 2.4. The chemical composition of the slabs is Tb_5M_4, because there is one cubo-octahedron for each double trigonal prism in the slab. The three distinct M-sites are occupied by Si(Ge) atoms which we designated by M1, M2 and M3: the last one (M3) is located on the slab surface thus playing a role in the interslab bonding, whereas the other two (M1 an M2) are found inside the slabs contributing to the stability of the slabs [18].

The rigid slabs can also be subdivided in five atomic planes and the order of the layers in each slab is the following: M3; Tb2/Tb3; M2/M1/Tb1; Tb2/Tb3; M3, as we can see in Fig. 2.5.

2.1.2 Structural Transition: Martensitic-like transformation

The two crystal structures that are observed in the $Tb_5Si_2Ge_2$ compound differ only in the different form of arrangements of the slabs. The first structure belongs to the orthorhombic Gd_5Si_4-type, in which all slabs are interconnected via short M3-M3 bonds, where the interatomic distance is approximately 2.6 $\dot{A}$

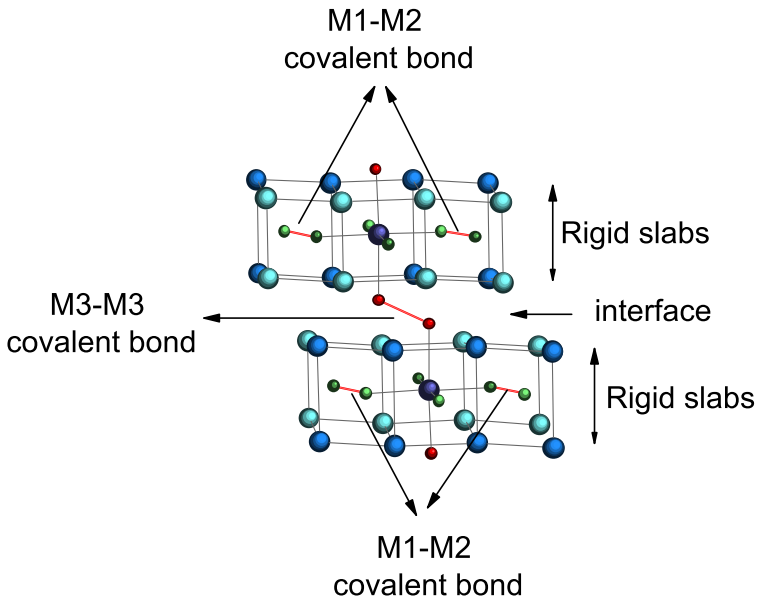

Figure 2.4: Schematic representation of two rigid slabs, in $Tb_5Si_2Ge_2$ alloy at 100 K, with the covalent bonds between M3 atoms in the interface.

(see Fig. 2.6). The second structure belongs to the monoclinic $Gd_5Si_2Ge_2$-type, with the slabs being identical to those from the Gd_5Si_4-type, but interconnected alternately forming pairs of slabs (see Fig. 2.6).

Above T_S, the interatomic distance between the unconnected pairs increases from 2.6 to 3.4 $\dot{A}$, while between the connected pairs remain equal to 2.6 $\dot{A}$. This happens because the slabs move parallel to the lattice a-axis, leading to a natural decrease of the corresponding bond strength and to the lowering of the Fermi level. In Fig. 2.7 a schematic diagram of the Fermi level in the cases of bonding and non-bonding is represented [18]. This process is denominated *Martensitic-like transformation* [19], occurring at $T_S \sim 100$ K.

This phase transformation occurs suddenly (at the speed of sound) and can be of two types - *thermic* or *athermic*. The athermic transitions are fast time-dependent martensitic transitions. The thermic transitions are martensitic transformations that occur practically instantaneously when reaching the transition temperature or when applying a magnetic field or pressure. In the present studied compound, the transformation is thermic. This transformation together with the magnetic transition originate the MCE, and can be induced

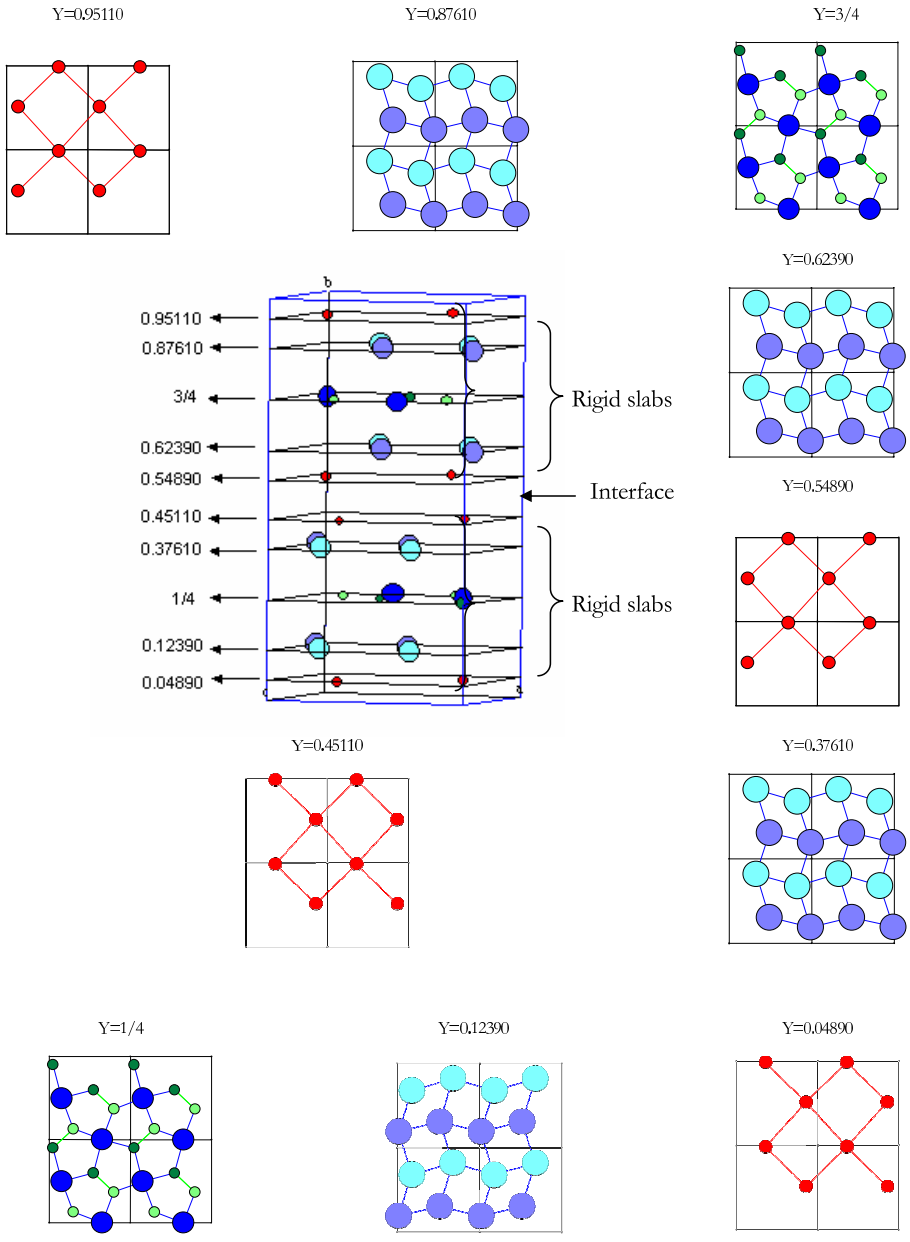

Figure 2.5: Nanostratified atomic slabs of the unit cell for $Tb_5Si_2Ge_2$ compound at 100 K.

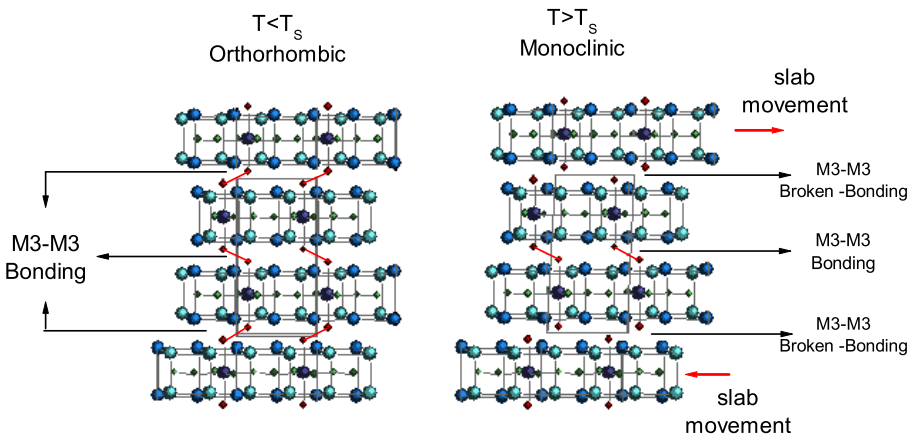

Figure 2.6: Schematic crystalline structures during the Martensitic-like transformation in $Tb_5Si_2Ge_2$ compound below and above T_S: Orthorhombic (left; at 100 K) and Monoclinic (right; at 250 K).

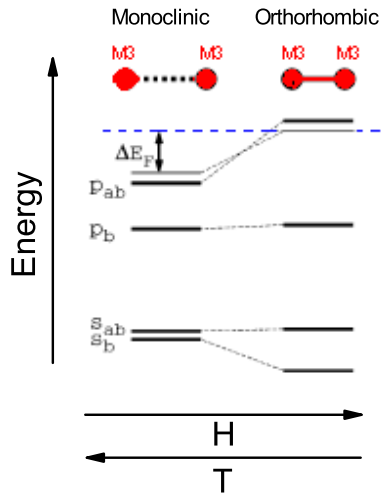

Figure 2.7: Schematic Fermi level for bonding and non-bonding structures: for monoclinic structure (left) and for the orthorhombic structure (right)[18].

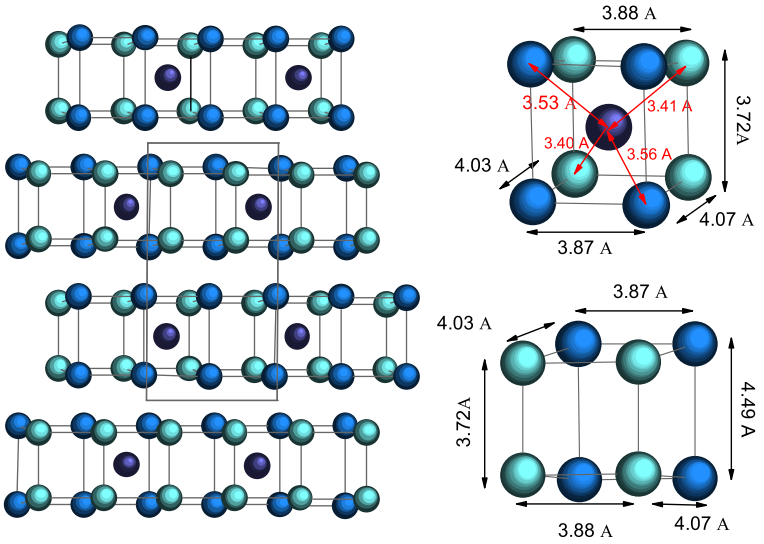

Figure 2.8: Magnetic structure of $Tb_5Si_2Ge_2$ at 100 K.

by a temperature variation or by application of a magnetic field, therefore its enormous potential for the application the magnetic refrigeration.

During this transformation, the respective charge-balanced formulas based on the Zintl-Klemn formalism change from $[(Tb_5^{3+})(M_2^{6-})_2(3e^-)]$ to $[(Tb_5^{3+})(M_2^{6-})_{1.5}(M^{4-})(2e^-)]$, where M represents a Si or Ge atom. Note that the number of electrons assigned to the conduction band drops as some of the M_2 bonds break [20].

2.2 Magnetic structure of $Tb_5Si_2Ge_2$ compound

In the previous section the crystalline structure of the compound was studied, being concluded that the Si(Ge) atoms have an important role, namely in the interslab bonding. The magnetic contribution is due to the Tb atoms.

In Fig. 2.8 we observe that the magnetic structure can be subdivided in the same away as the crystalline structure: an approximated body-centered cube and a double trigonal prism. The body-centered cube is the principal magnetic structure because the distance between the Tb atoms in the corners (Tb2, Tb3) and the Tb atom in the center (Tb1) are significantly less than in the double trigonal prism or between the corner atoms of the cubic structure.

The double trigonal prism only appears to establish the bonding between two body-centered cubes. In the structural transition, the rigid slabs remain almost equal, only varying the distance between the two principal magnetic structures (body-centered cube) in the two different slabs. The variation of this distance is important for the magnetic contribution because in these compounds the magnetic exchange coupling between Tb ions is mediated by the conduction electrons (RKKY - exchange interaction; chapter 3). Additionally, at lower temperature a spin reorientation transition occurs which we will study in detail in this work. As the name indicates, this transition consists in the realignment of the magnetic moment directions of the Tb atoms, from the FM1 into another FM2 phase at $T_{SR_1} \sim 65$K. This identification (T_{SR1}) was achieved through neutron diffraction intensity measurements of the purely magnetic (100)+(020) reflections [13].

A detailed and refined diffraction study of the magnetic structure (Rietveld refinements of neutron power diffraction data) was performed for the sample with x = 0.5 [13], for temperatures 85 K (above T_{SR_1}) and 2 K. Such study [13] shows that the different Tb directions depend on the three distinct types of positions in the unit cell: Tb1 (4c symmetry), Tb2 (8d) and Tb3 (8d). Different magnetic anisotropy site-constants exist and so different orientational processes occur as temperature change.

Additionally for each of the 8d positions (Tb2 and Tb3) the magnetic moment can still point in two distinct directions (γ and σ).

According to the neutron diffraction data [13], at T $\sim$ 85 K the Tb1, Tb2 and Tb3 magnetic moment components in the ac plane form slightly different angles with the a-axis, $\theta_1 = 5^0$, $\theta_2 = 13^0$ and $\theta_3 = 3^0$ respectively, whereas the corresponding angles (with a-axis) in the ab plane are ϕ_1=0^0, $\phi_2 \sim 11^0$ and ϕ_3 $\sim 4^0$. Therefore, at 85 K, the spontaneous magnetization (M_S) is quasi-parallel to the a-axis, if one disregards the small ϕ_i angles.

At T=2K the magnetic moments of each Tb site are splitted in two subsets with slightly different canting angles whose average values are $\theta_1 = 33^0$, $\theta_2 = 45^0$ and $\theta_3 = 34^0$. The values of the magnetic moment direction for the three Tb atoms obtained by neutron diffraction data are tabled in Appendix 2 of this work. These results are pictorially summarized in Figs. 2.9 a) and 2.10 a) for

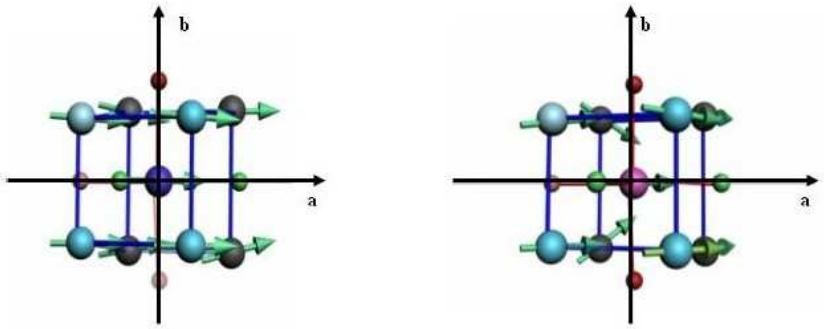

Figure 2.9: a) Magnetic structure for $Tb_5Si_2Ge_2$ projected (orthogonally) into the *ab*-plane at T=85 K (grey, black and white atoms correspond to Tb1, Tb2 and Tb3 atoms respectively). b) Magnetic structure projected into the *ab*-plane at T= 2K.

T = 85 K and in Figs. 2.9 b) and 2.10 b) for T = 2 K. It is very clear that above the spin reorientation transition (T = 85 K), all the Tb ions essentially lie in the *ac*-plane and most of them are oriented along the *a*-axis. Below the spin reorientation transition (T = 2 K), most of the Tb magnetic moments still lie close to the *ac*-plane, except half of the Tb2 ions, which point into a direction (β) making a large angle ($\sim 33^0$) with the *ac*-plane. One notes that the markedly out-of-plane moments at low temperatures represent only 20% of the total number of moments. Therefore, the major reorientational processes occur in the*ac* plane, as can be seen comparing Figs. 2.10 a) (T = 85K) and b) (T = 2K), likely influencing the behavior of different physical properties through the spin reorientation transition [15].

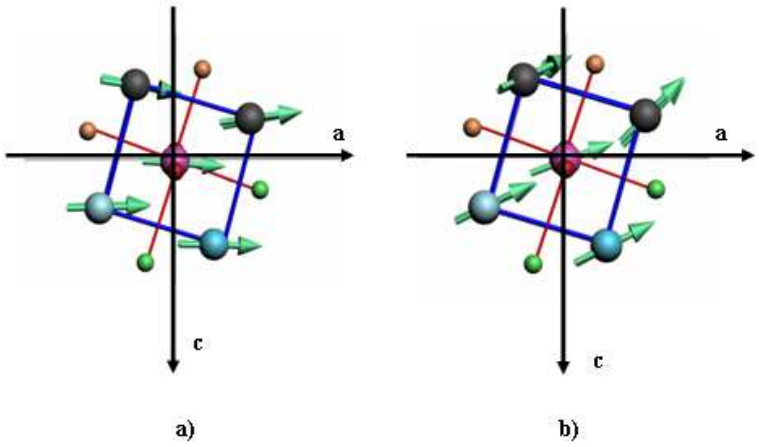

Figure 2.10: a) Magnetic structure of $Tb_5Si_2Ge_2$ (orthogonally) projected into the *ac*-plane at T=85 K (grey, black and white atoms correspond to Tb1, Tb2 and Tb3 atoms respectively). b) Magnetic structure projected into the *ab* plane at T=2 K.

Chapter 3

Quantum Theory of Magnetism

3.1 Introduction to Rare Earths

The rare-earth elements are located in the 6^{th} Period of the Periodic Table, forming the lanthanide series and are responsible for the strong magnetism observed in some compounds. The study of the magnetic properties of the rare-earth metals started in the 1930's, when the ferromagnetism of Gd was discovered and the paramagnetism of the other heavy elements was investigated. Their magnetic properties like magnetoresistance (MR) [21], magnetostriction (MS) and magnetocaloric effects (MCE) [22] form a vast area of research where new compounds and interesting phenomena are still being discovered. Therefore, the understanding of the magnetism of these elements is very important. The unusual properties (magnetic, electronic, transport and several other physical properties) observed in rare-earth compounds arise from the presence of $4f$ electrons, which are generally well separated in energy from the $6s$ electrons, since they are well embedded within the atom and shielded by the $5s$ and $5p$ shells (see Fig. 4.1). As a consequence, the $4f$ electrons do not take a significative role in chemical bonding. The incomplete screening of the increasing nuclear charge along the rare-earth series causes wavefunction contraction, which is reflected in the ionic and atomic radii in the solid state [23].

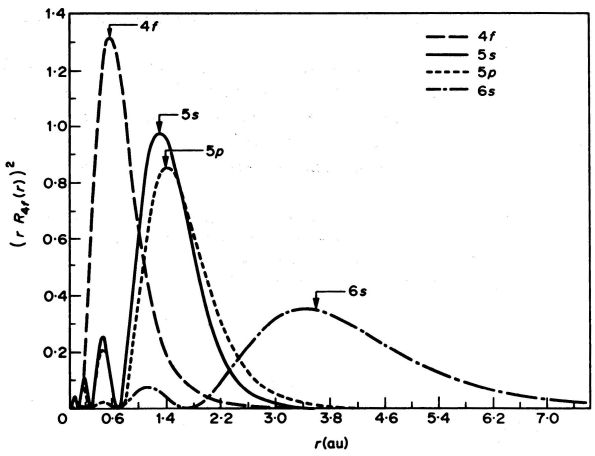

Figure 3.1: Radial components of atomic wavefunctions for $4f$, $5s$, $5p$ and $6s$

The rare-earth ions usually have the valence state 3^+ (trivalent) both in ionic crystals and in metals, except in the cases of europium (Eu) and ytterbium (Yb) which can form 2^+ (bivalent) ions and cerium (Ce) whose valence state can fluctuate between 3^+ and 4^+ (fourvalent).

Observing Fig. 3.2 one concludes that the spin-orbit coupling (L-S) in $4f$ metals is the strongest interaction. Therefore, the angular momentum $\vec{L}$ and the total spin-angular momentum $\vec{S}$ combine themselves, giving the total angular momentum $\vec{J}$, which is a good quantum number. The ground state multiplet (J) is determined by Hund's rules [23]. These quantum numbers for all rare-earth elements are given in an appendix C. The complicated magnetic structures of the pure rare-earth metals, their alloys and compounds result from the competition between different interactions, mainly because of the indirect exchange interaction through the RKKY (Ruderman-Kittel-Kasuya-Yosida) mechanism [24], which is critically affected by complexity and topology of Fermi surface.

In the present chapter, the theoretical background (principles) of magnetism will be introduced . Particular attention will be given to methods to calculate the spontaneous magnetization in a mean-field approach.

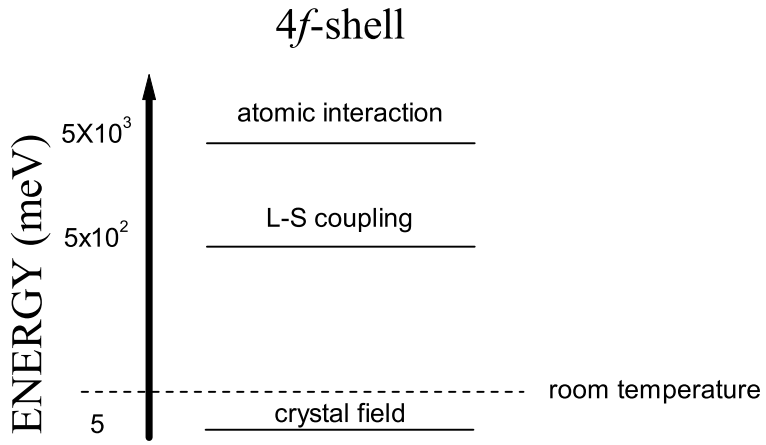

Figure 3.2: Crystal field and spin-orbital coupling in $4f$ ions.

3.2 Principles of Magnetism

3.2.1 Paramagnetism

Zeemann Hamiltonian

Introducing the total angular momentum operator J diagonalizes the spin orbit interaction, i.e. the hamiltonian for the spin-orbit interaction H_{LS} comutes with J^2 and J_z. In the presence of a magnetic field, these states are splitted. This effect is caused by the orbital and spin magnetic moments ($\vec{L}$ and $\vec{S}$) with an applied magnetic field ($\vec{B}$), giving a additional term to the general Hamiltonian - the *Zeeman hamiltonian* [23].

Consider a system with N not interacting identical magnetic atoms. Neglecting the small diamagnetic susceptibility, the interaction hamiltonian between the atomic magnetic moment and the magnetic field is given by Zeemann hamiltonian

$$\hat{\mathcal{H}}_Z = -\mu_B(\vec{L} + g_0\vec{S}) \cdot \vec{B} \tag{3.1}$$

where μ_B is the Bohr magneton, g_0 is the Landé factor which is for the electron g_0=2 and $\vec{B}$ is the magnetic flux density (magnetic induction) given by $\vec{B}$=$\mu_0(\vec{H} + \vec{M})$ where $\vec{H}$ is designated by applied magnetic field and $\vec{M}$ the magnetization.

Magnetic Susceptibility and Magnetization

The most natural way to classify the magnetic properties of a material is by its response to an applied magnetic field $\vec{H}$ [25]. This response is characterized by the susceptibility χ, given by the relation [26]

$$\chi = \frac{dM}{dH} \mid_{H=0} = \frac{M}{H}_{0} \tag{3.2}$$

where M is given by the derivative of the free energy $\mathcal{F}$ with respect to the magnetic field

$$\vec{M} = -\frac{1}{V}\frac{\partial \mathcal{F}}{\partial \vec{B}} \tag{3.3}$$

with the free energy being

$$\mathcal{F} = -\frac{N}{\beta} ln \sum_{N} e^{-\beta E_n(\vec{B})} \tag{3.4}$$

with E_n being the atomic energy levels of the magnetic hamiltonian and β=$1/k_B$T where k_B is the Boltzman constant. Using equations 3.3 and 3.4, the general form for the magnetization becomes

$$\vec{M} = \frac{N}{V}\frac{\Sigma_n \frac{\partial E_n}{\partial \vec{B}} e^{-\beta E_n(\vec{B})}}{\Sigma_n e^{-\beta E_n(\vec{B})}} \tag{3.5}$$

The Zeemann hamiltonian term gives a small $En(\vec{B})$ contribution to the energy that can be calculated using a first-order perturbation theory [23]

$$E_n(\vec{B}) = \mu_B \cdot \vec{B} < n|\vec{L} + 2\vec{S}|n > \tag{3.6}$$

Problems of degeneracy are solved using the $|JM_JLS >$ basis, whose degeneracy is completely lifted by the magnetic field. In this basis and within a particular JLS-multiplet, the Wigner-Eckart theorem implies that the matrix elements of $(\vec{L} + 2\vec{S})$ are proportional to those of $\vec{J}$. Considering the magnetic field $\vec{B}$ parallel to z-axis the eq.3.6 becomes

$$E_n(B) = g\mu_B \cdot B < JLSM_J|J_z|JLSM'_J >= g\mu_B \cdot BM_J\delta_{M_JM'_J} \tag{3.7}$$

where factor g, called the *Landé factor*, can be expressed by

$$g = \frac{3}{2} + \frac{S(S+1) - L(L+1)}{2J(J+1)} \tag{3.8}$$

and within the a given J multiplet considerer $\vec{L} + 2\vec{S} = g\vec{J}$. The effective moment of the atom is then given by

$$\vec{\mu} = -g\mu_B \vec{J} \tag{3.9}$$

In similar way we can use the projection theorem to find a similar

$$\vec{L} = (2-g)\vec{J} \tag{3.10}$$

and

$$\vec{S} = (g-1)\vec{J} \tag{3.11}$$

Once the eigenvalues are obtained by eq.3.7, the magnetization can be calculated from eq. 3.5 giving

$$\vec{M}(\vec{B}, T) = gn\mu_B J \mathcal{B}_J(\beta g \mu_B J B)\vec{u}_z \tag{3.12}$$

where n is concentration of magnetic moments (number of magnetic ions per volume unit), β=$1/k_BT$ and $\mathcal{B}_J(\beta g\mu_B JB)$=$\mathcal{B}_J(x)$ is the *Brillouin function* [23]

$$\mathcal{B}_J(x) = \frac{2J+1}{2J}\coth\frac{2J+1}{2J}x - \frac{1}{2J}\coth\frac{1}{2J}x \tag{3.13}$$

From eq. 3.12, we see that the magnetization depends on the magnetic field and temperature, as illustrated in Fig. 3.3. In Fig. 3.3 a) we can see that, when a magnetic field is applied, the magnetization grows rapidly (first linearly) and then saturates for higher magnetic fields [27]. In Fig. 3.3 b), it is clear that the magnetization decreases with temperature to M=0, upon heating.

If x«1 we can perform a Taylor expansion and the Brillouin function in 1st approximation becomes linearized 3.13, resulting the approximation [25]:

$$\mathcal{B}_J(x) = \frac{J+1}{3J}x \tag{3.14}$$

Within the above approximation eq.3.12 becomes

$$M = \frac{ng^2\mu_B^2 J(J+1)}{3k_BT}B \tag{3.15}$$

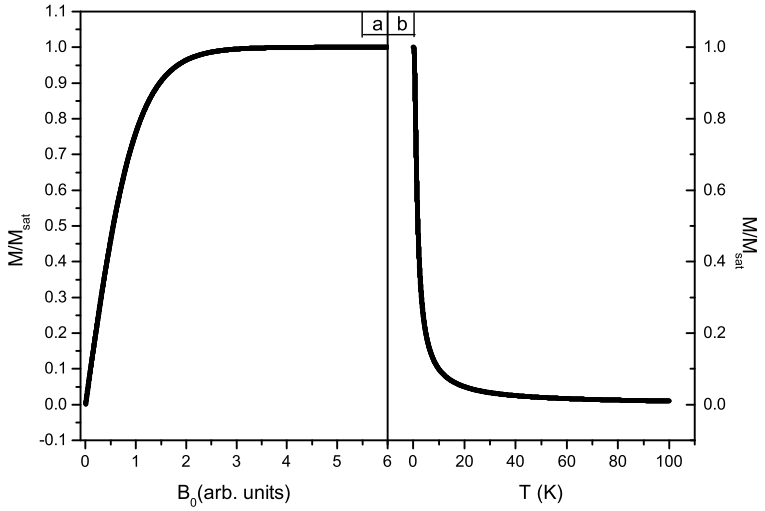

Figure 3.3: Variation of the magnetization (M) using the Brillouin function with: (a) Magnetic field (B_0) (b) Temperature (T)

Using the expression 3.2 and the previous approximation for the magnetization, the susceptibility in such a paramagnetic system is given by

$$\chi = \frac{ng^2\mu_B^2 J(J+1)}{3k_B T} = \frac{C}{T} \tag{3.16}$$

known as the *Curie's law*, where C is the Curie constant. Observing Fig. 3.4 it can be seen that the inverse susceptibility depends linearly with temperature, according with eq. 3.16 [27].

3.3 Exchange Interaction

3.3.1 Direct Exchange Interaction

In the last section we have discussed the properties of a paramagnetic system, but it is known that some materials become magnetized spontaneously at low temperatures. This spontaneous magnetization appears essentially because of the exchange interaction processes between magnetic atoms [28]. For simplicity we consider a simple model with two electrons A and B (S=$\frac{1}{2}$) which have spatial coordinates r_1 and r_2, respectively [29]. In a real crystal, the spins of these electrons interact with each other and the main contributions are the

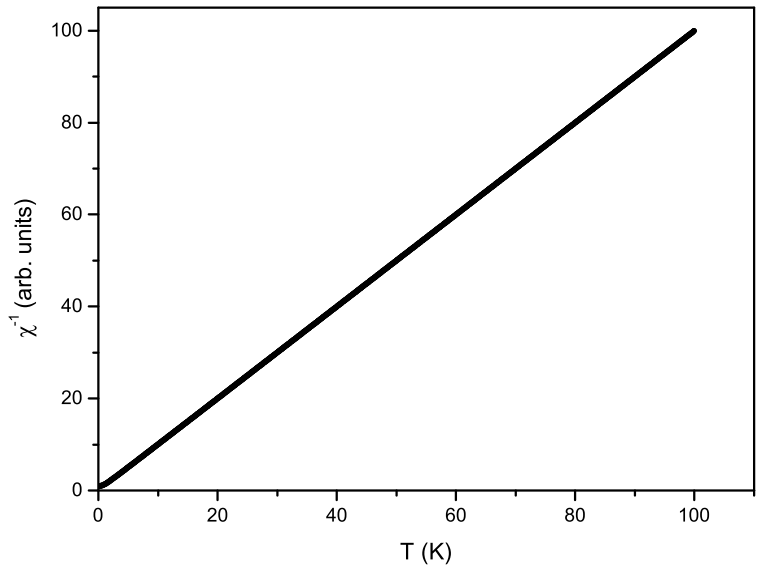

Figure 3.4: Temperature dependence of the susceptibility inverse in a paramagnetic system using the Brillouin function

Coulomb interaction and the exchange symmetry for two electrons instead of the dipole-dipole magnetic interaction. The *Coulomb hamiltonian term* is

$$\hat{\mathcal{H}}_c = \frac{1}{4\pi\epsilon_0}\frac{e^2}{r_{12}} \tag{3.17}$$

The wavefunctions of two neighboring electrons are $\psi_A(r_1)$ and $\psi_B(r_2)$ which are localized functions in neighboring points of the lattice. The overall wavefunctions must be antisymmetric accordingly with Pauli's exclusion principle, so the spin part of the wavefunction must be either an antisymmetric singlet state χ_S (S=0) in the case of a symmetric spatial state, or a symmetric triplet state χ_T (S=1) in the case of an antisymmetric spatial state [29]:

$$\begin{aligned} \chi_S &= \frac{|\uparrow\downarrow> - |\downarrow\uparrow>}{\sqrt{2}} \\ \chi_T &= \begin{cases} |\uparrow\uparrow> \\ |\downarrow\downarrow> \\ \frac{|\uparrow\downarrow>+|\downarrow\uparrow>}{\sqrt{2}} \end{cases} \end{aligned}$$

So we can write the system wavefunctions for the singlet ψ_S and triplet ψ_T respectively as

$$\begin{aligned}\psi_S &= [\psi_A(r_1)\psi_B(r_2) + \psi_A(r_1)\psi_B(r_2)]\chi_S \\ \psi_T &= [\psi_A(r_1)\psi_B(r_2) - \psi_A(r_1)\psi_B(r_2)]\chi_T\end{aligned} \tag{3.18}$$

where both the spatial and spin parts of the wavefunctions are included, and the respective energy of each state is

$$\begin{aligned}E_S &= \int \psi_S^* \hat{\mathcal{H}}_c \psi_S dr_1 \\ E_T &= \int \psi_T^* \hat{\mathcal{H}}_c \psi_T dr_2\end{aligned} \tag{3.19}$$

assuming that the spin parts of the wavefunction χ_S and χ_T are normalized. The difference between the two energy states is

$$E_S - E_T = \int \psi_A^*(r_1)\psi_B^*(r_2)\hat{\mathcal{H}}_c\psi_A(r_1)\psi_B(r_2)dr_1dr_2 \tag{3.20}$$

For S=$\frac{1}{2}$ particles the eigenvalues of the operator $(\vec{S}_A \cdot \vec{S}_B)$ are (S are the quantum number of the system total spin operator $=_A + \vec{s}_B$) :

$$\vec{S}_A \cdot \vec{S}_B = \begin{cases} \frac{1}{4} & if \quad s = 1 \quad (triplet \quad state) \\ -\frac{3}{4} & if \quad s = 0 \quad (singlet \quad state) \end{cases} \tag{3.21}$$

So we can write the effective hamiltonian for two electrons as

$$\hat{\mathcal{H}}_c = \frac{1}{4}(E_S + E_T) - (E_S - E_T)\vec{S}_A \cdot \vec{S}_B \tag{3.22}$$

In this hamiltonian the first term is a sum of constant terms being thus irrelevant and the second one depends on the spin and the energy difference between the two states. This energy difference is directly related with the so called *exchange constant* $\mathcal{J}$ defined by

$$\mathcal{J} = \frac{E_S - E_T}{2} = \int \psi_a^*(r_1)\psi_b^*(r_2)\hat{\mathcal{H}}_c\psi_a(r_1)\psi_b(r_2)dr1dr2 \tag{3.23}$$

In this way, the hamiltonian term for the interaction between two spins is given by

$$\hat{\mathcal{H}}_c = -2\mathcal{J}\vec{S}_1 \cdot \vec{S}_2 \tag{3.24}$$

If $\mathcal{J}$ is positive, $E_S > E_T$ the triplet state (S=1) is the ground state corresponding to a ferromagnetic interaction between spin. On the other hand, if $\mathcal{J}$ is negative, the singlet state (S=0) is the most favorable one corresponding

to an antiferromagnetic ground state. These arguments can be generalized for a system with many particles.

3.3.2 Indirect-Exchange Interaction - RKKY

In rare-earths, the $4f$ electrons are strongly localized (as seen previously) and lie very close to the nucleus with biggest density probability, occupying about one tenth of the interatomic spacing. This means that the direct exchange interaction is unlikely to be very effective in rare-earths, being indirect instead. The indirect coupling of magnetic moments by conduction electrons is referred as the *Ruderman-Kittel-Kasuya-Yosida* ($RKKY$) interaction [24]. The form of the RKKY interaction is obtained within the framework of generalized susceptibility. Assuming the exchange interaction between a localized spin $\vec{S}_\alpha$ located at r=0 and the conduction spins $\vec{s}_i$, using expression 3.24 we have

$$\hat{\mathcal{H}} = -\mathcal{J} \sum_i \vec{S}_\alpha \cdot \vec{s}_i \delta(r_i) \tag{3.25}$$

Each conduction spin therefore experiences an effective magnetic field given by

$$\vec{B}_{ef}(r) = -\frac{\mathcal{J}}{g\mu_B} \vec{S}_\alpha \delta(r) \tag{3.26}$$

Performing a Fourier transform on this field, we obtain

$$\vec{B}_{ef}(k) = -\frac{\mathcal{J}}{g\mu_B} S_\alpha \delta(k) \tag{3.27}$$

so the spin density at r is given by

$$s(r) = -\frac{\mathcal{J}}{g^2 {\mu_B}^2 V} \Sigma_k \chi(k) e^{ikr} S_\alpha \tag{3.28}$$

where $\chi(k)$ is the susceptibility. For a free-electron gas, $\chi(k)$ is given by

$$\chi(k) = -\frac{3g^2\mu_B^2 \frac{N}{V}}{8\epsilon_F} F\left(\frac{k}{2k_F}\right) \tag{3.29}$$

where

$$F\left(\frac{k}{2k_F}\right) = \frac{1}{2} + \frac{k_F}{2k}\left(1 - \frac{k^2}{4k_F^2}\right) log\left|\frac{2k_F + k}{2k_F - k}\right| \tag{3.30}$$

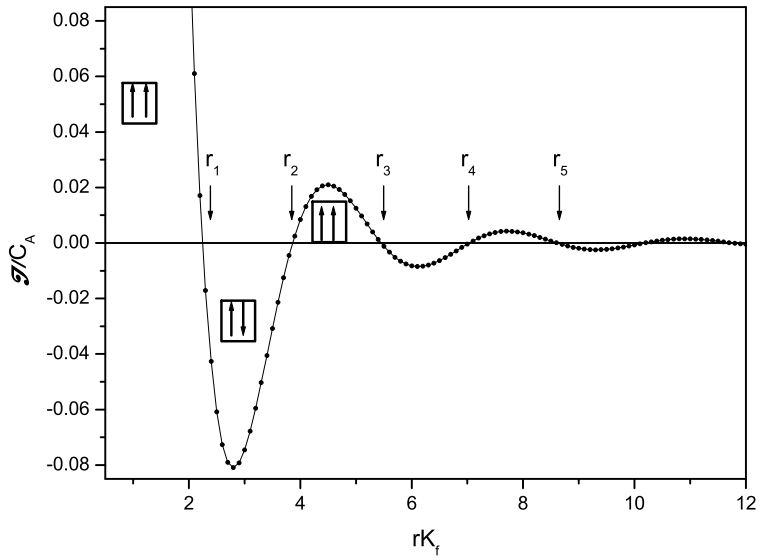

Figure 3.5: Distance dependence of conduction electron spin density (RKKY exchange-$\mathcal{J}$) where C_A is given by $\frac{3g^2\mu_B(N/V)}{8\epsilon_F}\frac{k_F^3}{16\pi}$. The r_n marked give the nodes of $\mathcal{J}$ where $\mathcal{J}$ inverts its signal.

.

The exchange coefficient is given by

$$\mathcal{J} = \frac{1}{V}\Sigma_k \chi(k) e^{ik\cdot r} = \frac{3g^2\mu_B^2 n}{8\epsilon_F}\frac{k_F^3}{2\pi^2 r}\int dk k F\left(\frac{k}{2k_F}\right) sin(kr) \tag{3.31}$$

From the calculation of expression 3.31, we arrive to the general formula for the RKKY exchange [24]

$$\mathcal{J} = \frac{3g^2\mu_B n}{8\epsilon_F}\frac{k_F^3}{16\pi}\left\{\frac{sin2k_F r - 2k_F cos2k_F r}{(k_F r)^4}\right\} \tag{3.32}$$

In Fig.3.5, we see that a localized moment is introduced and the conduction spins develop an oscillating polarization in the vicinity of this moment. The r_n marked give the nodes of $\mathcal{J}$ where $\mathcal{J}$ inverts its signal.

3.4 Molecular Field Theory of Ferromagnetism

3.4.1 Heisenberg Hamiltonian

In section 3.3.1 we have built the hamiltonian for the direct interaction between two electron spins 3.24 using the Heisenberg model. A real magnetic system is composed by N magnetic particles and thus we must considerer the interaction between all magnetic particles. Substituting the spin (S) by the total angular momentum (J) using the eq.3.11 in the expression , the 3.24 Heisenberg hamiltonian becomes

$$\hat{\mathcal{H}}_{ex} = -(g-1)^2 \sum_{ij} \mathcal{J}_{ij} \vec{J}_i \cdot \vec{J}_j \tag{3.33}$$

where $\mathcal{J}_{ij}$ is the exchange coefficient. This Hamiltonian is very attractive to use as a starting point for the calculation of the spontaneous magnetization, particularly because it allows us to apply the powerful spin operator technics to this problem.

The general magnetic hamiltonian in the presence of a flux $\vec{B}$ is given by

$$\hat{\mathcal{H}}_{mag} = \hat{\mathcal{H}}_{ex} + \hat{\mathcal{H}}_Z = -(g-1)^2 \sum_{ij} \mathcal{J}_{ij} \vec{J}_i \cdot \vec{J}_j - g\mu_B \vec{J} \cdot \vec{B} \tag{3.34}$$

Mean-Field approximation

The simplest method used to obtain approximated solutions is the mean-field approximation [23, 25, 26]. In this approximation, we assume that each atom experiences the action of a magnetic exchange field $\vec{B}_{ex}$ proportional to the magnetization of its nearest neighbors:

$$\vec{B_{ex}} = \lambda \vec{M} \tag{3.35}$$

where λ is the mean field constant. According to this expression, each spin feels the average magnetization of all other spins. We can considerer in a simple approximation that all nearest neighbors atoms have the same exchange interaction $\mathcal{J}$. In this way the hamiltonian 3.33, can be simply written as

$$\hat{\mathcal{H}}_{ex} = \sum_i -2(g-1)^2 \mathcal{J} \vec{J}_i \cdot \sum_{j=1}^{z} \vec{J}_j \tag{3.36}$$

where the sum is extended over the z nearest neighbors of the i-*th* atom. Now we can replace the interactions by an effective magnetic field so that $\mathcal{H}_{ex}$ has the form

$$\hat{\mathcal{H}}_{ex} = -\sum_i \mu_B g \vec{B}_{ex} \cdot \vec{J}_i \tag{3.37}$$

and from expressions 3.36 and 3.37 we find

$$\vec{B}_{ex} = \frac{2(g-1)^2\mathcal{J}}{g\mu_B} \sum_{j=1}^{z} \vec{J}_j \tag{3.38}$$

In the context of mean-field, we assume that each $\vec{J}_j$ can be replaced in the Heisenberg term by its average value $< \vec{J}_j >$. So, as all magnetic atoms are identical and equivalent, $< \vec{J}_j >$ is replaced by the total magnetic spin $< \vec{J} >$ magnetization is given by the

$$\vec{M} = ng\mu_B < \vec{J} > \tag{3.39}$$

Thus, the exchange magnetic field becomes

$$\vec{B}_{ex} = \frac{2z(g-1)^2\mathcal{J}}{g\mu_B} < \vec{J} >= \ = \frac{2z(g-1)^2\mathcal{J}}{g^2\mu_B^2 n}\vec{M} \tag{3.40}$$

and the molecular-field parameter is

$$\lambda = \frac{2z(g-1)^2\mathcal{J}}{ng^2\mu_B^2} \tag{3.41}$$

The molecular-field coefficient (λ) defined in this way depends on the number of atoms of the sample. However $\vec{B}_{ex}$ (eq. 3.40) is independent of n, as one would expect. For simplify an energy variable J_0 defined as

$$J_0 = \frac{2z(g-1)^2\mathcal{J}}{n} \tag{3.42}$$

Since we also want to consider the effects of an applied magnetic field H ($\vec{B} = \mu_0\vec{H}$), so that the total induction acting on the i^{th} atom is

$$\vec{B_T} = \vec{B} + \vec{B}_{ex} \tag{3.43}$$

Using a simple model with no anisotropy we can consider a collinear alignment of $\vec{M}$, $\vec{B}_{ex}$, $\vec{B}$ and $\vec{B_T}$ and $\vec{J}$ along the z-axis. For one atom, the Hamiltonian is

$$\hat{\mathcal{H}}_{mag} = -g\mu_B J_z B_T \tag{3.44}$$

and has eigenvalues given by

$$E_M = -g\mu_B M B_T \qquad M = -J, -J+1, ..., J \tag{3.45}$$

3.4.2 Weiss Magnetization

Using identical processes presented in section 3.2.1 and taking in account the mean-field approximation, we can calculate the spontaneous susceptibility and the spontaneous magnetization. Particularly, in the molecular-field theory, the magnetization is given by expression

$$M = ng\mu_B J B_J(\beta g\mu_B J B_T) \tag{3.46}$$

Since for sufficiently high temperatures the magnetization is small one can use approximation 3.14 and the magnetization is:

$$M = \frac{ng^2\mu_B^2 J(J+1)}{3k_B T} B_T \tag{3.47}$$

considering that $M = UB_T$ where $U = \frac{ng^2\mu_B^2 J(J+1)}{3k_B T}$ but using the relation that $B_T = B + \lambda M$ the fraction M/B is given by:

$$\frac{M}{B} = \frac{U}{1-\lambda U} \tag{3.48}$$

and using the definition of the paramagnetic susceptibility 3.2

$$\chi = \frac{M}{H}_0 = \mu_0 \frac{M}{B} \tag{3.49}$$

we obtain

$$\chi = \mu_0 \frac{\frac{ng^2\mu_B^2 J(J+1)}{3k_B}}{T - \frac{2z(g-1)^2 J(J+1)\mathcal{J}}{3k_B}}$$

This expression is known as the Curie-Weiss susceptibility and can be written

$$\chi = \frac{C}{T - \Theta_c} \tag{3.50}$$

where C is the Curie constant and Θ_c is the Curie Temperature is a critical temperature, both given by:

$$C = \mu_0 \frac{ng^2\mu_B^2 J(J+1)}{3k_B} \tag{3.51}$$

$$\Theta_c = \frac{2z(g-1)^2 \mathcal{J} J(J+1)}{3k_B} \tag{3.52}$$

In conclusion, within a mean field approximation model the magnetic hamiltonian (Zeemann and Heisenberg hamiltonian), if the direction of magnetization is taken along z-axes, we have

$$\hat{\mathcal{H}}_{mag} = -g\mu_B B_T J_z \tag{3.53}$$

where

$$g\mu_B B_T = g\mu_B B + J_0 J_z \tag{3.54}$$

The eigenvalues of the magnetic hamiltonian are

$$E_M = -g\mu_B B_T M, \qquad M = -J, -J+1, ..., J \tag{3.55}$$

Analyzing the eq. 3.55 the magnetic hamiltonian within the $\mid J, M >$ basis can be described by a square matrix with (2J+1)×(2J+1) elements and all are zero except for the diagonal elements (diagonal matrix).

Chapter 4

Crystal Field and Magnetic Anisotropy

4.1 Crystal Field

When atoms condense to form a crystal, the electronic state of each atom is modified from the free-atom state because of the interaction with surrounding atoms. The $4f$ electrons in a rare earth ion are thus subject to a variety of interactions with their surroundings. These forces may be broadly classified into two categories: the *single-ion interactions* and the *two-ion interactions*. the *single-ion interactions* act independently at each ionic site, so that their influence on the state $4f$ at a particular site is unaffected by the magnetic state of neighbors [23]. The corresponding contribution to the Hamiltonian therefore contains sums extended over terms located at the ionic sites i of the crystal, but without any coupling between different ions. On the other hand, the *two-ion interactions* couple the $4f$-electron clouds at pairs of ions, giving terms which involve two sites i and j. The first treatment is made considering a paramagnetic ion as a quantum system and the second process considers it as a classical system. In this chapter the crystal field interactions in a single crystal will be presented using the Steven's operator methods. A model for magnetic anisotropy will be also presented considering the anisotropic hamiltonian. At the end of this chapter a phenomenological approach will be presented to determine

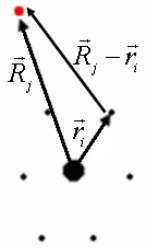

Figure 4.1: Scheme of the point charge model

the easy direction of magnetization.

4.1.1 The crystal field potential

The $4f$ electrons of a given Rare earth ions are subject to the electrostatic charge distribution $\rho(\vec{R})$. This electrostatic potential is given by

$$V_{cf}(\vec{r}_i) = \int \frac{e\rho(\vec{R}_i)}{\mid \vec{r}_i - \vec{R} \mid} d\vec{R} \tag{4.1}$$

$\vec{r}_i$ is the i-th electron coordinate [30]. Two models can be used for the crystal field and are described below.

The point charge model

If we consider that the electrostatic potential of the surroundings arises from point electric charges located at the center of the atoms of the crystal at a point R_j the eq. 4.1 can then be written as [27]:

$$V_{cf}(\vec{r}_i) = -e \sum_j \frac{q_j}{\mid \vec{R}_j - \vec{r}_i \mid} \tag{4.2}$$

where q_j is the charge of the ion j of the surroundings. If one knows the charge q_j, this potential can be calculated precisely. Although this model sometimes gives the correct signal of the coefficients, it fails in most cases [31]. This happens because this simples model neglects the finite extent of charges on the ions and the overlap of the magnetic ion wavefunctions with those of neighboring ions. Also this model does not consider the conduction electrons which give rise to a strong contribution to the crystal field Hamiltonian.

The spherical harmonics potential

This model consists in writing the potential as a series of spherical harmonics with the nucleus in the center of the ion:

$$V_{cf}(\vec{r_i}) = \sum_{l,m} A_l^m f_l(r_i) Y_l^m(\theta_i, \phi_i) \tag{4.3}$$

The linear combinations of $Y_l^m(\theta_i, \phi_i)$ remain invariant under the symmetry operations of $\hat{R}$, $\hat{R}$ stands for an element of the point symmetry group, but the A_l^m is not invariant and depends directly on the site symmetry as we shall explain latter.

4.1.2 Perturbing Hamiltonian of Crystal Field

Let $V(\vec{r_i})$ be the electrostatic potential acting on the electron i of the studied magnetic ion. The perturbing Hamiltonian due to the crystalline electric field can be written as:

$$\hat{\mathcal{H}}_{cf} = \Sigma_i q_i V(\vec{r_i}) = -e\Sigma_i V(\vec{r_i}) \tag{4.4}$$

The sum is restricted to electrons in unfilled shells ($4f$ in the case of rare earth metals), as the crystal field does not affect closed shells to a first order of perturbation [23].

Calculation of the matrix elements of the perturbing Hamiltonian $\hat{\mathcal{H}}_C$

In the basis $\mid J, M_J >$ of the considered multiplet, the matrix elements within first-order perturbation are:

$$< J, M_J \mid \hat{\mathcal{H}}_c \mid J, M_J > = < J, M_J \mid -e\Sigma_i V(r_i) \mid J, M_J > \tag{4.5}$$

Direct integration

The free-ion wave function $\mid J, M_J >$ is obtained from states involving single-electron wave function [26]:

$$\Psi_n^k \sim R(r_k) Y_n^k(\theta_k, \phi_k) \tag{4.6}$$

Using the definition of the angular multiplication, equation 4.5 is written as:

$$\int \Psi_{l_3}^{m_3^*} \Psi_{l_2}^{m_2^*} \Psi_{l_1}^{m_1^*} = \left[\frac{(2l_1+1)(2l_2+1)}{4\pi(2l_3+1)}\right]^{\frac{1}{2}} C(l_1 l_2 l_3; m_1 m_2 m_3) C(l_1 l_2 l_3; 000) \tag{4.7}$$

where the C's are the Clebsch-Gordan coefficients. These coefficients are non zero only if $l_3 = l_1 + l_2, l_1 + l_2 - 1, ..., |l_1 - l_2|$ and $m_3 = m_1 + m_2$.

In the matrix element components for the present case, the subscripts 1 and 3 refer to the atomic f-electrons ($l_1 = l_3 = 3$) and index 2 stands for a spherical harmonic of the potential expansion and is restricted to $0 \leq l_2 \leq 6$. As was refereed above the potential has to be invariant under rotation or inversion. Let us consider first the group of inversion through the origin (r→-r) . This contains two elements and hence two one-dimensional irreducible representations. One easily shows that Y_l^m with l even and l= 2n (n=integer) transforms according to the identity representation, while it occurs for l=2n+1 for the inversion symmetry. Therefore for 4f-atoms l is restricted to the values 2, 4 and 6. The term l=0 in the expansion is a constant. This term shifts all the levels of the given configuration by the same amount. Being $\hat{R}$ an element of the point symmetry group $\hat{R}$V=V$\hat{R}$ we can use this relation to show that some coefficient A_l^m of expansion 4.3 are zero.

For example, if the crystal field has a C_3 local point symmetry (hexagonal symmetry), where the generating elements of C_3 group are r→-r, $\theta \rightarrow \theta$, $\phi \rightarrow \phi - \frac{2\pi}{3}$. So

$$\hat{C}_3 V_{cf} = \sum_{l,m} e^{-im\frac{2\pi}{3}} A_l^m r^l Y_l^m(\theta, \phi) \hat{C}_3 \tag{4.8}$$

Since $\hat{R}$V=V$\hat{R}$, so we must have

$$e^{-im\frac{2\pi}{3}} A_l^m = A_l^m \tag{4.9}$$

hence A_l^m=0 (if m $\neq \pm 3$ and ± 6). Consequently, the potential in a C_3 point symmetry is

$$V(C_3) = \sum_{l=2,4,6} \sum_{m \pm 3, \pm 6} A_l^m r^l Y_l^m(\theta, \phi) \tag{4.10}$$

Therefore for rare earth atoms we have 9 crystal field parameters, A_2^0, A_4^0, $A_4^{\pm 3}$,A_6^0, $A_6^{\pm 3}$and $A_6^{\pm 6}$, for the C_3 point symmetry.

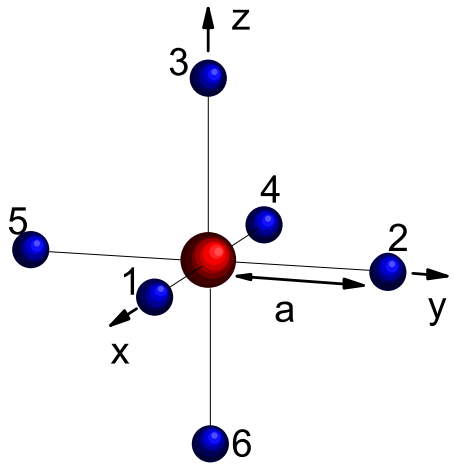

Figure 4.2: Sixfold cubic coordination

As an alternative we can proceed by representing the lattice ions as point charges, using directly the formula for the crystal field potential (eq. 4.3) and substituting directly the angular positions, for example considering a sixfold cubic symmetry. Observing Fig.4.2 it is obvious that the angular positions (ϕ,θ) are P_1=($\frac{\pi}{2}$,0), P_2=($\frac{\pi}{2}$,$\frac{\pi}{2}$), P_3=(0,0), P_4=($\frac{\pi}{2}$,π), P_5=($\frac{\pi}{2}$,$\frac{3\pi}{2}$) and P_6=(π,0). Substituting in eq.4.3 the non-zero terms are the terms with l=4 and 6 and m=0 and $\pm$4.

4.2 The Stevens "Equivalent Operator" Method

The Stevens equivalent operator method is by far the most convenient method for evaluating the matrix elements of the crystalline potential between coupled wave functions specified by J (or L). It eliminates the need to go back to single electron wave functions by the use of an "equivalent operator" to $\hat{H}_{cf}$ consisting of angular momentum operators which act on the angular part of the wave function. This is an application of the *Wigner-Eckart* theorem. Due to the fact that the angular momentum J and the position of an electron $\mathbf{r}$ are both vectors, to find the operator equivalents of terms as $\sum_i f(x_i, y_i, z_i)$ occurring in $\hat{\mathcal{H}}_c$, one replaces x, y and z by J_x, J_y and J_z respectively, always allowing for the non-commutation of J_x, J_y and J_z. This is done by replacing products of x, y and z by an expression consisting of all the possible different combinations

of J_x, J_y and J_z, divided by the total number of combinations, we for example obtain [23, 26]:

$$x^2 - y^2 \rightarrow J_x^2 - J_y^2, \qquad 3z^2 - r \rightarrow 3J_z^2 - J(J+1), \qquad xy \rightarrow \frac{1}{2}(J_xJ_y + J_yJ_x) \tag{4.11}$$

In this way we can write the matrix elements for example as:

$$< J, M_J \mid \sum_i (3z_i^2 - r_i) \mid J, M_J > \equiv \alpha_J < r^2 >< J, M_J \mid 3J_z^2 - J(J+1) \mid J, M_J > \tag{4.12}$$

The multiplicative factor α_J is a constant depending on the quantum number l of the electron (3 in the case of a rare-earth), and J of the considered rare-earth element. The constants are commonly named β_J and γ_J for fourth- and the sixth-order terms, respectively. Their values are tabulated in appendix D. The values and expressions of the equivalent operators O_l^m are given in appendix E. Using the formalism of the equivalent operator for the case of sixfold cubic symmetry we obtain [32]

$$\begin{aligned} \hat{\mathcal{H}}_{cf} &= C_4[\frac{7}{2}Y_4^0 + \frac{\sqrt{70}}{4}(Y_4^4 + Y_4^{-4})] + C_6[\frac{3}{4}Y_6^0 - \frac{3}{8}\sqrt{14}(Y_6^4 + Y_6^{-4})] \\ &= B_4^0(O_4^0 + 5O_4^4) + B_6^0(O_6^0 - 21O_6^4) \end{aligned} \tag{4.13}$$

where

$$B_n^m = A_l^m \alpha_l < r^l > \tag{4.14}$$

are the crystal field parameters.

4.2.1 The crystal field parameters B_n^m

The crystal field parameters can be either measured experimentally (by neutron diffraction) or calculated by means of simple models such as the point charge model [33, 34]. In the case of a cubic symmetry the point charge model yields

$$B_4^0 = b_4 \frac{|e|q}{d}^5 \beta < r^4 >; \qquad B_6^0 = -b_6 \frac{|e|q}{d}^7 \beta < r^6 >; \tag{4.15}$$

and b_4 and b_6 depends on the type of symmetry (tetrahedric, cubic and octahedric) and are tabulated in 4.1 [35] and d is the distance of the nearest newborns to the RE site and $|e|q$ is the effective charge placed on them. The

Table 4.1: Parameters for the crystal field.

Type of coordination	b4	b6
Tetrahedric (4)	$-\frac{7}{36}$	$\frac{1}{16}$
Octahedric (6)	$+\frac{7}{16}$	$+\frac{3}{64}$
Cube	$-\frac{7}{18}$	$+\frac{1}{9}$

most common eigenfunctions and eigenvalues of the hamiltonian 4.13 have been determinate and tabulated for different J by Lea *et al* [35]. In order to cover all possible values of the ratio between the fourth and sixth degree terms we put [36, 37, 38]:

$$B_4F(4) = Wx; \qquad B_6F(6) = W(1-|x|); \tag{4.16}$$

where -1<x<1. It follows that

$$\frac{B_4}{B_6} = \frac{x}{1-|x|}\frac{F(6)}{F(4)}; \tag{4.17}$$

so that B_4/B_6=0 for x=0, while B_4/B_6=$\pm\infty$ for x=$\pm$1. The factors F(4) and F(6) are the common factors to the matrix O_4^n and O_6^n respectively.

Rewriting the equation 4.13 we have:

$$\mathcal{H}_{cf} = W\left[x\frac{1}{F(4)}(O_4^0+5O_4^4) + (1-|x|)\frac{1}{F(6)}B_6^0(O_6^0-21O_6^4)\right] \tag{4.18}$$

Expressed in this form the term in square bracket represents a matrix whose eigenvectors correspond to the most general combination of the fourth and sixth degree crystal fields, and whose eigenvalues are related to the crystal field energy levels by a scale factor W defined in equation 4.16 and 4.18 [33].

4.3 Magnetic Anisotropy

In a ferromagnetic material, both the energy and the magnetization depend on the orientation of the magnetization relative to the crystal axes, and the interactions between magnetic atoms favor a parallel alignment of the atomic magnetic moments. At absolute zero temperature, the alignment is complete and the spontaneous magnetization has its maximum possible value. As the temperature increases, the effects of thermal fluctuations which favor random orientation of the magnetic moment become important. In the sixties, Callen and Callen first pointed out that the existence of energy anisotropy implies anisotropy the magnetization. This gives an anisotropy hamiltonian $\hat{\mathcal{H}}_{ani}$ with two components. The exchange $\hat{\mathcal{H}}_{mag}$ (chapter 3) and the crystal field hamiltonian given in this chapter $\hat{\mathcal{H}}_{cf}$. The anisotropic hamiltonian are expressed by $\hat{\mathcal{H}}_{ani} = \hat{\mathcal{H}}_{mag} + \hat{\mathcal{H}}_{cf}$ [26].

4.3.1 Relation between Crystalline and Magnetization Coordinate Systems

As we have seen in Chapter 3, the magnetic hamiltonian for simplification is considered that magnetization direction is along the z-axis and is given by

$$\hat{\mathcal{H}}_{mag} = -g\mu_B B_T M \tag{4.19}$$

where M = -J,-J+1....J-1, J. The crystal field Hamiltonian has the simple form given in eq. 4.18 because it was considered the coordinates (x,y,z) are along the crystallographic (a,b,c)-axes. However to use the magnetic hamiltonian ($\mathcal{H}_{mag}$) we have to project the lattice coordinates to obtain the c-axis parallel to the magnetization direction.

In order to distinguish the two systems, we will denote the Stevens operators $O_n^m(J)$ in $\hat{\mathcal{H}}_{cf}$ with respect to the crystallographic axis, i.e. in the (ξ,η,ζ)-coordinate system, by $Q_n^m(J_\xi,J_\eta,J_\zeta)$, as H_{cf}=$\Sigma B_n^m Q(\vec{J})$ [23, 26]. The direction of magnetization (z-axis) is specified by the transformation of the angular momentum operator in $Q_n^m(\vec{J})$ (by projecting J_x, J_y, J_z onto J_ξ, J_η, J_ζ) (see Fig.4.3).

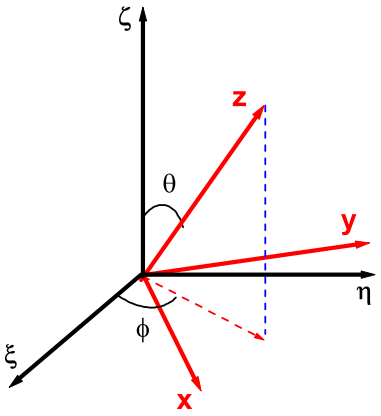

Figure 4.3: Relationship between the crystalline J_x, J_y, J_z and magnetic coordinates (J_ξ,J_η,J_ζ).

This projection results in the following expressions [39]:

$$\begin{aligned} J_\zeta &= J_z cos(\theta) - J_x sin(\theta) \\ J_\xi &= J_x cos(\theta)cos(\phi) + J_z sin(\theta)cos(\phi) - J_y sin(\phi) \\ J_\eta &= J_x cos(\theta)sin(\phi) + J_z sin(\theta)sin(\phi) + J_y cos(\phi) \end{aligned} \tag{4.20}$$

With such transformation, we have the expressions of $Q_n^m(J_\xi,J_\eta,J_\zeta)$ in terms of $O_n^m(J_x,J_y,J_z)$ (see appendix E) [39]. As an example we transform Q_2^0:

$$Q_2^0 = 3J_\zeta^2 - J(J+1) \tag{4.21}$$

Using equation 4.20 we obtain:

$$\begin{aligned} Q_2^0 &= 3(J_z cos(\theta) - J_x sin(\theta))^2 - J(J+1) = 3J_z^2 cos^2(\theta) + 3J_x^2 sin^2(\theta) + \frac{3}{2}(J_z J_x + J_x J_z)sin(2\theta) \\ &\quad -J(J+1) \\ &= \frac{1}{2}(3cos^2(\theta)-1)(3J_z^2 - X) + 3sin(2\theta)\left[\frac{1}{2}(J_z J_x + J_x J_z)\right] + \frac{3}{2}sin^2(\theta)\frac{1}{2}(J_+^2 + J_-^2) \\ &= \frac{1}{2}(3cos^2(\theta)-1)O_2^0 - 3sin(2\theta)O_2^1 + \frac{3}{2}sin^2(\theta)O_2^2 \end{aligned} \tag{4.22}$$

To obtain the other operators a similar process is used [39].

4.4 The anisotropy Hamiltonian

If we specifically consider the sixfold cubic axis we have

$$\hat{\mathcal{H}}_{cf} = B_4^0(Q_4^0 + 5Q_4^4) + B_6^0(Q_6^0 - 21Q_6^4) \tag{4.23}$$

and we obtain the matrix of the $\hat{\mathcal{H}}_{anis}$ as:

$$\begin{aligned} &< JM_J|H_{anis}|JM'_J > =< JM_J|H_{ex} + H_{cf}|JM'_J > \\ &=< JM_J|B_4^0(Q_4^0 + 5Q_4^4) + B_6^0(Q_6^0 - 21Q_6^4) - g\mu_B B_{ex} J_z|JM'_J > \end{aligned} \tag{4.24}$$

and more simply we express the above equation by

$$\mathcal{H} = -J_0 J_Z + W\left[x\frac{1}{F(4)}(O_4^0 + 5O_4^4) + (1-|x|)\frac{1}{F(6)}B_6^0(O_6^0 - 21O_6^4)\right] \tag{4.25}$$

with

$$\begin{aligned} Q_4^0 &= \frac{35}{8}sin^4(\theta)O_4^4 \\ &\quad -35sin^3(\theta)cos(\theta)O_4^3 \\ &\quad +\frac{5}{2}sin^2(\theta)(7cos^2(\theta)-1)O_4^2 \\ &\quad -\frac{5}{2}sin(2\theta)(7cos^2(\theta)-3)O_4^1 \\ &\quad +\frac{1}{8}(35cos^4(\theta) - 30cos^2(\theta) + 3)O_4^0 \end{aligned} \tag{4.26}$$

$$\begin{aligned} Q_4^4 &= \frac{1}{8}cos(4\phi)(cos^4(\theta) + 6cos^2(\theta) + 1)O_4^4 \\ &\quad +\frac{1}{2}sin(2\theta)cos(4\phi)(cos^2(\theta)+3)O_4^3 \\ &\quad +\frac{1}{2}sin^2(\theta)cos(4\phi)(cos^2(\theta)+1)O_4^2 \\ &\quad +sin^3(\theta)cos(4\phi)cos(\theta)O_4^1 \\ &\quad +\frac{1}{8}sin^4(\theta)cos(4\phi)O_4^0 \end{aligned}$$

$$
\begin{aligned}
&-sin^3(\theta)sin(4\phi)O_4^{-1}\\
&+sin^2(\theta)sin(4\phi)cos(\theta)O_4^{-2}\\
&-sin(\theta)sin(4\phi)(3cos^2(\theta)+1)O_4^{-3}\\
&-\frac{1}{2}sin(4\phi)cos(\theta)(cos^2(\theta)+1)O_4^{-4}
\end{aligned}
\tag{4.27}
$$

$$
\begin{aligned}
Q_6^0 \;=\;& \frac{231}{32}sin^6(\theta)O_6^6\\
&-\frac{693}{8}sin^5(\theta)cos(theta)O_6^5\\
&+\frac{63}{1}6sin^4(\theta)(11cos^2(\theta)-1)O_6^4\\
&-\frac{105}{8}sin^3(\theta)cos(\theta)(11cos^2(\theta)-3)O_6^3\\
&+\frac{105}{3}2sin^2(\theta)(33cos^4(\theta)-18cos^2(\theta)+1)O_6^2\\
&-\frac{21}{8}sin(2\theta)(33cos^4(\theta)-30cos^2(\theta)+5)O_6^1\\
&+\frac{1}{16}(231cos^6(\theta)-315cos^4(\theta)+105cos^2(\theta)-5)O_6^0
\end{aligned}
\tag{4.28}
$$

$$
\begin{aligned}
Q_6^4 \;=\;& \frac{11}{32}sin^2(\theta)cos(4\phi)(cos^4(\theta)+6cos^2(\theta)+1)O_6^6\\
&-\frac{11}{16}sin(2\theta)cos(4\phi)(3cos^4(\theta)+10cos^2(\theta)-5)O_6^5\\
&+\frac{1}{16}cos(4\phi)(33cos^6(\theta)+35cos^4(\theta)-65cos^2(\theta)+13)O_6^4\\
&+\frac{5}{16}sin(2\theta)cos(4\phi)(11cos^4(\theta)+2cos^2(\theta)-5)O_6^3\\
&+\frac{5}{32}sin^2(\theta)cos(4\phi)(33cos^4(\theta)-10cos^2(\theta)+1)O_6^2\\
&+\frac{1}{4}sin^3(\theta)cos(\theta)cos(4\phi)(33cos^2(\theta)-13)O_6^1\\
&+\frac{1}{16}sin^4(\theta)cos(4\phi)(11cos^2(\theta)-1)O6^0\\
&-\frac{1}{2}sin^3(\theta)sin(4\phi)(11cos^2(\theta)-1)O_6^{-1}\\
&-\frac{5}{8}sin^2(\theta)cos(\theta)sin(4\phi)(11cos^2(\theta)-5)O_6^{-2}\\
&-\frac{5}{4}sin(\theta)sin(4\phi)(11cos^4(\theta)-8cos^2(\theta)+1)O_6^{-3}\\
&-\frac{1}{2}cos(\theta)sin4\phi(5cos^4(\theta)-1)O_6^{-4}\\
&+\frac{11}{4}sin(\theta)sin(4\phi)(5cos^4(\theta)-1)O_6^{-5}\\
&-\frac{11}{8}sin^2(\theta)cos(\theta)sin(4\phi)(cos^2(\theta)+1)O_6^{-6}
\end{aligned}
\tag{4.29}
$$

4.5 Determination of easy direction of magnetization

In a free rare earth ion, each J level is $(2J+1)$-fold degenerated. However, on placing the ion in lattice, the $(2J+1)$-fold state degeneracy is partial or totally removed due to the crystalline electric field produced by the charges surrounding the rare earth ion. Given a magnetic rare-earth, we have a definite J, then M_J=-J,-J+1,-J+2,...,J. In this thesis we developed a computer program where we determine the matrix elements of Stevens operator $< JM_J|O_n^m(J_x, J_y, J_z)|JM'_J >$ and then the anisotropic Hamiltonian matrix [23]. In this way we can obtain the first-order energy correction E_i to the $2J+1$ sublevel which is used to calculate the partition function [28]:

$$Z(\vec{n}, T) = \sum_i e^{-\beta E_i} \tag{4.30}$$

and immediately we can obtain the free energy using eq. 4.31 [28]

$$F(\vec{n}, T) = -\frac{1}{\beta} ln \sum_i e^{-\beta E_i} \tag{4.31}$$

The minimum of free energy at a given temperature gives the direction of the easy magnetization. An estimate of the magnitude of $\mu_B\ B_{ex}$ can often be obtained for the compound considered from available magnetic data considering a selfconsistent method (see chapter 6).

4.6 Phenomenological Approach

4.6.1 The expression of the free energy

The magnetic anisotropy properties of crystals are often expressed in terms of the bulk magnetic anisotropy constants. In the phenomenological treatment, the magnetic free energy of a **cubic crystal** can be expanded into a polynomial series in α_i, the direction cosine of the direction of magnetization with respect to the cubic edges [29, 40]:

$$F(\vec{n}, T) = K_0 + K_1(\alpha_1^2\alpha_2^2 + \alpha_2^2\alpha_3^2 + \alpha_3^2\alpha_1^2) + K_2(\alpha_1^2\alpha_2^2\alpha_3^2) \tag{4.32}$$

with $\alpha_1^2 + \alpha_2^2 + \alpha_3^2 = 1$. The $K's$ are the anisotropy constants and depend strongly on temperature. It is commonly accepted that only terms up to the sixth power of the direction cosine should be retained. It can be easily shown by differentiation with respect to the angles β and γ ($\alpha = cos^{-1}\alpha_1, \beta = cos^{-1}\alpha_2, \gamma = cos^{-1}\alpha_3$) that the only minima for the free energy occur in the major axes of symmetry [100], [110] and [111] in case of a cubic system. Which of these axes become an easy axis of magnetization, depends on the relative values of K_1 and K_2. On the other hand, the easy direction of magnetization may not be along the such major symmetry axes so that the expression would be expanded to include the eighth-power terms:

$$F(\vec{n},T) = K_0+K_1(\alpha_1^2\alpha_2^2+\alpha_2^2\alpha_3^2+\alpha_3^2\alpha_1^2)+K_2(\alpha_1^2\alpha_2^2\alpha_3^2)+K_3(\alpha_1^4\alpha_2^4+\alpha_2^4\alpha_3^4+\alpha_3^4\alpha_1^4) \tag{4.33}$$

4.6.2 The easy direction of magnetization with anisotropy constants

To determine the easy directions, first we start substituting α_1^2 to 1-α_2^2-α_3^2 in eq.4.32 and changing the notation to α_1=cos(α), α_2=cos(β) and α_3=cos(γ). Mathematically, the conditions for an extremum in $F(\vec{n},T)$ are

$$\frac{\partial F}{\partial \beta} = 0 \qquad \frac{\partial F}{\partial \gamma} = 0 \tag{4.34}$$

The extremum is a minimum if

$$\frac{\partial^2 F}{\partial \beta^2} > 0 \qquad and \qquad \frac{\partial^2 F}{\partial \gamma^2} > 0 \tag{4.35}$$

Using the eq.4.34 for the extremum, one obtains [40]

$$\begin{aligned} \frac{\partial F}{\partial \beta} &= 2sin\beta cos\beta(2cos^2\beta - 1 + cos^2\gamma) \\ \cdot[K_1 + K_2cos^2\gamma - 2K_3(cos^4\beta - cos^2\beta + cos^2\beta cos^2\gamma + cos^4\gamma)] &= 0 \\ \frac{\partial F}{\partial \gamma} &= 2sin\gamma cos\gamma(2cos^2\gamma - 1 + cos^2\beta) \\ \cdot[K_1 + K_2cos^2\beta - 2K_3(cos^4\gamma - cos^2\gamma + cos^2\gamma cos^2\beta + cos^4\beta)] &= 0 \end{aligned} \tag{4.36}$$

Each derivative is a product of four factors. These derivatives will simultaneously satisfy condition 4.34 whenever one of the four factors vanish as follows.

Case 1: The [100] axes and equivalent direction by rotation ([010], [001]) of magnetization corresponds to

$$cos\beta = cos\gamma = 0 \qquad cos\beta = sin\gamma = 0 \qquad sin\beta = cos\gamma = 0 \tag{4.37}$$

Case 2: The [110] axes of magnetization corresponds to

$$cos\beta = 0 \qquad and \qquad 2cos^2\gamma - 1 + cos^2\beta = 0$$

or to

$$cos\gamma = 0 \qquad and \qquad 2cos^2\beta - 1 + cos^2\gamma = 0 \tag{4.38}$$

Case 3: The [111] axes of magnetization corresponds to

$$2cos^2\gamma - 1 + cos^2\beta = 0 \qquad and \qquad 2cos^2\beta - 1 + cos^2\gamma = 0 \tag{4.39}$$

Substituting the values of cosβ and cosγ in each case into the quadratic form, eq.4.33 , yields the limiting values of K1 for which the above-mentioned major axes of symmetry becomes easy axes of magnetization.

Case 4: The nonmajor axes of easy magnetization are obtained by the vanishing of the second and fourth factors, respectively, in the two derivatives, i.e.,

$$cos\beta = 0$$

$$and$$

$$K1 + K2cos^2\beta - 2K3(cos^4\gamma - cos^2\gamma + cos^2\gamma cos^2\beta + cos^4\beta) = 0 \tag{4.40}$$

This yields the [uv0] directions, the angle ϕ between the direction of magnetization and [100] axes being in this case $sin^2 2\phi = sin^2 2\beta = \frac{-2K_1}{K_3}$. The magnetic anisotropy free energy $F_{uv0} = \frac{-3K_1}{4K_3}$.

Case 5: Finally the vanishing of the third factor in one derivative and the four in the second or the vanishing of both fourth factors, yields the minima for the [uuW] directions, i.e.,

$$2cos^2\beta - 1 + cos^2\gamma = 0$$

$$and$$

$$K1 + K2cos^2\beta - 2K3(cos^4\gamma - cos^2\gamma + cos^2\gamma cos^2\beta + cos^4\beta) = 0$$

$$or$$

$$K1 + K2cos^2\gamma - 2K3(cos^4\beta - cos^2\beta + cos^2\gamma cos^2\beta + cos^4\gamma) = 0$$

$$and$$

$$K1 + K2cos^2\beta - 2K3(cos^4\gamma - cos^2\gamma + cos^2\gamma cos^2\beta + cos^4\beta) = 0 \qquad (4.41)$$

The angle θ in this case is

$$cos\theta = 1 - 2cos^2\beta$$

$$and$$

$$cos\beta = \frac{(K2 + 2K3)[(K_2 + 2K_3)^2 + 24K_1K_3]^{\frac{1}{2}}}{12K_3} \qquad (4.42)$$

Substituting in eq. 4.33, one obtains the boundaries of region ABDGECA in Fig. 4.4. The results indicates that such minima can exist for direction of $\vec{n}$ parallel to the major axes of symmetry and also for crystallographic directions of type [uuw] ($\alpha = \beta$) and of type [uv0] ($\gamma = \frac{\pi}{2}$). These additional directions exist only for $K_3 > 0$. For the sake of conciseness, it is helpful to express K_1 and K_2 in units of K_3, and therefore define $K_1' = K_1/K_3$ and $K_2' = K_2/K_3$. A straightforward calculation allows one to determine the conditions imposed on the $K_i's$ which account for the presence of axes of symmetry. These conditions for [uuw]-type direction are

$$-2 < K_2' < 2 \qquad and \qquad -\frac{1}{24}(K'2 + 2)^2 < K'1 < 0$$

or

$$2 < K_2' < 4 \qquad and \qquad -\frac{1}{24}(K'2 + 2)^2 < K'1 < \frac{1}{2}(K'1 - 1) \qquad (4.43)$$

The conditions for a [uv0]-type direction are

$$-\frac{1}{2} < K_1' < 0 \qquad and \qquad 2 < K'2 \qquad (4.44)$$

The figure 4.4 represents, in the K1', K2' plane, the regions with the different possible axes of magnetization. Within the approximately triangular region

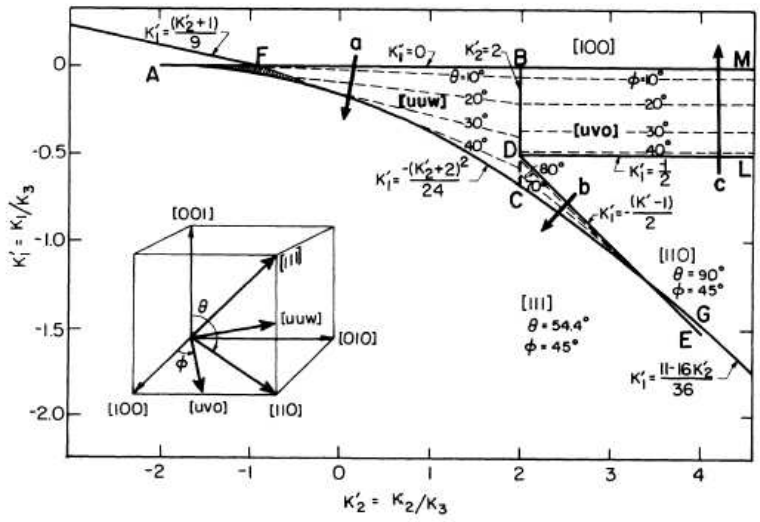

Figure 4.4: Boundaries of regions to different easy axis of magnetization in the K_1' and K_2'.

ABC, the axis of magnetization is of type [uuw]. Within this region θ=$cos^{-1}\alpha_3$, defined as the angle between $\vec{n}$ and the [001] axis, has values between 0 and 54.4°. Lines of constant θ change continuously across the AB boundary, but show a discontinuity when crossing the AC and BC boundaries. The cross hatched region in the neighborhood of A corresponds to a region of local minima of F for [uuw] types of magnetization. Such direction will therefore not be stable. Region CED is similar to ABC in that the direction of easy magnetization is of type [uuw]; the angle θ within this region varies between 54.4° and 90°. Between points E and G there is again a very narrow band corresponding to non-stable (local minima of F) axes of type [uuw]. Region DBML is part of the area in which the direction of magnetization is of type [uv0], i.e., θ=90^0 and ϕ=$tan^{-1}(\frac{v}{u})$. Lines of constant ϕ have also been plotted in this region, which continues indefinitely towards the right, bounded by the straight lines K_1'=0 and K_2'=-$\frac{1}{2}$ [40].

In chapter 2 we describe the spin reorientation of the compound where study ($Tb_5Si_2Ge_2$) and conclude that in a simple description the magnetic moments at high temperatures are almost all parallel to a-axis (the direction [100]). In the spin reorientation process the magnetic moments modify to [101] direction at low temperatures. Using the Fig.4.4 we represent the angular dependence (θ,

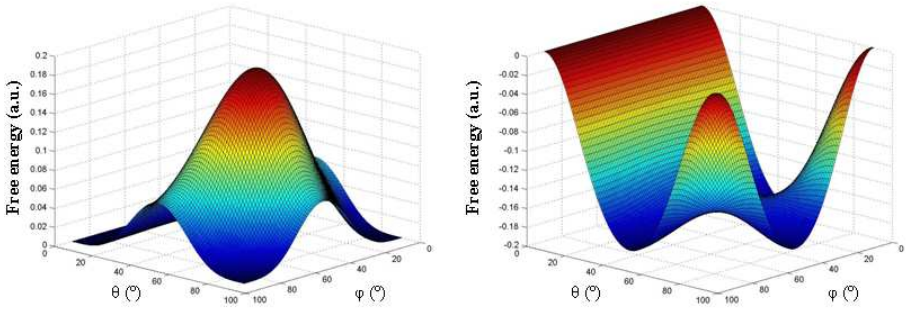

Figure 4.5: Angular dependence of magnetocrystalline energy for K_1'=0 and K_2'=4 (left). Angular dependence of magnetocrystalline energy for K_1'=-1 and K_2'=4(right)

ϕ) of the energy surface considering K_1'=0 and K_2'=4 that correspond to the easy direction on [100] and the equivalent direction ([010],[001]) (see Fig. 4.5 a). Observing the Fig. 4.5a) it is clear that the minimum energy correspond to the direction [100] and the other minimums are the equivalent direction. In Fig.4.5 b) we considerer K_1'=-1 and K_2'=4 and we can observe the three minimums that correspond to [110], [101] and [011] direction.

With above results we conclude that the spin reorientation process can occur due to the alteration of K_1'.

4.7 Relation between macroscopic and microscopic free anisotropic energy

The macroscopic anisotropy parameters are known to be the coefficients in a symmetry-determined expansion of the free energy in terms dependent on the magnetization direction as specified by polar coordinates (θ,ϕ) relative to the crystallographic axes. For cubic symmetry, the free energy may be written in a expansion of spherical harmonics as

$$F(\vec{n},T) = F_0(T) + k_4^0(T)Y_4^0(\theta,\phi) + k_4^4(T)Y_4^4(\theta,\phi) + k_6^0(T)Y_6^0(\theta,\phi) \quad (4.45)$$

$$+K_6^4(T)Y_6^4(\theta,\phi) \quad (4.46)$$

The spherical harmonics are normalized over a solid angle 4π.

An expansion in powers of sin θ has been employed, however the spherical harmonics form an orthogonal basis and are thus more appropriate.

Chapter 5

Experimental results

To understand the spin reorientation process for $Tb_5Si_2Ge_2$ compound, some physical properties namely transport and magnetic properties were measured. In this chapter we first give some experimental details related with the results obtained. Afterwards, a detailed analysis of the electrical resistance R(T), thermopower S(T), neutron diffraction and magnetization of $Tb_5Si_2Ge_2$ compound is reported, on the vicinity of the spin reorientation transition. A simple model based on an approximate magnetic anisotropy energy is presented, which gives a satisfactory qualitative description of the main features of the reorientation process.

5.1 Experimental details

5.1.1 Preparation of samples by arc melting technique

The $Tb_5Si_2Ge_2$ compound was synthesized by arc melting of 99.9 % wt pure Tb and 99.9999 % wt pure Si and Ge under high-purity argon atmosphere. This process consists in melting the pure elements which constitute the sample, in the desired stoichiometric quantities, through an electric arc discharge caused by the application of a high voltage between two near electrodes. Weight losses during melting were negligible and, therefore, the initial composition was assumed unchanged. The quality of the sample was checked by scanning electron microscopy and X-ray diffraction at room temperature. The measurements

confirmed the presence of a monoclinic ($P112_1/a$) main phase with unit cell parameters a=7.5080(5) $\AA$, b=14.652(1) $\AA$ and c=7.7117(5) $\AA$. A parallelepiped sample with cross-section 0.89×0.76 mm ^{2} and length 1.9 mm was cut from the initial ingot for our transport property measurements. The samples obtained are very shiny, porous and generally have microcracks. This method has a disadvantage: when the melting process ends, the process is not as fast and homogeneous as desired. The lower side of the sample, in contact with the water-cooled copper hearth cools faster than the upper part of the sample. This cooling difference is visible in the form acquired by the samples. During the brief cooling process, the upper part of the sample crystallizes with a shiny aspect and a spherical form, whereas the lower part does not crystallize.

5.1.2 Methods of measurement of transport and magnetic properties at cryogenic temperatures

Cryogenic systems

The determination of the transport properties, namely the electric resistivity and thermoelectric power was performed closed cycle refrigerators based in circulation of helium which, in our case can reach temperatures of 3.7 K and 10 K. In the determination of the magnetic properties, the cryogenic system used is a helium, with a temperature range between 4 and 300K cryostat coupled to a evercool system.

5.1.3 Electrical resistivity measurement

The sample holder is a cylindrical block of copper with a thread which incases in the cold tip of the cryostat. On its surface is placed a thin leaf of shroud paper absorbed in a GE-varnish which is a good electric insulator and good thermal conductor. This varnish allows the fixation of the sample to the sample holder, where the sample is placed on the shroud paper. On the sample holder plate, there are two connection wires to establish the electric contacts - generally two wires for the voltage of the sample (V) and the other two for the electric current of the sample (I).

After being established the electric contacts in the sample, it is inserted

in the cryostat, making the experimental setup represented in Fig. 5.1. The electric resistance measurement was made by the 4-probe technique as one can see in Fig. 5.1.

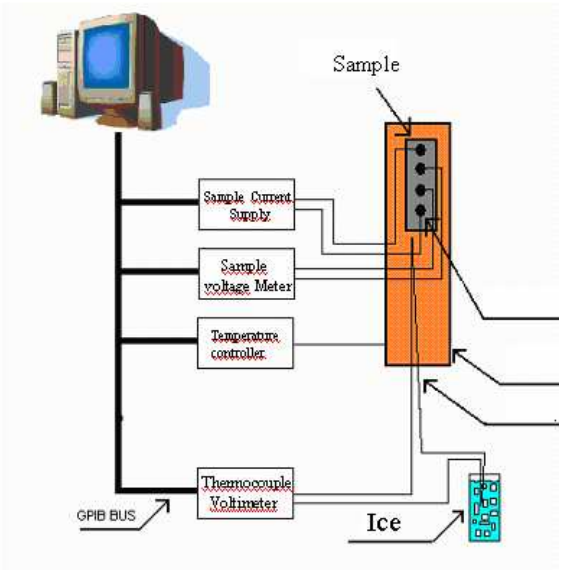

Figure 5.1: Experimental montage for electrical resistivity data using 4-probe technique.

During the experiment, the temperature is changed using a temperature controller thermocouple are used for measuring temperatures. The temperature variation rate has to be very small (about 1 K/min to 0.5 K/min) so that the thermal equilibrium of the sample can be established. This time variation of the temperature is so reduced that it allows obtaining a reasonable number of experimental values.

The software used allows monitoring graphically the experimental results, in real-time, early enabling the verification of the measured data.

5.1.4 Thermopower Measurements

The method used was the differential method. This method consists in the measurement of the thermoelectric voltage (ΔV) generated by a temperature gradient (ΔT) between the two tips of the sample, as is schematized in Fig. 5.2.

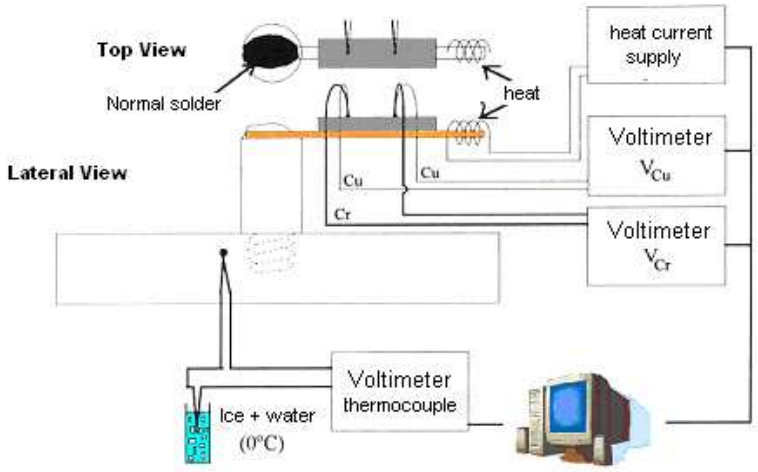

Figure 5.2: Schematic montage of thermopower measurements

As one can see from Fig.5.2 there are two connection points in the sample, each one with two connection wires (one of copper - Cu - and the other of Kromel - Cr). Each pair of wires is linked to the nanovoltmeters. During the thermoelectric power experiment, the average temperature of the sample is varied, acting in the temperature regulation system of the cryostat. The temperature gradient is increased almost continually (turning the heater on) up to a maximum value (usually $\Delta T_{max} \sim 0.5$ K). Typically, a temperature increases takes about a minute, being registered the successive voltage values of the copper and is kromel wires. After the ΔT_{max} being reached, the process repeat until reach ΔT = 0 along the sample. As the temperature gradient value is small and because the temperature of the sample and contacts is the same (for contacts sufficiently small and fixed with a silver ink which is a good heat conductor), one can build the graphic of V_{Cu} as a function of V_{Cr}, obtaining a straight line with slope $\alpha = \Delta V_{Cu}/\ \Delta V_{Cr}$. To obtain the thermoelectric power value, one has to consider the following equations

$$\Delta V_{Cu} = S_{a,Cu} \Delta T \tag{5.1}$$

$$\Delta V_{Cr} = S_{a,Cr} \Delta T \tag{5.2}$$

Since

$$\Delta V_{Cu} - \Delta V_{Cr} = (S_{a,Cu} - S_{a,Cr})\Delta T = S_{Cr,Cu}\Delta T \tag{5.3}$$

it is obtained the following expression to the thermoelectric power of the sample in respect comparison to the thermoelectric power of the copper:

$$S_{a,Cr} = \frac{\alpha}{\alpha - 1} S_{Cr,Cu} \tag{5.4}$$

Now it only lacks to know the thermoelectric power of copper in relation to the one of kromel as a function of temperature. Those values are obtained through a calibration made previously in the laboratory that allows determining the value of as a function of the temperature. The absolute value of the thermoelectric power of the sample S_A(T) is obtained by the following expression

$$S_A = S_{a,Cr}(T) + S_{Cr}(T) \tag{5.5}$$

Where the values of $S_{A,Cu}$ are obtained experimentally using eq.5.4 and the values of S_{Cu} are tabulated.

5.2 Experimental results

5.2.1 Electrical Resistivity

Figure 5.3 displays the temperature dependence of the electrical resistivity of $Tb_5(Si_{0.5}Ge_{0.5})_4$ from 10 K to 75 K, after subtracting the (large) residual resistivity ρ_0=500 $\mu\Omega$cm, together with its temperature derivative dρ/dT. Two clear anomalies are observed in dρ/dT near T_{SR_1}=57K and T_{SR_2}=40K. At T_{SR_1} the temperature dependence of dρ/dT changes abruptly, which we associate with the onset of the spin reorientation transition (see section D). At T_{SR_2} the temperature dependence of dρ/dT again changes suddenly, marking the end of the spin reorientation process, i.e. completing which makes the transformation of the FM1 phase into the FM2 phase. Between T_{SR_1} and T_{SR_2}, dρ/dT exhibits an irregular behavior. To investigate this effects, two further ρ(T) measurements were performed, taking the numerical (local) dρ/dT derivatives. These experiments confirmed the irregular behavior of dρ/dT between T_{SR_1} and T_{SR_2}. The anomalies cannot be attributed to artifacts of differentiation (coupled with

finite accuracy of experimental data), since as soon as T decreases below T_{SR_1} (or increases above T_{SR_2}) a smooth dρ/dT curve is systematically observed. These results suggest erratic steps in the reorientation of the Tb1, Tb2 and Tb3 magnetic moments during the spin reorientation process.

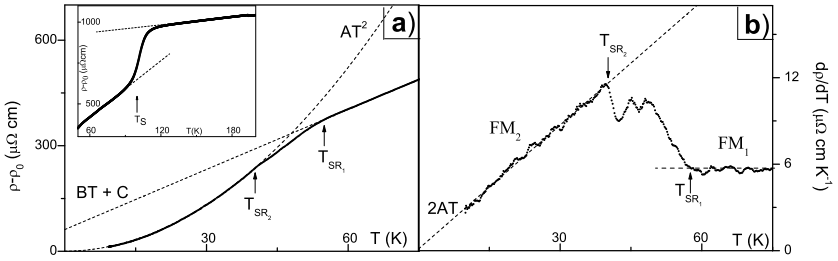

Figure 5.3: (a) Temperature dependence of the electrical resistivity (ρ) of $Tb_5(Si_{0.5}Ge_{0.5})_4$ between 10K to 75K, after subtraction of the residual resistivity (ρ_0). Inset: temperature dependence ρ(T) between 50K and 180K): (b)Temperature derivative of the electrical resistivity (dρ/dT) between 10K and 75K.

Below T_{SR_2} and all the way to the lowest measured temperatures, dρ/dT exhibits a linear temperature dependence extrapolating through the origin, which means a quadratic resistivity dependence, $\rho(\mathrm{T}) = \rho_0 + \mathrm{AT}^2$ with A=0.14 $\mu\Omega\mathrm{cm}K^{-2}$. We associate this behavior with spin wave electron scattering in the ferromagnetic FM2 phase, suggesting a quadratic spin wave dispersion relation, $w \propto k^2$ [41].

Remarkably, at T_{SR_1} and above ρ(T) increases almost linearly with temperature but does not extrapolate through the origin, i.e. $\rho(\mathrm{T})=B\mathrm{T}+\mathrm{C}$ with $B \simeq 5.73\mu\Omega\mathrm{cmK}^{-1}$ and C=70 $\mu\Omega$cm. This linear behavior is the same both in decreasing and increasing temperatures, being intrinsic of the FM1 phase just above T_{SR_1}. The finite intercept (at the origin) of the linear ρ(T) part above T_{SR_1}, indicates an extra constant resistivity in the FM1 phase, besides the residual resistivity ρ_0. This suggests some temperature-independent spin-disorder within the FM1 phase (orthorhombic I), in a scale of the order or below the electron mean free path. With regard to the linear term one could think on the usual electron-phonon contribution to ρ. Such term is clearly seen in the PM phase (monoclinic) above T_S~100K, but its slope ($0.88\mu\Omega\mathrm{cmK}^{-1}$;

see inset of Fig.1a) is much smaller that the B coefficient in ρ(T) just above T_{SR_1}, unless the orthorhombic-I structure (T<T_S) exhibits an extremely high electron-phonon resistivity. It is thus unlikely that phonon resistivity dominates ρ(T) near T_{SR_1}. One recalls that, according to the available neutron diffraction data [12], below T_{SR_1} the magnetic moments are essentially aligned along the ac bisecting direction, whereas above T_{SR_1} they are oriented along the a-axis. Therefore, another possible explanation could be a significant change in the spin wave spectrum, in such a way as to give a resistivity linear contribution, ρ=BT in the FM1 phase.

5.2.2 Thermoelectric power

The behavior of the thermoelectric power at low temperatures also confirms the two critical temperatures associated with the reorientation processes in $Tb_5(Si_{0.5}Ge_{0.5})_4$. This is clearly seen in Fig.5.4a, which displays the S(T) data from 10 to 70 K.

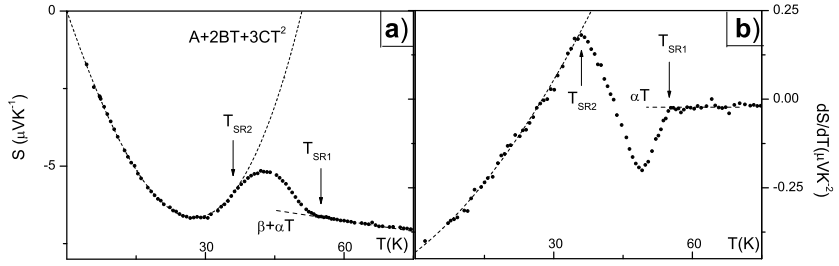

Figure 5.4: (a) The temperature dependence of the thermoelectrical power (S) of $Tb_5(Si_{0.5}Ge_{0.5})_4$ between 75 K to 10 K (b) The temperature derivative of the thermoelectrical power (dS/dT).

Above $\sim$ 57 K the thermopower exhibits a linear temperature dependence, S(T)=β+αT with $\beta \simeq$ -5.73 μVK^{-1} and $\alpha \simeq$ -0.017 μVK^{-2}, leading to a strictly constant dS/dT behavior (Fig. 5.4b)

Upon cooling, the S(T) behavior changes at T_{SR_1}=57K (Fig. 2a), corresponding to the onset of the spin reorientation process, similarly to what was observed in dρ/dT. At T_{SR_2}=40K one observes an inflexion point in S(T), marking the end of the spin reorientation process. From T_{SR_1} to T_{SR_2}, a

non-monotonic behavior is observed in dS/dT (Fig. 2b), suggesting competing effects in the reorientation process: dS/dT first decreases below T_{SR_1}, reaches a minimum at T$\sim$44K and then rises as T approaches T_{SR_2}. When we compare the dS/dT and the dρ/dT curves (Figs 5.4b and 1b), the latter one appears much more irregular between T_{SR_1} and T_{SR_2}. This could be due to the dominant dependence of the electrical resistivity on the electron scattering processes, which are very sensitive to short-range order effects. Therefore, ρ is essentially linked with the averaged electron collision time over the Fermi surface. In contrast, S(T) depends strongly on the energy derivatives and density of states of the conduction electrons near the Fermi surface (besides electron scattering) i.e. on the electron band features.

At temperatures below T_{SR_2} the S(T) data is well described by a polynomial fit $S(T) = AT + BT^2 + CT^3$ with A= -0.432 μVK^{-2}, B= 0.005 μVK^{-3} and C= 6.83 $\times$ 10^{-5} μ VK^{-4}. This behavior is more neatly confirmed in the dS/dT curve (Fig.5.4b), described by a quadratic polynomial below T_{SR_2}.

The quadratic term (B), usually characteristic of electron-spin wave scattering [42, 41], again suggests the dominance of such excitations below T_{SR_2}. The cubic term coefficient (C), which begins to be important at temperatures around $\sim T_{SR_2}$, is likely associated with the phonon drag contribution, which at temperatures T$\ll\Theta_D$ should be proportional to $(T/\Theta_D)^3$ [43]. At low temperatures ($<$10K) the S(T) dependence is practically linear indicating the dominance of impurity scattering [43].

5.2.3 Magnetization and neutron diffraction

The temperature dependence of the magnetization M(T) and its derivative dM/dT obtained field-cooled (FC) regimes for an applied magnetic field of 10 Oe, are displayed in Figs 5.5 a) and 5.5 b) respectively. The dM/dT curves were obtained from numerical differentiation of high resolution M(T) data (0.5 K steps). The spin reorientation process is well observable in the M(T) curve with a decrease of magnitude between 67K and 40K also confirmed by dM/dT curve. The important anomaly observed at T^*= 67 K, where dM/dT exhibits a well defined maximum, however such anomaly is not detected in our transport property measurements (Figs. 5.3 and 5.4). Besides the referred SQUID

magnetization data, we have also information on the basal plane component of the spontaneous magnetization as a function of temperature, from neutron diffraction data [12]. This data (inset of Fig.5.5a) shows that the reorientation transition actually starts at T^*= 67 K, apparently persisting down to $T_{SR_2} \simeq$ 40K.

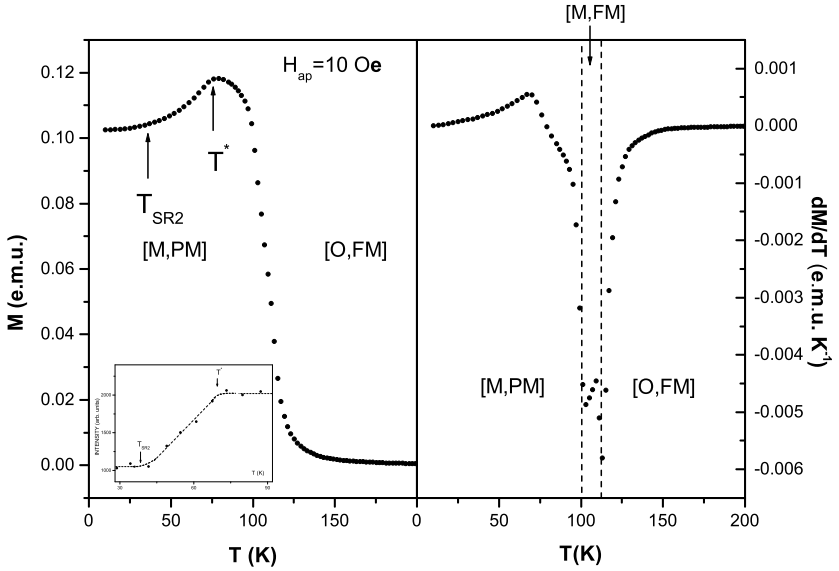

Figure 5.5: a) M(T) in $Tb_5(Si_{0.5}Ge_{0.5})_4$ as a function of the temperature, both in the zero-field-cooled (ZFC) and field-cooled (FC) regimes. Inset: Temperature dependence of the neutron diffraction intensity of the purely magnetic (100)+(020) reflection, obtained in the $Tb_5(Si_{0.5}Ge_{0.5})_4$ sample. b) dM/dT in $Tb_5(Si_{0.5}Ge_{0.5})_4$ as a function of the temperature

5.2.4 Magnetic anisotropy and spin reorientation processes

Considering only a dominant rotation of the Tb moments in the ac plane, from $\theta = 0°$ to $\theta = 45°$, and disregarding the small ϕ_i variations in the ab plane, we consider an approximate anisotropy magnetic energy (E_a) with the required symmetry:

$$E_a = K_1 sin^2(2\theta) + K_2 sin^4(2\theta) \tag{5.6}$$

Near T_{SR1} we assume that the first anisotropy coefficient has the usual form K_1 (T)$\simeq$ α $(T - T_{SR_1})+$ $\beta(T - T_{SR_1})^2$, with α and $\beta > 0$. K_2 is the 2nd-anisotropic constant and the positive α and β coefficients ensure θ=0 for T>T_{SR_1}. Minimizing the energy with respect to θ and considering the above approximation for K_1(T) over the whole reorientation range one obtains three possible spin structures: $\theta = 0$ for T>T_{SR_1}, θ=$\pi/4$ for T$\leq T_{SR_2}$ (see below) and $0<\theta<\pi/4$ between T_{SR_1} and T_{SR_2} (as follows):

$$\theta = \frac{1}{2} sin^{-1} \sqrt{-\frac{\alpha(T - T_{SR_1}) + \beta(T - T_{SR_1})^2}{2K_2}} \tag{5.7}$$

This shows that a spin-reorientation transition at T=T_{SR_1} requires $K_2 > 0$ and K_1<0, whereas the transition at T_{SR_2} requires $(\alpha(T_{SR_2} - T_{SR_1}) + \beta(T_{SR_2} - T_{SR_1})^2)/2K_2$=-1 , i.e. $K_1(T_{SR_2})$=-$2K_2(T_{SR_2})$.

One can also calculate the θ(T) dependence directly from the experimental ρ(T) values. For this one recalls that ρ should satisfy the condition $\rho(\theta)$=$\rho(\theta \pm \pi/4)$ implicit in eq.5.6 and a second-order development of ρ (in powers of cos(2θ)) is generally sufficient to account for the mean effect of the reorientation process [44]:

$$\rho(T) = \rho_0 + a(T) + b(T) cos^2(2\theta) \tag{5.8}$$

Here ρ_0 is the residual resistivity, $a(T)$=AT^2 is the low temperature resistivity (extrapolated into the reorientation range) and the anisotropy coefficient b(T) $\propto$ M_S^2(T) gives the magnitude of the spin re-orientation effects on the electrical resistivity. Assuming b$\simeq$constant in the small temperature range where the spin reorientation occurs, we can estimate b since at T_{SR_1} one has θ=0^0, so b= $\rho(T_{SR_1}) - a(T_{SR_1}) - \rho_0$. We can then extract, from $\rho(T)$, the θ(T) dependence between T_{SR_2} and T_{SR_1} [44]:

$$\theta(T) = \frac{1}{2} \cos^{-1} \sqrt{\frac{\rho(T) - a(T) - \rho_0}{\rho(T_{SR_1}) - a(T_{SR_1}) - \rho_0}} \tag{5.9}$$

Such θ(T) behavior is shown in Fig.5.6 (heavy points), together with the best fit to the anisotropy-model formula (eq.2; dotted line), obtained with $\alpha/2K_2 \sim 0.096$ K^{-1} and $\beta/2K_2 \sim 0.0023$ K^{-2}.

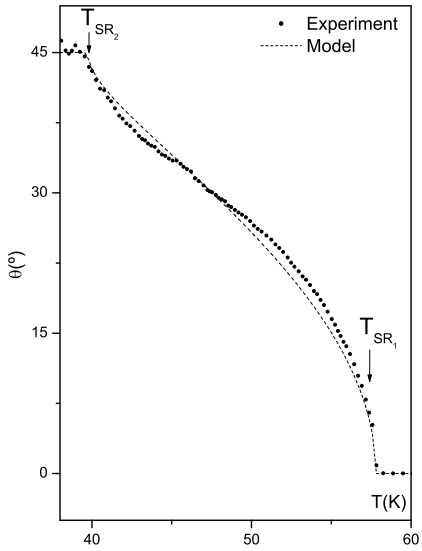

Figure 5.6: Temperature dependence of the angle θ taking of experimental results ρ(T) in $Tb_5(Si_{0.5}Ge_{0.5})_4$ compound (point) between 58 K to 38 K, the dotted line given the theoretical results accordingly to eq.5.7.

It is clear that the agreement is only qualitative, which may be due to the oversimplified model used. In fact we only considered a common θ-rotation in the ac plane, disregarding the θ_i differences among the Tb1, Tb2 and Tb3 ions, as well as the ϕ-rotations in the ab plane (that occur in Tb2 and Tb3 ions). We also assumed $K_1(T) = \alpha(T - T_{SR_1}) + \beta(T - T_{SR_1})^2$ between T_{SR_1} and T_{SR_2} and b=constant over such range.

It seems desirable to have refined neutron diffraction data covering in greater detail the temperature range between T_{SR_2} and T_{SR_1} in detail, to provide direct information on the corresponding θ(T) dependence, so as to compare with the approximate results obtained in the present work. In addition, such data may help in the (independent) discrimination between T_{SR_1}, T_{SR_2} and T^*.

This simple model gives a satisfactory phenomenological description of the main features of the reorientation process, but lacks in explaining the microscopic causes of this type of transition. It remains to understand the microscopic nature of such spin transitions and we will devote the next chapter to this issue. It is the main objective to of these work arising from the numerically the crystal

field interaction and understand the effect of this interaction in magnetic and thermodynamic properties.

Chapter 6

Numerical Results

In this chapter, we summarize several numerical investigations related with crystal field interaction and these effects on 4f systems. In the first part we study the influence of *strong* and *weak* crystal field interactions on the magnetic properties. We also study the temperature dependence of relevant thermodynamic properties namely magnetization, free energy and susceptibility, considering a mean field approximation for these two strengths of interactions. We study the magnetocrystalline anisotropy, determine the easy direction of magnetization and understand microscopically the influence of CF-interactions in spin reorientation transition process. An application of the crystal field interaction on a spin reorientation transition will be analyzed for the compound $Tb_5Si_2Ge_2$. In all the results here presented we considered the Tb^{+3} ion as the rare earth element (J=6).

6.1 Introduction

The simplest lattice symmetry for the crystal field interaction is the cubic symmetry that has been introduced in chapter 4. However, in a number of situations, the symmetry is not far from cubic and it is convenient to regard the crystal field as a combination of a large cubic term with smaller terms of lower symmetry [35]. In our study we are going to consider a cubic symmetry as a simple approach where $\vec{B}$ is parallel to c-axis and an external applied magnetic field ($\vec{H}$), in this case the hamiltonian can be expressed by:

$$\mathcal{H} = -J_0 J_z + W\left[x\frac{1}{F(4)}(O_4^0 + 5O_4^4) + (1-|x|)\frac{1}{F(6)}B_6^0(O_6^0 - 21O_6^4)\right] \quad (6.1)$$

where J_0, W and x are in principle unknown parameters.

In the next section we will study the influence of J_0, W and x on the magnetic and thermodynamic properties. For this study, it was created a computer program.

6.2 Computational Methods

The numerical code elaborated in this work was made using the MatLab 6.5 software. The choice of MatLab software was made essentially because of its simple programming language and because this program presents some important packages of numerical methods (diagonalization, differentiation, etc...) that are helpful in the study of the physical problem. In brief the program calculates the hamiltonian matrix using the quantum mechanic operators (J_+, J_- and J_Z) given by the following common definitions:

$$\begin{aligned} < JM_J|J_Z|JM'_J > &= M_J\delta_{M_J M'_J} \\ < JM_J|J^2|JM'_J > &= J(J+1)\delta_{M_J M'_J} \\ < JM_J|J_\pm|JM'_J > &= \sqrt{(J \mp M'_J)(J \pm M'_J + 1)}\delta_{M_J M'_{J\pm 1}} \end{aligned} \quad (6.2)$$

The crystal field hamiltonian was calculated using the Steven's operator methods (see table D.1 in D appendix). The eigenvalues and eigenvectors of the hamiltonian matrix were determined for a certain magnetic molecular field.

The eigenvalues allow the calculation of the magnetization at a certain temperature T and to calculate a better estimation for the molecular field, closing a self-consistent loop. The program stops when the magnetization converges to a given percentage (e.g. ΔM/M=0.1 %). Once the convergence is obtained, it is straightforward to calculate different thermodynamic functions (susceptibility, energy levels, occupation number and magnetization).

6.3 Numerical Results

6.3.1 Crystal Field Energies

The main frame of this work is study the influence of CF-interactions in rare-earth system. The first part of the calculation was the determination of the energy levels of the crystal field hamiltonian using the equation

$$\mathcal{H} = W\left[\frac{x}{F(4)}(O_4^0 + 5O_4^4) + \frac{(1-|x|)}{F(6)}B_6^0(O_6^0 - 21O_6^4)\right] \tag{6.3}$$

and the determination of the energy as a function of the x parameter. The results are given by Fig. 6.1, and are in agreement with the *Lea et al* work [35]. In Fig.6.1 we can see that the energy levels are very dependent of the x parameter.

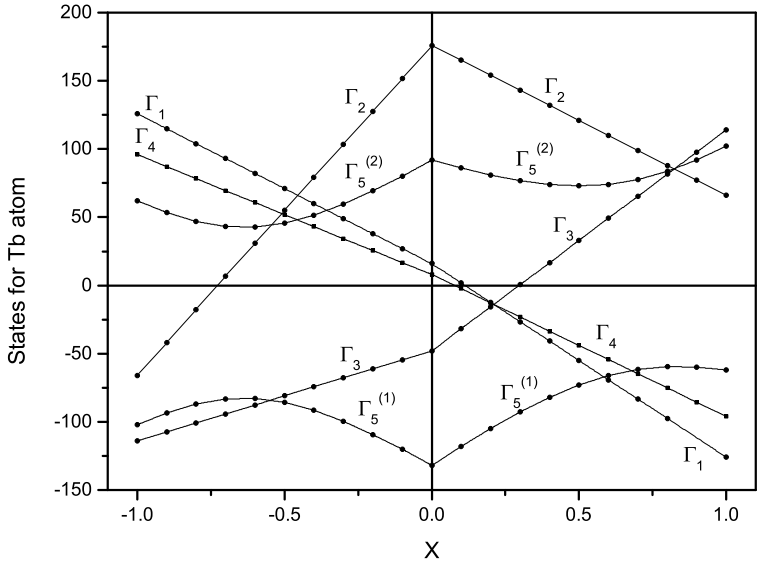

Figure 6.1: x dependence of crystal field states

The eigenvectors were also determined and the eigenvectors corresponding to Γ_1, Γ_2, Γ_3, Γ_4 eigenvalues are presented table 6.1. The eigenvector corresponding to Γ_5 varies with the x concentration. All results are in agreement with *Lea* et al work [35], which means that the developed program is performing the correct calculation for the crystal field hamiltonian. The results performed were

Table 6.1: Steven's Equivalent Operators

Γ_1 :	-0.6614|4>+0.3536|0>-0.6614|-4>
Γ_2 :	-0.3953|6>+0.5863|2>+0.5863|-2>-0.3953|-6>
Γ_3 :	0.5863|6>+0.3953|2>+0.3953|-2>+0.5863|-6> 0.2500|4>+0.9354|0>+0.25|-4>
Γ_4 :	$0.6846\|\pm 3> -0.4330\|\mp 1> +0.5863\|\mp 5>$ -0.7071|4>+0.7071|-4>

also compared with other previous works [23, 36, 37, 38] and the results fully in agreement with previous literature.

6.3.2 The Effect of Crystal Field Interaction on Magnetization

In the last chapter we presented the experimental data of transport and magnetic properties. However the transport properties are not easily accessed by numerical calculation due to the complexity of the transport theory models. Like was mentioned in chapter 4, the magnetization is the property that is more directly related with crystal field splitting and indirect exchange. To determine the temperature dependence of the magnetization is used the following relation:

$$M(T) = Ng\mu_B \frac{Tr\left(S_z e^{-\frac{\hat{H}_i}{kT}}\right)}{Tr\left(e^{-\frac{\hat{H}_i}{kT}}\right)} \tag{6.4}$$

However to obtain M(T) it is necessary to know the crystal field parameters solve the following hamiltonian finding corresponding the eigenvalues an the eigenvectors. It is helpful to study the effect of the crystal field and exchange parameters on magnetization. However, the crystal field parameters can only be determined experimentally for example by neutron diffraction. In present

case these parameters are unknown. Our first purpose will be to describe the influence of these parameters in the magnetic properties and thermodynamics functions.

$\frac{W}{J_0}$ and x dependence on magnetization

We divide the crystal field interactions in two types: *strong interactions* with $1<\frac{W}{J_0}<1/10$ and *weak interactions* with $\frac{W}{J_0} < 1/100$.

The parameter J_0 is directly related with the molecular field and an increase of J_0 causes an increase in T_C as well in the magnetic moment with a maximum value of 9 (g.J). This is well known for systems where it is only considered the exchange term.

It is interesting to study the effect of the coefficient $\frac{W}{J_0}$ in thermal magnetization for the two distinct regions of this parameters. This effect is represented in Fig. 6.2. For a weak CF-interaction (Fig.6.2 a) it can be observed that this effect does not affect a significantly T_C. At very low temperatures, an absolute increase in M originates an anomalous behavior,which is more evident when $\frac{W}{J_0}$ < 0 because the magnetic momentum decreases.

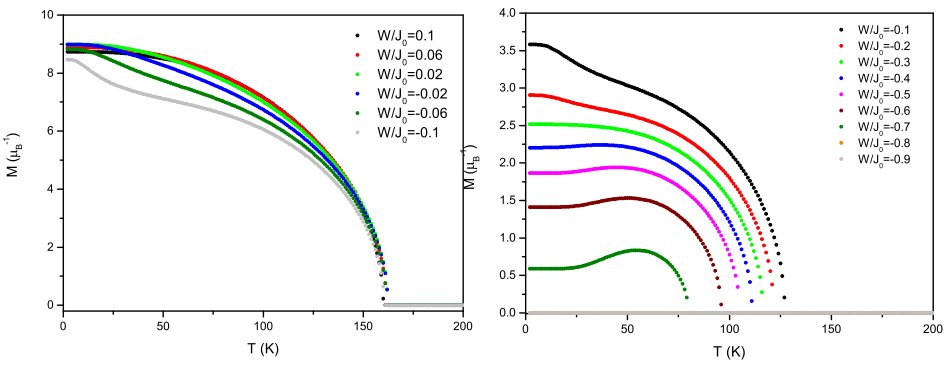

Figure 6.2: a)Temperature dependence of magnetization for a weak CF-interaction with variation of $\frac{W}{J_0}$ parameter (left). b) Temperature dependence of magnetization for a strong CF-interaction with variation of $\frac{W}{J_0}$ parameter (right).

For the strong crystal field interactions, we can observe that a variation of the crystal field parameter gives a large variation on the M(T) curve at low

temperatures and also a significant variation of T_C. The variation of the critical temperature with the free parameter $\frac{W}{J_O}$ is represented in Fig. 6.3

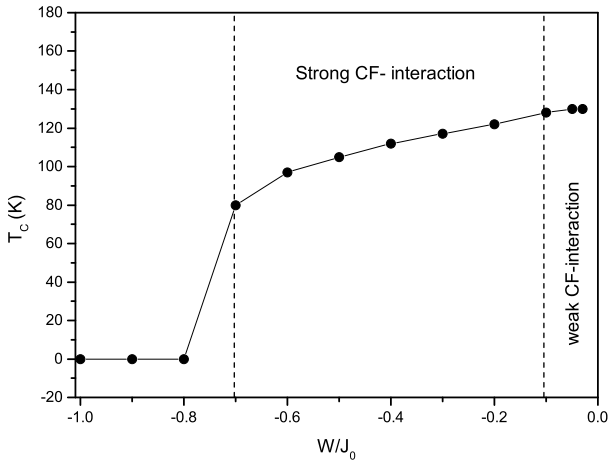

Figure 6.3: Variation of the critical temperature with $\frac{W}{J_0}$ parameter.

For $\frac{W}{J_0}$<-0.8 the system is always in the paramagnetic state (T_C=0). In range -0.8<$\frac{W}{J_0}$<-0.1, the critical temperature increases with $\frac{W}{J_0}$. This increase slows down in weak interaction regime.

Another important parameter is the x value that is related with the relative amplitude between 4^{th} and 6^{th} elements of the Steven's Operators.

Observing the Fig.6.4 it is clear that for negative values of x (the most common case), a large change in the M(T) curve is observed as well as a variation of the critical temperature.

In conclusion we see that M(T) dependents largely with $\frac{W}{J_0}$ and x parameters causing a deviation of the "normal" behavior (the Brillouin function). With the eigenvalues and eigenvectors obtained with our programm we can study other important physical properties presented in next section.

6.3.3 Statistical and Thermodynamical Functions

Statistical state

In this subsection we study some statistical and thermodynamics functions, namely the temperature dependence of the occupation number and the energy

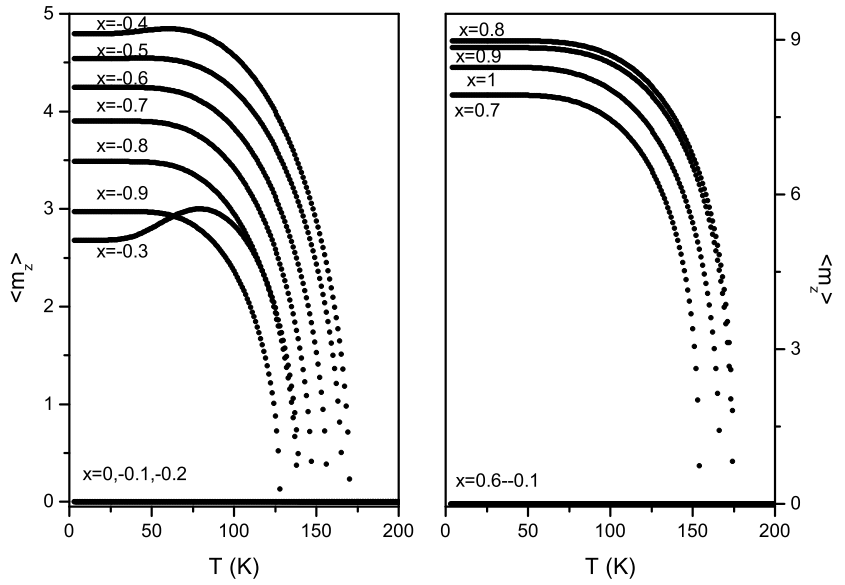

Figure 6.4: a) Temperature dependence of magnetization for a weak CF-interaction with variation of x parameter (left). b) Temperature dependence of magnetization for a strong CF-interaction with variation of x parameter (right).

splitting, in order to understand the mechanisms implicit in a strong and weak crystal field interaction. For these two interactions we have selected the parameter x=0.5 $\frac{W}{J_0}$=-0.5 μ_B^2 and W/J_0=-0.05 μ_B^2 for strong and weak CF-interaction respectively.

In Fig.6.5 a) the temperature dependence of the energy levels splitting is represented. Below T_C, the levels split giving 2J+1 levels (13) due to the magnetic contribution. It is clear that the crystal field interaction does not contribute significatively to the splitting of the energy levels which means that only for low temperatures the crystal field becomes important.

For a strong CF-interaction, presented in Fig. 6.5 b), above T_C, there are six energy levels populated, which appear because of the CF-interactions, although the total magnetization is zero. Below T_C, the magnetic hamiltonian (J_Z) splits the degenerated levels causes an increase of M(T). Also in Fig. 6.5 b), when we show the effect of a strong CF-interaction, it is clear that strong CF-interaction causes a large splitting of the energy levels above and below T_C. The most important levels below T_C have a splitting from the ground state to the first

excitated state of ΔE$\sim$ 25.06 meV, demonstrating that the ground state is the most important one. On the other hand, in a weak CF-interaction we observe that ΔE is only of $\sim$ 3.00 meV and is essentially due to the magnetic interaction (J_z).

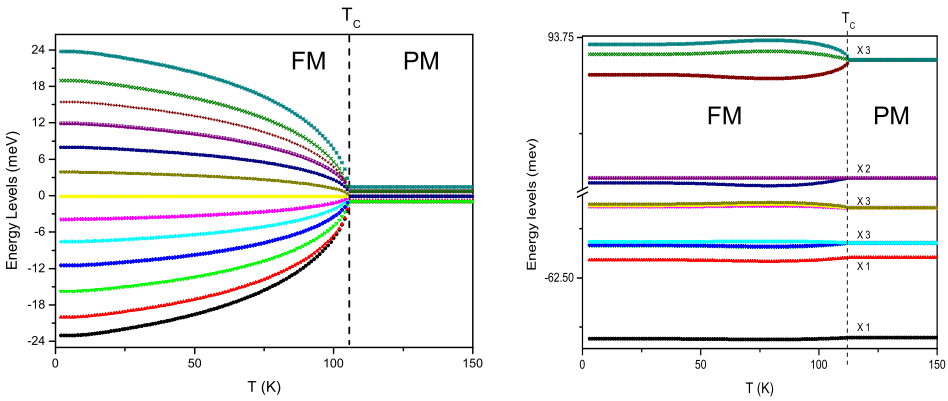

Figure 6.5: a) Temperature dependence of energy states for a weak CF-interaction (left). b)Temperature dependence of energy states for strong CF-interaction (right)

Another important statistical property is the occupation number (probability) which gives the states occupied on each level, having an important role in the physical properties. Statistically the probability of a certain level E_i being occupied is given by:

$$P(E_i) = \frac{e^{-\frac{E_i}{kT}}}{Tr\left(e^{-\frac{E_i}{kT}}\right)} \tag{6.5}$$

In Fig. 6.6 we represent $P(E_i)$ in the two limiting cases. In a weak CF-interaction (see Fig. 6.6a)) where we observed that all states are occupied and that only at very low temperatures a strong decrease on the population of the excited states occur. However in a strong CF-interactions, (see Fig. 6.6 b) we can see that, at very low temperatures, only one state is occupied (the ground energy state). With an increase of temperature, an increase of the number of occupation of the first excited state is observed, making an alteration in the linear combination of the quantum states. This new linear combination is the same as an alteration of the magnetization direction. However, the splitting

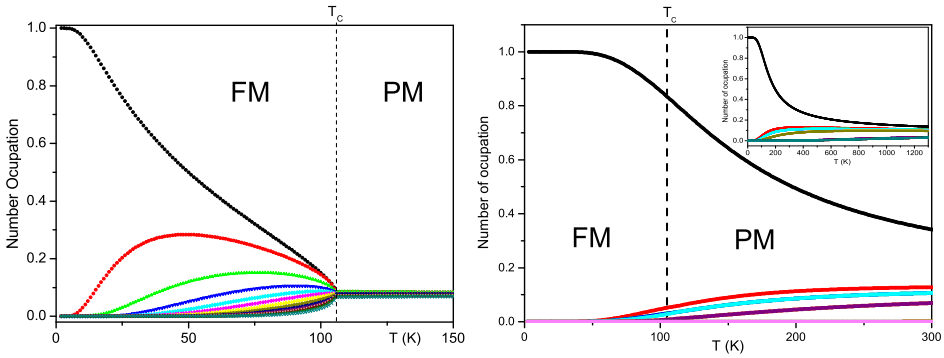

Figure 6.6: a)(left) Temperature dependence of number of occupation for a weak CF-interaction. b) (right) Temperature dependence of number of occupation for strong CF-interaction

of states is very high corresponding to an intense crystal field interaction (uncommon in 4f ions) because, observing the inset of Fig. 6.6b), for T $\sim$ 1300 K the states are not equally occupied contrasting with the T $\sim$ 110 K on a weak crystal field (more common in 4f ions).

Thermodynamic functions: susceptibility

The thermodynamic functions are also important to understand the microscopic process due to crystal field interactions. One of them is the magnetic susceptibility (χ), that is defined as the response of a material when a magnetic field is applied (eq. 4.2). The method of determination of the magnetic susceptibility is to consider two small applied magnetic fields (H=1 Oe and H=4 Oe), to make the difference between the magnetization and divide it by the variation of the applied magnetic field. It is interesting to plot the inverse of susceptibility with temperature for CF-interactions, whose results are represented in the Fig. 6.7.

Observing Fig. 6.7 it can be seen that at high temperatures, χ^{-1} varies linearly with temperature, i.e. it follows the Curie-Weiss law for both interaction (eq.3.50). For both cases the linear contribution gives a 9.72 μ_B that are in good agreement to what we expected. Also we can determined the Curie temperature and the results were θ_p = 145.7 K and 110 K in the case of strong and weak CF-interaction respectively. Near T_C, the weak CF-interaction follows the χ^{-1}

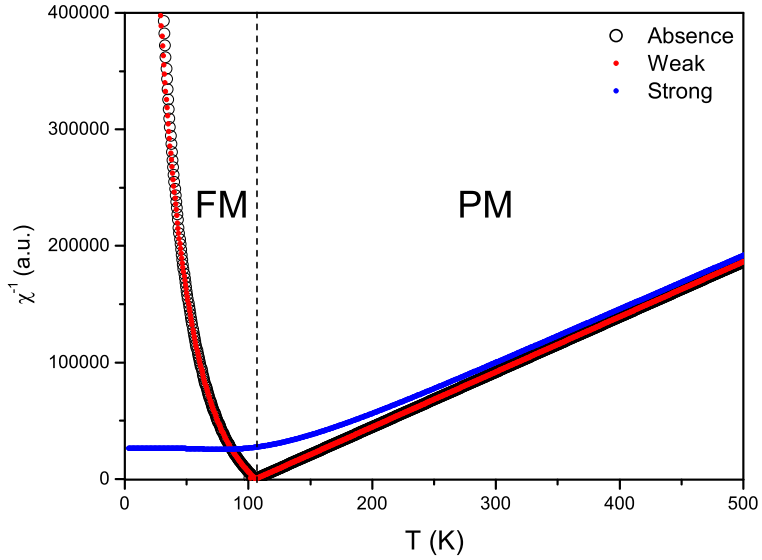

Figure 6.7: Temperature dependence of χ^{-1} in the absence of CF-interaction (black line), with a weak interaction (line red) and in a strong CF-interaction (line blue).

in the absence of CF-interaction. In the case of strong interaction we observe a deviation of this linear regime (blue line) which is in disagreement with the Curie Weiss law because the crystal field splitting is very high. This means that the CF-interactions causes a decrease of critical temperature when we have a strong crystal field interaction. Below T_C the weak interaction behavior is almost the same as without the *CF*-interaction. For a strong *CF*-interaction at low temperatures we observe a much smaller slope in the inverse of susceptibility than in the cases of weak or in the absence of CF-interaction.

6.3.4 Anisotropy studies

Until now we presented the effect of CF-interaction, but these results are only applied to isotropic systems or considering only the magnetic contribution parallel to z-axis. In general the real systems are not isotropic being called anisotropic systems. These anisotropies are directly related with the surroundings atoms and the CF-interaction is one of the causes. The magnetic anisotropy systems have a preferential direction called the easy-axis corresponding to the direction

where the magnetic moment is maximum. However, in some of these systems, the easy-axis change its direction with temperature, and this process is called the **spin reorientation transition**. In other cases this anisotropy is unchangeable with temperature maintaining the same direction. To study this anisotropy we use the theory described in section 4.3.4.

Weak CF-interaction

To study the anisotropy it is better to study the free energy of a system and the condition that minimizes the free energy which gives the direction of the easy-axis. Using the crystal field parameters for a weak interaction B_4^0∼1E-5 meV and $B_6^0 \sim$ 1E-6 meV, making a variation for ϕ=[0°,90°] and θ=[0°,90°] and using the eq. 5.29, we obtain the free energy results for temperatures of 2K, 15K, 30K and 65K.

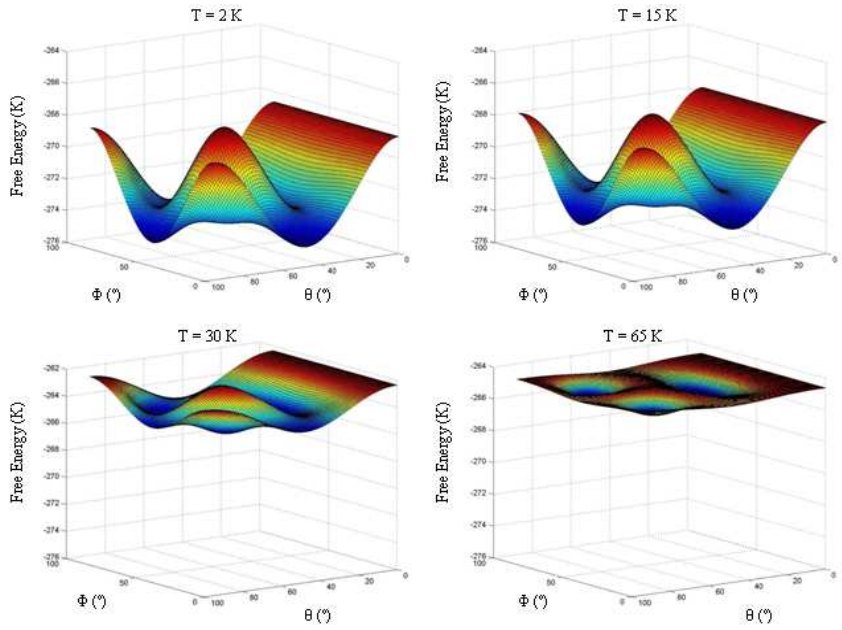

Figure 6.8: a)Free energy for a anisotropic system considering a weak CF-interaction for T=2K (up left), b) T=15K (up right), c) T=30K (down left) and d) for T=65K (down right)

We clearly observe in Fig. 6.8 a) that the free energy has three minimums at low temperature corresponding to (90°,45°), (45°,0°) and (45°,90°) for θ

and ϕ respectively. These three directions are the same by symmetry and correspond to possible directions of the easy-axis. This figure can be compared with Fig.4.5 obtained within by the phenomenological theory (see chapter 4) concluding that both have the same behavior and the same minimums. These means that the microscopical theory (CF-interaction) is in agreement with phenomenological theory for a cubic symmetry. With an increase of temperature these minimums decrease (see Fig. 6.8 b) and c)) and at approximately 65K they almost disappear (see Fig. 6.8) and "any" direction can be the easy direction.

The weak CF-effects only predict the easy-directions where their contribution to free energy anisotropy becomes more important (always at low temperature). So the easy direction for high temperature has to be due other interactions, for example, dipolar interactions very characteristic in case of Gd ion. The above process described can be responsible for rotation of magnetic momentum being called spin reorientation transition.

Strong CF-interactions

A similar study was performed considering strong CF-interactions and the results for the angular dependence of free energy are represented in Fig. 6.9.

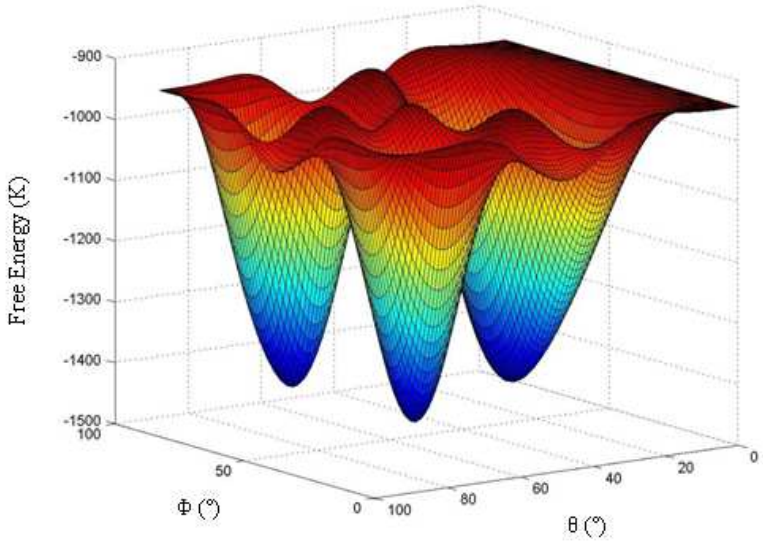

Figure 6.9: a)Free energy for a anisotropic system considering a strong CF-interaction for T=2K.

Analyzing Fig. 6.9 we can see that the free energy surface presents three minimums corresponding to 45° and 28°, 22° and 72°, 69° and 22° for ϕ and θ respectively. These minimums are not common in a cubic symmetry except if we consider higher terms in the phenomenological free energy equation as we presented in eq. 5.32. These minimums present a significant variation of free energy (ΔF$\sim$500K) relatively to F$\sim$-950K and do not disappear when increasing the temperature like in the case of a weak CF-interaction. So in this case the easy-direction remains the same and is invariant with temperature, this means that for strong CF-interaction a spin reorientation is not expected due to a very marked deep of minimums of free energy.

Until now we have studied the CF-interaction in general for a cubic system. However this study can be applied for any symmetry being only needed the CF-parameters. In the next section we will demonstrate an application of spin reorientation process in $Tb_5Si_2Ge_2$ and try to understand these transition within a crystal field theory.

6.4 An application of CF-interaction in $Tb_5Si_2Ge_2$

As we have presented in chapter 2 the compound $Tb_5Si_2Ge_2$ has a spin reorientation transition at low temperatures. We have seen that this compound has three types of Tb sites (one 4c and two in 8d symmetry). The Tb in 4c symmetry has six neighbors forming almost a regular octahedron symmetry. The other sites do not have a regular symmetry, presenting a complex one. This transition can be essentially described as a rotation on ac-plane from 0° (at high temperatures) to 45° with respect to a-axis. In this section will only studied the Tb atom in 4c-symmetry because it is expected that the process is "identical" in other sites. In a 4c-symmetry the number crystal field parameters (B_n^m's) on the hamiltonian are 9 parameters. However for this system, the crystal field parameters are still unknown which makes more complex the task of describing the CF-interaction. As we have seen along of this chapter a variation on CF-parameters gives distinct and diversifies behavior on physics properties. But as we refereed in chapter 3 we can calculated in a first approximation we can simplify the study of these application considering a cubic system and the other

terms in hamiltonian can be consider as secondary terms less important.

6.4.1 Point Charge Model

The principal unknown variables for a cubic system are the B_4^0 and B_6^0 parameters. Theoretically, there are only one possibility to try to obtain the CF-parameters called the point charge model, described in chapter 4. Using equation 4.15 and table 4.1 we obtain the values of B_4^0= -1.17E-5 meV and B_6^0=3.49E-5 meV, B_4^0= 5.86E-6 meV and B_6^0=-1.74E-5 meV and B_4^0= 1.32E-5 meV and B_6^0=-1.472E-5 meV for cubic, tetrahedric and octahedric symmetries respectively using an average distance of d=3.2 . The effective charge is considered the charge of Si or Ge atoms (-4 e). With these coefficients was calculated the temperature dependence of magnetization and the corresponding results are presented in Fig. 6.10. The only free parameter is J_0 which corresponds to the critical temperature T_C with a value equal to the one obtained experimentally, that is $\sim$ 105 K. The values obtained for J_0 are 0.87 meV, 0.75 meV and 0.72 meV for cubic, tetrahedric and octahedric symmetry respectively. Comparing results obtain with experimental results M(T) curve (see Fig.5.5), the behavior are different concluding that the point charge model does not explain these results for $Tb_5Si_2Ge_2$ compound.

These results are not surprising because according to ref. [31] the point charge model in almost all cases does not give a correct information of coefficients, inclusively the signal can be wrong. Also the approximation model for a cubic symmetry and the average distance used can cause some differences between a real system and the simple model here presented.

6.4.2 Complementar studies

In the present chapter we concluded that only the weak CF-interaction explained the spin reorientation transition premising a change in the easy-axis direction. For the easy-axis direction have to be in the $\phi\sim45^o$ and $\theta\sim0^o$ at low temperature we obtain the following parameters $B_4^0 \sim$ 3.2736E-5 meV and $B_6^0 \sim$ 9.6706E-7 meV. For these parameters we can determine the anisotropic magnetization. The results are only made for the plane ac for ϕ=0^o and 45^o because it is in this plane that our system occurs.

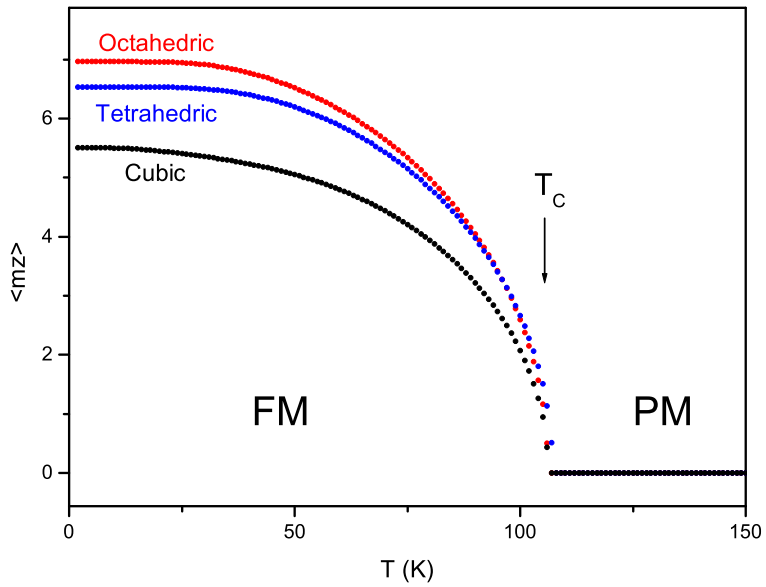

Figure 6.10: Temperature dependence of magnetization using point charge model parameters for a cubic, tetrahedron and octahedron symmetry.

Observing the Fig.6.11 we can see the anisotropy is very small almost negligible and this result is in disagreement with the experimental results (see Fig.6.12), only for very low temperatures there is a difference between two direction. The next step was to determine the unknown variables that fit the experimental results. After making some attempts to discover the best parameters, finally we obtained the ones that fit our experimental results which are J_0=1.22 meV, W=-0.97 meV and x=0.37 corresponding to a strong CF-interactions. The comparison of the M(T) curves are represented in Fig. 6.12.

We refereed above that in these cases the minimums of free energy are very well defined and unchangeable with temperature variation not predicting a spin reorientation transition. However by Fig.6.12 we observed that below $T_C \sim$ 70K, a decrease of magnetization occurs.

A complementary study of the anisotropy magnetization was performed and we could see that for this case a large anisotropy occurred. With these results from the magnetization variation can be interpreted as a variation of the magnetic moment because in some direction there is a decrease and in the other direction there is an increase contrasting with free energy where predict only

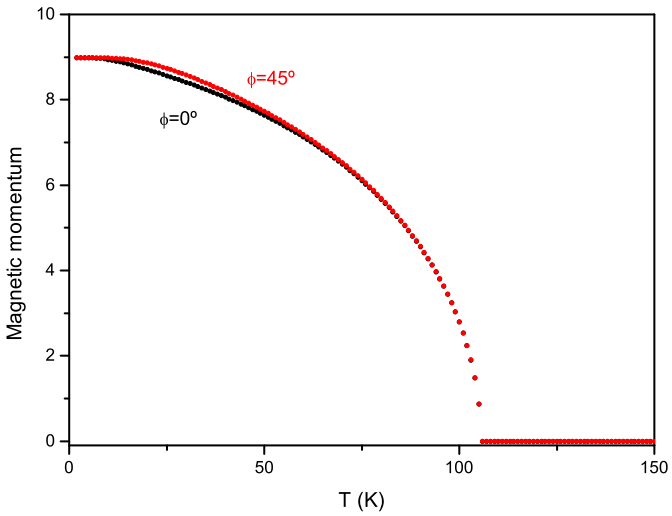

Figure 6.11: Temperature dependence of magnetization in ac plane with ϕ=0° and ϕ=45°.

one unchangeable direction.

This process can not be seen as a classic model of a momentum change because is purely quantic (change of eigenstates).

In summary, we observed that the crystal field interaction explain the spin reorientation transition. Comparing the numerical results with experimental data we obtain the best fit if we consider a strong crystal field interaction. However the compound studied here is polycrystalline and this condition was not taken in account. Also a very simplified model was made and this can change the magnitude of the CF-interaction. The ideal is to obtain the crystal field parameters experimentally and afterwards substitute these values in this programme and predicting the M(T) curves to understand the CF-interaction in $Tb_5Si_2Ge_2$ compound.

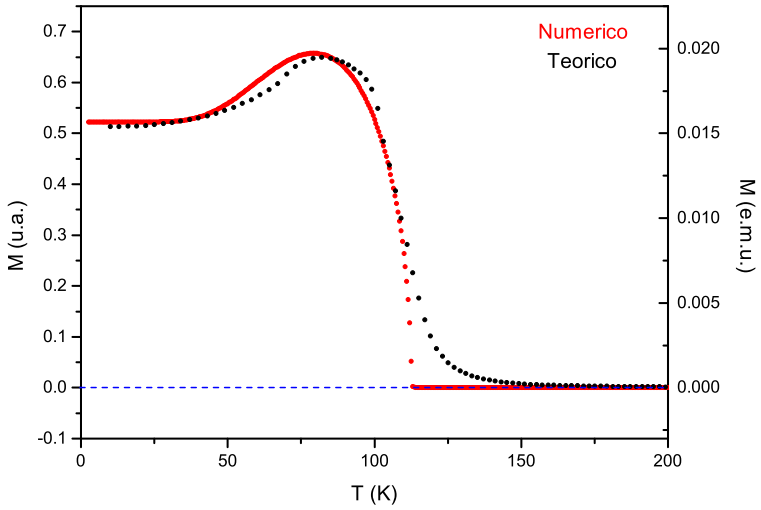

Figure 6.12: Temperature dependence of M(T) in a strong CF-interaction (red line) comparing with experimental data.

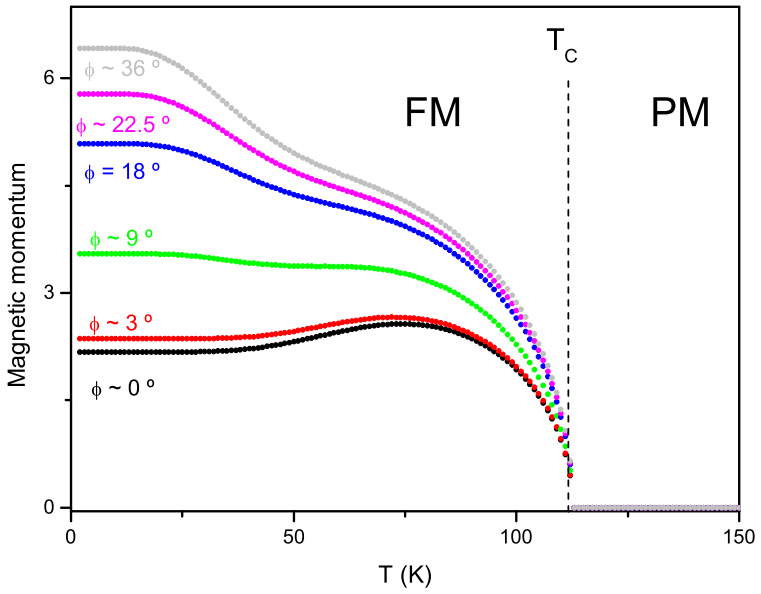

Figure 6.13: Temperature and angle dependence (ϕ) of magnetic anisotropy.

Chapter 7

Conclusions

This Thesis presents a study of several fundamental physical properties on Giant magnetocaloric compound $Tb_5Si_2Ge_2$ combining numerical and physical property measurements.

In the $Tb_5Si_2Ge_2$ compound the spontaneous magnetization in rare-earths is a consequence of the exchange interaction due to localized $4f$ electrons via conduction electrons and the magnetic anisotropy arises from the crystal field effects. We modeled the effect of crystal field arising at a given site by means of a single-ion crystal-field Hamiltonian. We observed that in a number of physical situations in which symmetry is not far from cubic, it is sufficient to regard the crystal field as a combination of a large cubic term with smaller terms of lower symmetry. The strength of the exchange interactions could be estimated by a mean-field approximation. We developed a computer programm which, once fixed the crystal field parameters and use a self-consistent method to calculate the temperature dependence of magnetization and other relevant physics properties.

This work also shows that the magnetic properties depend strongly of crystal field parameters. Two regimes of crystal field interactions (strong and weak interaction) are presented and we concluded that weak crystal field parameters gives small contribution to magnetic properties. Strong CF-interaction, on the other hand contributes strongly to the anomalous behaviors of magnetization. We studied the free energy and showed numerically that the strength of the

crystal field interaction plays an important role on determining of the easy direction of magnetization as also as in the magnitude of the minimum of free energy (ΔF).

Our transport (ρ, dρ/dT, S, dS/dT) and magnetic property measurements (M, dM/dT) in $Tb_5Si_2Ge_2$ reveal the existence of a complex spin reorientation process within the FM phase at low temperatures. According to our magnetic data and previous neutron diffraction work [12], the spin reorientation process clearly starts at T^*=67K and ends at T_{SR2}=40K. However, due to the different site-anisotropies (Tb1, Tb2, Tb3), corresponding spin reorientation transitions may occur at slightly different temperatures involving different numbers of Tb ions. In particular, the transport properties are virtually insensitive to the spin reorientations, occurring between T^*=67K and T_{SR1}=57K. They are however very sensitive to the reorientation processes between T_{SR1}=57K and T_{SR2}=40K.

A simple phenomenological treatment, based on an approximate model of the magnetic structure of $Tb_5Si_2Ge_2$ at low temperatures, gives a satisfactory description of the main features of the reorientation process and corresponding effect on the electrical resistivity, between T_{SR1} and T_{SR2}.

Applying the developed computer to this specific system we showed that the weak CF-interactions predicted a change of the easy direction as a function of temperature. At low temperatures the easy direction with θ=90^o and ϕ=45^o was obtained for B_4^0=1E-5 meV and B_6^0=1E-6 meV, in agreement with a phenomenological model also developed in this work. At higher temperatures, the free energy becomes isotropic implying other physical processes are responsible for the new easy direction of magnetization found experimentally.

In the case of a strong CF-interaction, the free energy showed a clear minimum at ϕ=45^o and θ=28^o directions corresponding to the easy direction (the other minimums are obtained by symmetry). The free energy is strongly anisotropic which is reflected in the magnetization along different directions. and important changes in magnetization were observed.

Without any crystal field parameters obtained experimentally (by for example inelastic neutron scattering) the task of fitting the magnetization at different temperatures becomes very complex of finding the scanned parameters phase spaces in order to understand the M(T) behavior obtained experimentally. We

found B_4^0=6.1E-3 meV and B_6^0=-7.955E-5 meV parameters for the best fit of data. These parameters showed that only a strong CF-interaction could explain the experimental data. However this interaction does not predict a change in the easy direction according to the free energy but only changes on magnitude of magnetic momentum of the ion.

In summary, we think that main objective of this work that consisted in developed the numerical methods to study the influence of the crystal field interaction was attained. We are now considering to perform in mean future inelastic neutron scattering to obtain the CF-parameters.

Also important is for instance a magnetic study in a single crystals to fit our results and understand the real magnitude of crystal field parameters. Also a statistical approach for polycrystal systems can be important to explain ours experimental results.

Finally and probably the most promising is study a new family of compounds $PrNi_{5-x}Cu_x$ and $PrNi_{5-y}Co_y$ that presents a simple structure (cubic symmetry) and understand the influence of crystal field interactions in this compounds in particular the anomalous magneto caloric effect that they present.

Bibliography

[1] V. K. Pecharsky and K. A. Gschneidner Jr., "Some common misconceptions concerning refrigerant materials", *J. Appl. Phys.*, vol. 90, pp. 4614–4622, 2001.

[2] V. K. Pecharsky and K. A. Gschneidner Jr., "Magnetocaloric effect and magnetic refrigeration", *J. Magn. Magn. Mat.*, vol. 200, pp. 44–56, 1999.

[3] V. K. Pecharsky and K. A. Gschneidner Jr., "Tunable magnetic regenerator alloys with a giant magnetocalloric effect for magnetic refrigeration from $\sim$ 20 to $\sim$ 290 k", *Appl. Phys. Lett.*, vol. 70, pp. 3299–3301, 1997.

[4] V. K. Pecharsky and K. A. Gschneidner Jr., "Giant magnetocaloric effect in $Gd_5Si_2Ge_2$", *Phys. Rev. Lett.*, vol. 78, pp. 4494–4497, 1997.

[5] W. Choe J. Meyers, S. Chumbley and G. J. Miller, "Microstructural analysis of twinned $mathrm\beta - gd_5si_2ge_2$", *Phys. Rev. B*, vol. 66, pp. 012106, 2002.

[6] K. A. Gschneidner Jr. and V. K. Pecharsky, "Magnetic refrigeration materials", *J. Appl. Phys*, vol. 85, pp. 5365–5368, 1999.

[7] C. Magen L. Morellon, P. A. Algarabel and M. R. Ibarra, "Giant magnetoresistance in the ge-rich magnetocaloric compound, $Gd_5(Si_{0.1}Ge_{0.9})_4$", *J. Magn. Magn. Mat.*, vol. 237, pp. 119–123, 2001.

[8] X. Batlle F. Casanova and A. Labarta, "Entropy change and magnetocaloric effect in $Gd_5(Si_xGe_{1-x})_4$", *Phys. Rev. B*, vol. 66, pp. 100401, 2002.

[9] V. Provenzano et al, "Reduction of hysteresis in the magnetic refrigeration $Gd_5Si_2Ge_2$ by addition of iron", *Nature*, vol. 429, pp. 853–857, 2004.

[10] F.C.Correia J.M.Teixeira J.P.Araujo R.P.Pinto M.E.Braga L. Morellon P.A.Algarabel C.Magen J.B.Sousa, A.M.Pereira and M.R.Ibarra, "Multi-step and anomalous reproducible behavior of the electrical resistivity near the first-order magnetostructural transition of $Gd_5(Si_{0.1}Ge_{0.9})_4$", *J. Phys: Condens. Matter*, vol. 17, pp. 2461, 2005.

[11] C. Magen C. Ritter O. Proklnenko Y. Skorokhod P. A. Algarabel M.R. Ibarra L. Morellon, Z. Arnold and J. Kamarad, "Pressure enhancement of giant magnetocaloric effect in $tb_5si_2ge_2$", *Phys. Rev. Lett.*, vol. 93, pp. 137201, 2004.

[12] K. A. Gschneidner Jr. M. Levin and V. K. Pecharsky, "Magnetic correlations induced by magnetic field and temperature in Gd_5Ge_4", *Phys. Rev. B*, vol. 65, pp. 214427, 2002.

[13] P.A. ALgarabel C. Magen C. Ritter, L. Morellon and M.R. Ibarra, "Magnetic and structural phase diagram of $Tb_5(Si_xGe_{1-x})_4$, journal=Phys. Rev. B, volume=65, year=2002, pages=094405,".

[14] L. Morellon M.R. Ibarra C. Ritter J.P.Araujo C. Magen, P. A. Algarabel and J.B. Sousa, "Pressure enhancement of giant magnetocaloric effect in $Tb_5Si_2Ge_2$", *submitted to Phys. Rev. B*, vol. 0, pp. 0, 0.

[15] J.M. Teixeira R. P. Pinto M. E.Braga F. C. Correia J. B. Sousa L. Morellon P. A. Algarabel C. Magen J.P.Araujo, A.M.Pereira and M.R.Ibarra, "Transport and magnetic study of the spin-reorientation transition in $Tb_5(Si_{0.5}Ge_{0.5})_4$ magnetocaloric compound", *submited to J. Phys: Condens. Matter.*

[16] C. Magen P.A. Algarabel L. Morellon, C. Ritter and M.R.Ibarra, "Magnetic-martensitic transition of $tb_5si_2ge_2$ studied with neutron powder diffraction", *Phys. Rev. B*, vol. 68, pp. 024417, 2003.

[17] D. Viterbo F. Scordari G. Gilli G. Zanotti M.Catti Giacovazo, H.L Monaco, *Fundamentals of Crystallography*, Oxford Science publications, Oxford, 1995.

[18] V. P. Antropov A. O. Pecharsky V. K. Pecharsky, G. D. Samolyuk and K. A. Gschneidner Jr., "The effect of varying the crystal structure on magnetism, electronic strucure and thermodynamics in the $Gd_5(Si_xGe_{1-x})_4$ system near x$\sim$ 0.5", *J. Solid State Chem.*, vol. 171, pp. 57–68, 2003.

[19] M. Levin, "Spontaneous generation of voltage in $Gd_5Si_xGe_{4-x}$ during a first-order phase transition induced by temperature or magnetic field", *Phys. Rev. B*, vol. 63, pp. 174110, 2001.

[20] Shriver and Akins, *Inorganig Chemestry*, Oxford University Press, Oxford, 1999.

[21] K. A. Gschneidner Jr. M. Levin and V. K. Pecharsky, "Magnetic properties of $Gd_5Si_{1.5}Ge_{2.5}$ near the temperature and magnetic field induced first order phase transition $Gd_5(Si_{0.1}Ge_{0.9})_4$", *J. Magn. Magn. Mat.*, vol. 231, pp. 135–145, 2001.

[22] V.K. Pecharsky K.A. Gschneider and A.O. Tsokol, "Recent developments in magnetocaloric materials", *Rep. Prog. Phys. 68*, vol. 68, pp. 1479–1539, 2005.

[23] Jens Jensen and Allan R. Mackintosh, *Rare Earth Magnetism*, Clarendon Press Oxford, Oxford, 1991.

[24] Robert M. White, *Quantum Theory of Magnetism*, MacGRAW-HILL Book Company, New York, 1970.

[25] J. Samuel Sart, *Effective Field Theories of Magnetism*, W.B. Saunders Ccompany, Philadelphia, 1966.

[26] Kangying Wang, *Crystal-Field Study of Magnetic Anisotropy in Rare-Earth Compounds*, PhD thesis, The American University, Faculty of the College of Arts and Science, Statistics, & Computing Science, 1999.

[27] Derek Craik, *MAGNETISM - Principles and Applications*, Wiley, Chichester, 1995.

[28] Torsten Fliebach, *Curso de Fisica Estatistica*, Fundação Calouste Gulbenkian, Portugal, 1999.

[29] Stephen Blundell, *Magnestism in Condensed Matter*, Oxford University Press, Oxford, 2000.

[30] D.K. Ray M.T. Hutchings, "Investiagtion into the origin of crystalline electric field effects on rare earth ions", *Proc. Phys. Soc.*, vol. 81, pp. 663, 1962.

[31] D.J. Newman and B.K. Ng, *Crystal Field Handbook*, Cambridge University Press, Cambrige, 2000.

[32] K.W.H. Stevens, "Matrix elements and operator equivalents connected with the magnetic properties of rare earth ions", *Proc. Phys. Soc.*, vol. A65, pp. 209, 1952.

[33] Michael Loewenhaupt Peter Fulde, "Magnetic excitations in crystal-field split 4f systems", *Adv. in Phys.*, vol. 34, pp. 589–661, 1986.

[34] Taylor and Darby, *Physics of Rare Earth Solids*, Chapman and Hall Ltd, London, 1972.

[35] W.P.Wolf K.R.Lea, M.J.M. Leask, "The raising of angular momentum degenaracy of f-electron terms by cubic crystal fields", *J.Phys.Chem.Solids*, vol. 23, pp. 1381–1405, 1963.

[36] L. Palermo A. Caldas, P.J. von Ranke, "The existance of a gap between the para- and ferromagnetic phases in a group of pr intermetallics observed through a doublet-triplet model", *Phys. Stat. Sol.*, vol. 175, pp. 497, 1993.

[37] X.A. da Silva A. Caldas L. Palermo, P.J. von Ranke, "The determination of te lande factors and effective exchange parameters for a group of $(pr_x y_{1-x})al_2$ alloys using a doublet-triplet model", *J. Magn. Magn. Mat.*, vol. 115, pp. 265–270, 1992.

[38] W.E. Wallace, *Rare Earth Intermetallics*, Academic Press, New York and London, 1973.

[39] Czeslaw Rudowicz, "Transformation relations for the conventional o_k^q and normalized q_k^q stevens operator equivalents with k=1 to 6 and -k<q<k", *J.Phys.C: Solid State Phys.*, vol. 18, pp. 1415–1430, 1985.

[40] M.P. Dariel U. Atzmony, "Nonmajor cubic symmetry axes of easy magnetization in rare-earth-iron laves compounds", *Phys. Rev. B*, vol. 13, pp. 4006–4014, 1976.

[41] T. Kasuya, "Spin waves on trnasport properties in magnetic materials", *Prog. Theor. Phys.*, vol. 22, pp. 227, 1959.

[42] F. C. Correia J.P. Araújo M. E. Braga A.M. Pereira L. Morellon P. A. Algarabel R.P. Pinto, J. B. Sousa and R. Ibarra, "Thermopower behavior in the $Gd_5(Si_{0.1}Ge_{0.9})_4$ magnetocaloric compound from 4 to 300 k", *J. Magn. Magn. Mater.*, vol. 290/291, pp. 661, 2005.

[43] R. D. Barnard, *Thermoelectricity in Metals and Alloys*, London: Taylor and Francis, London, 1972.

[44] A. Del Moral P. Algarabel J. B. Sousa, J. M. Moreira and R. Ibarra, "Spin reorientation process", *J. Phys.:Condensed Matter*, vol. 2, pp. 3897, 1990.

Appendix A

X-ray Crystallographic data for $Tb_5Si_2Ge_2$ compound

Table A.1: Space group, lattice parameters, unit-cell, volume and fractional atomic coordinates at 250 K and 2K [13].

	250 K		100 K
Space group	$P112_1/a$		$Pnma$
a($\dot{A}$)	7.5080(5)		7.4340(3)
b($\dot{A}$)	14.652(1)		14.6290(6)
c($\dot{A}$)	7.7117(5)		7.7171(3)
γ (deg)	93.042(5)		
V($\dot{A}^3$)	847.1(1)		839.25(6)
Tb1 (4e):x	0.3241	Tb1 (4c):x	0.3476(6)
y	0.2466(6)	y	$\frac{1}{4}$
z	0.0033(9)	z	-0.099(4)
Tb2A (4e):x	-0.000(1)	Tb2 (8d):x	0.0202(4)
y	0.0994(5)	y	0.0966(1)
z	0.179(1)	z	0.8192(4)
Tb2B (4e):x	0.019(1)		
y	0.4002(5)		
z	0.182(1)		
Tb3A (4e):x	0.359(1)	Tb3 (8d):x	0.1763(4)
y	0.8820(5)	y	0.1227(2)
z	0.168(1)	z	0.3217(3)
Tb3B (4e):x	0.331(1)		
y	0.8820(5)		
z	0.168(1)		
M1 (4e):x	0.953(1)	M1 (4c):x	0.997(1)
y	0.2522(6)	y	$\frac{1}{4}$
z	0.893(1)	z	0.1047(9)
M2 (4e):x	0.207(1)	M2 (4c):x	0.977(1)
y	0.2528(6)	y	$\frac{1}{4}$
z	0.206(1)	z	0.634(1)
M3A (4e):x	0.206(1)	M3 (8d):x	0.15379
y	0.9581(6)	y	0.9597(4)
z	0.469(1)	z	0.5299(7)
M3B (4e):x	0.153(1)		
y	0.5435(6)		
z	0.466(1)		
R_P/R_{wp} (%)	2.6/3.2		3.6/4.4

Appendix B

Neutron diffraction data for $Tb_5Si_2Ge_2$ compound

Table B.1: Components of the Tb magnetic moments for $Tb_5Si_2Ge_2$ determined form the Rietveld refinements at 100 K, 85 K and 2 K[13].

T(K)		$\mu_{Tb1}(\mu_B)$	$\mu_{Tb2}(\mu_B)$	$\mu_{Tb3}(\mu_B)$
	μ_x	8.51(9)	7.20(8)	7.61(8)
100 K	μ_y	0	1.5(1)	0.4(1)
	μ_z	0.8(1)	1.26(8)	0.2(1)
	μ_x	8.50(8)	7.45(7)	8.04(7)
85 K	μ_y	0	1.54(8)	0.67(9)
	μ_z	0.7(1)	1.76(6)	0.40(8)
	μ_x	9.3(3)	7.2(3)	8.7(2)
	μ_y	0	0.1(1)	0.0(2)
	μ_z	3.7(2)	7.0(2)	5.6(2)
2K				
	μ_x	7.7(3)	6.6(3)	8.2(2)
	μ_y	0	4.3(2)	1.0(2)
	μ_z	5.1(3)	5.4(2)	3.7(2)

Appendix C

Table of Rare Earth properties

Table C.1: Properties of the tripositive rare-earth ions [23].

$4f^n$	Ion^{+++}	L	S	J	g	$(g-1)^2$ J(J+1)	Δ(K)
0	La	0	0	0	-		
1	Ce	3	$\frac{1}{2}$	$\frac{5}{2}$	$\frac{6}{7}$	0.18	3150
2	Pr	5	1	4	$\frac{4}{5}$	0.80	3100
3	Nd	6	$\frac{3}{2}$	$\frac{9}{2}$	$\frac{8}{11}$	1.84	2750
4	Pm	6	2	4	$\frac{3}{5}$	3.20	2300
5	Sm	5	$\frac{5}{2}$	$\frac{5}{2}$	$\frac{2}{7}$	4.46	1450
6	Eu	3	3	0	–		500
7	Gd	0	$\frac{7}{2}$	$\frac{7}{2}$	2	15.75	
8	Tb	3	3	6	$\frac{3}{2}$	10.50	
9	Dy	5	$\frac{5}{2}$	$\frac{15}{2}$	$\frac{4}{3}$	7.08	4750
10	Ho	6	2	8	$\frac{5}{4}$	4.50	7500
11	Er	6	$\frac{3}{2}$	$\frac{15}{2}$	$\frac{6}{5}$	2.55	9350
12	Tm	5	1	6	$\frac{7}{6}$	1.17	11950
13	Yb	3	$\frac{1}{2}$	$\frac{7}{2}$	$\frac{8}{7}$	0.32	14800
14	Lu	0	0	0	–		

Appendix D

Values of α, β and γ for Ground States of Rare Earth Ions

Table D.1: Values of α, β and γ for Ground States of Rare Earth Ions

			α	β	γ
$4f^1$	Ce^{3+}	$^2F_{\frac{5}{2}}$	-2/35	$2/7 \cdot 45$	0
$4f^2$	Pr^{3+}	$^3H_4$	-52/11 $\cdot$ 15^2	-4/55·33·3	$17 \cdot 16/7 \cdot 11^2 \cdot 13 \cdot 5 \cdot 3^4$
$4f^3$	Nd^{3+}	$^4I_{\frac{9}{2}}$	$-7/33^2$	$-8 \cdot 17/11^2 \cdot 13 \cdot 297$	$-17 \cdot 19 \cdot 5/13^2 \cdot 11^3 \cdot 3^3 \cdot 7$
$4f^4$	Pm^{3+}	$^5I_4$	$14/11^2 \cdot 15$	$952/13 \cdot 3^3 \cdot 11^3 \cdot 5$	$2584/11^2 \cdot 13^2 \cdot 3 \cdot 63$
$4f^5$	Sm^{3+}	$^6H_{\frac{5}{2}}$	$13/7 \cdot 45$	$26/33 \cdot 7 \cdot 45$	0
$4f^6$	Eu^{3+}	$^6F_0$	0	0	0
$4f^7$	Gd^{3+}	$^8S_{\frac{7}{2}}$	0	0	0
$4f^8$	Tb^{3+}	$^7F_6$	-1/99	$2/11 \cdot 1485$	$-1/13 \cdot 33 \cdot 2079$
$4f^9$	Dy^{3+}	$^6H_{\frac{15}{2}}$	$-2/9 \cdot 35$	$-8/11 \cdot 45 \cdot 273$	$4/11^2 \cdot 13^2 \cdot 3^3 \cdot 7$
$4f^10$	Ho^{3+}	$^5I_8$	$-1/30 \cdot 15$	$-1/11 \cdot 2730$	$-5/13 \cdot 33 \cdot 9009$
$4f^11$	Er^{3+}	$^4H_{\frac{15}{2}}$	$4/45 \cdot 35$	$2/11 \cdot 15 \cdot 273$	$8/13^2 \cdot 11^2 \cdot 3^3 \cdot 7$
$4f^12$	Tm^{3+}	$^3H_6$	1/99	$8/3 \cdot 11 \cdot 1485$	$-5/13 \cdot 33 \cdot 2079$
$4f^13$	Yb^{3+}	$^2F_{\frac{7}{2}}$	2/63	$-2/77 \cdot 15$	$4/13 \cdot 33 \cdot 63$

Appendix E

Stevens Equivalent Operators

Table E.1: Stevens Equivalent Operators

$O_2^2 = \frac{1}{2}(J_+^2 + J_-^2)$
$O_2^1 = \frac{1}{2}(J_z J_x + J_x J_z) = \frac{1}{4}[J_z(J_+ + J_-) + (J_- + J_+)J_z]$
$O_2^0 = 3J_z^2 - X$
$O_2^{-1} = \frac{1}{2})(J_z J_x + J_x J_z) = \frac{i}{4}[J_z(J_+ - J_-) + J_z(J_+ + J_-)]$
$O_2^{-2} = \frac{1}{2i}(J_+^2 - J_-^2)$
$O_4^4 = \frac{1}{2}(J_+^4 + J_-^4)$
$O_4^3 = \frac{1}{4}[J_z(J_+ + J_-) + (J_+ + J_-)J_z]$
$O_4^2 = \frac{1}{4}[(7J_z^2 - X - 5)(J_+ + J_-) + (J_+ + J_-)(7J_z^2 - X - 5)]$
$O_4^1 = \frac{1}{4}[(7J_z^3 - (3X + 1)J_z)(J_+ + J_-) + (J_+ + J_-)(7J_z^3 - (3X + 1)J_z)]$
$O_4^0 = 35J_z^4 - (30X - 25)J_z^2 + 3X^2 - 6X$
$O_4^{-1} = \frac{i}{4}[(7J_z^3 - (3X + 1)J_z)(J_+ - J_-) + (J_+ - J_-)(7J_z^3 - (3X + 1)J_z)]$
$O_4^{-2} = \frac{1}{4i}[(7J_z^2 - X - 5)(J_+ - J_-) + (J_+ - J_-)(7J_z^2 - X - 5)]$
$O_4^{-3} = \frac{1}{4i}[J_z^2(J_+^3 - J_-^3) + (J_+^3 - J_-^3)J_z^2]$
$O_4^{-4} = \frac{1}{2i}(J_+^4 - J_-^4)$
$O_6^6 = \frac{1}{2}(J_+^6 + J_-^6)$
$O_6^5 = \frac{1}{4}[J_z(J_+^5 + J_-^5) + (J_+^5 + J_-^5)J_z]$
$O_6^4 = \frac{1}{4}[(11J_z^2 - X - 38)(J_+^4 + J_-^4) + (J_+^4 + J_-^4)(11J_z^2 - X - 38)]$
$O_6^3 = \frac{1}{4}[(11J_z^3 - (3X - 59)J_z)(J_+^3 + J_-^3) + (J_+^3 + J_-^3)(11J_z^3 - (3X - 59)J_z)]$

Table E.2: Stevens Equivalent Operators-continuation

$$O_6^2 = \tfrac{1}{4}[33J_z^4 - (18X - 123)J_z^2 + X^2 + 10X + 102](J_+^2 + J_-^2)$$
$$+(J_+^2 + J_-^2)[33J_z^4 - (18X - 123)J_z^2 + X^2 + 10X + 102]$$

$$O_6^1 = \tfrac{1}{4}[33J_z^5 - (30X - 115)J_z^3 + (5X^2 - 10X + 12)]$$
$$(J_+ + J_-) + (J_+ + J_-)[33J_z^5 - (30X - 115)J_z^3 + (5X^2 - 10X + 12)]$$

$$O_6^0 = 231J_z^6 - (315X - 735)J_z^4 + (105X^2 - 525X + 294)J_z^2 - 5X^3 + 40X^2 - 60X$$

$$O_6^{-1} = \tfrac{i}{4}[33J_z^5 - (30X - 115)J_z^3 + (5X^2 - 10X + 12)](J_+ - J_-)$$
$$+(J_+ - J_-)[33J_z^5 - (30X - 115)J_z^3 + (5X^2 - 10X + 12)]$$

$$O_6^{-2} = \tfrac{i}{4}[33J_z^4 - (18X - 123)J_z^2 + X^2 + 10X + 102](J_+^2 - J_-^2)$$
$$+(J_+^2 - J_-^2)[33J_z^4 - (18X - 123)J_z^2 + X^2 + 10X + 102]$$

$$O_6^{-3} = \tfrac{i}{4}[(11J_z^3 - (3X - 59)J_z)(J_+^3 - J_-^3) + (J_+^3 - J_-^3)(11J_z^3 - (3X - 59)J_z)]$$
$$O_6^{-4} = \tfrac{i}{4}[(11J_z^2 - X - 38)(J_+^4 - J_-^4) + (J_+^4 - J_-^4)(11J_z^2 - X - 38)]$$
$$O_6^{-5} = \tfrac{i}{4}[J_z(J_+^5 - J_-^5) + (J_+^5 - J_-^5)J_z]$$

$$O_6^{-6} = \tfrac{1}{2i}(J_+^6 - J_-^6)$$

Appendix F

Programme code

```
% %%%%%%%%%%%%%%%%%%%%%%%%%%%%%%%%%%%%%%%%%%%%%%%%%%%%%%%%%%%%%%%%%%%%%%%%%%%
%    Programme for determination the energy of crystal field for the      %
%                       Tb trivalente ion in a self consistent            %
%                             Made by Andre Pereira                       %
%                                Version 3.0                              %
%                                2005-09-29                               %
%%%%%%%%%%%%%%%%%%%%%%%%%%%%%%%%%%%%%%%%%%%%%%%%%%%%%%%%%%%%%%%%%%%%%%%%%%%%%%

format long
clear
%%%%%%%%INPUT%%%%%%%%%%%%%%%%%%
J=input('Entre com o valor de J:   ');
plsv=input('Deseja (1) salvar os dados ou (2) "plotar":   ');

L=2*J+1; % number of Mj
Z=0;
Jz=zeros(L,L);
J2=zeros(L,L);
JMais=zeros(L,L);
Jmenos=zeros(L,L);
Id=zeros(L,L);

%%%%%%CONSTANTES%%%%%%%%%%%%%%%
g=3/2; k=1.380658e-16; mibor=9.27e-21; %%%%%k em erg.K-1%%%mibor em erg.G-1%%%%
difmag=1;mag3=[]; valores=[]; concx=[]; concW=[]; concJ0=[]; magt=[];temp=[];Ftemp=[];b↙
molecular=[];


% Quantic operators
for i=1:L
    for j=1:L
if i==j
    Id(i,j)=1;
else
   Id(i,j)=0;
end
end
end

for i=1:L
    for j=1:L
if i==j
    X(i,j)=J*(J+1);
else
   X(i,j)=0;
end
end
end

% operator Jz
for i=1:L
    for j=1:L
if i==j
    Jz(i,j)=i-J-1;
else
    Jz(i,j)=0;
end
end
end

% operator J2
```

```
for i=1:L
    for j=1:L
if i==j
    J2(i,j)=J*(J+1);
else
    J2(i,j)=0;
end
end
end

%operator J+

for i=1:L
    for j=1:L
         if i==j+1
            JMais(i,j)=sqrt((J-(j-J-1))*(J+(j-J-1)+1));
        else
             JMais(i,j)=0;
        end
    end
end

%operador J-

for i=1:L
    for j=1:L
if i==j-1
    Jmenos(i,j)=sqrt((J+(j-J-1))*(J-(j-J-1)+1));
else
    Jmenos(i,j)=0;
end
end
end


%Coeficientes de steven's

O22=1/2*(JMais^2+Jmenos^2);

O21=1/4*(Jz*(JMais+Jmenos)+(JMais+Jmenos)*Jz);

O20=3*Jz^2-X;

O2menos1=1/2i*(Jz*(JMais-Jmenos)+(JMais-Jmenos)*Jz);

O2menos2=1/2i*(JMais^2-Jmenos^2);


O44=1/2*(JMais^4+Jmenos^4);

O43=1/4*((Jz*(JMais^3+Jmenos^3)+(JMais^3+Jmenos^3)*Jz));

O42=1/4*((7*Jz^2-X-5*Id)*(JMais^2+Jmenos^2)+(JMais^2+Jmenos^2)*(7*Jz^2-X-5*Id));

O41=1/4*((7*Jz^3-(3*X+1*Id)*Jz)*(JMais+Jmenos)+(JMais+Jmenos)*(7*Jz^3-(3*X+1*Id)*Jz));

O40=35*Jz^4-(30*X-25*Id)*Jz^2+3*X^2-6*X;

O4menos1=1/4i*((7*Jz^3-(3*X+1*Id)*Jz)*(JMais-Jmenos)+(JMais-Jmenos)*(7*Jz^3-(3*X+1*Id)*↙
Jz));
```

```
O4menos2=1/4i*((7*Jz^2-X-5*Id)*(JMais^2-Jmenos^2)+(JMais^2-Jmenos^2)*(7*Jz^2-X-5*Id));

O4menos3=1/4i*((Jz*(JMais^3-Jmenos^3)+(JMais^3-Jmenos^3)*Jz));

O4menos4=1/2i*(JMais^4-Jmenos^4);



O66=1/2*(JMais^6+Jmenos^6);

O65=1/4*((Jz*(JMais^5+Jmenos^5))+((JMais^5+Jmenos^5)*Jz));

O64=0.25*[(11*Jz^2-X-38*Id)*(JMais^4+Jmenos^4)+(JMais^4+Jmenos^4)*(11*Jz^2-X-38*Id)];

O63=1/4*[(11*Jz^3-(3*X+59*Id)*Jz)*(JMais^3+Jmenos^3)+(JMais^3+Jmenos^3)*(11*Jz^3-(3*X+5↙
9*Id)*Jz)];

O62=1/4*[(33*Jz^4-(18*X-123*Id)*Jz^2+X^2+10*X+102*Id)*(JMais^2+Jmenos^2)+(JMais^2+Jmeno↙
s^2)*(33*Jz^4-(18*X-123*Id)*Jz^2+X^2+10*X+102*Id)];

O61=1/4*[(33*Jz^5-(30*X-15*Id)*Jz^3+(5*X^2-10*X+12*Id)*Jz)*(JMais+Jmenos)+((JMais+Jmeno↙
s)*(33*Jz^5-(30*X-15*Id)*Jz^3+(5*X^2-10*X+12*Id)*Jz))];

O60=231*Jz^6-(315*X-735*Id)*Jz^4+(105*X^2-525*X+294*Id)*Jz^2-5*X^3+40*X^2-60*X;

O6menos1=1/4i*[(33*Jz^5-(30*X-15*Id)*Jz^3+(5*X^2-10*X+12*Id)*Jz)*(JMais-Jmenos)+((JMais↙
-Jmenos)*(33*Jz^5-(30*X-15*Id)*Jz^3+(5*X^2-10*X+12*Id)*Jz))];

O6menos2=1/4i*[(33*Jz^4-(18*X-123*Id)*Jz^2+X^2+10*X+102*Id)*(JMais^2-Jmenos^2)+(JMais^2↙
-Jmenos^2)*(33*Jz^4-(18*X-123*Id)*Jz^2+X^2+10*X+102*Id)];

O6menos3=1/4i*[(11*Jz^3-(3*X+59*Id)*Jz)*(JMais^3-Jmenos^3)+(JMais^3-Jmenos^3)*(11*Jz^3-↙
(3*X+59*Id)*Jz)];

O6menos4=1/4i*[(11*Jz^2-X-38*Id)*(JMais^4-Jmenos^4)+(JMais^4-Jmenos^4)*(11*Jz^2-X-38*Id↙
)];

O6menos5=1/4i*(Jz*(JMais^5-Jmenos^5)+(JMais^5-Jmenos^5)*Jz);

O6menos6=1/2i*(JMais^6-Jmenos^6);



%for J0=0.81
for J0=1.22
    lambda=J0*1.6E-15/(g*g*mibor*mibor);

%for W=-0.315
for W=-0.97
%for x=0.671
 for x=-0.38

F4=60;

F6=7560;

Vcf2=W*(x/F4*(O40+5*O44)+((1-abs(x))/F6)*(O60-21*O64));
```

```
for T=2:1:150
    mag=10;

    d=10;

    while d >= 0.001


b0=0.001;

b=b0+lambda*mag*mibor;

Hm=-g*mibor*Jz*b;


HamG=Hm+Vcf2*1.6E-19*1E-3/1E-7;
%HamG=Hm;

[Vectores_propriosl,Valores_propriosl] = eig(HamG);


Valores_Propriosm=eig(HamG);


Q=0;


VPexp=expm(-Valores_propriosl/(k*T));


Jzdiag=Vectores_propriosl'*Jz*Vectores_propriosl;


Q=trace(VPexp);


M1=trace(Jzdiag*VPexp)/Q;

    d=abs(mag-g*M1)/(g*M1);

    mag=g*M1;

Valores_magn = eig(HamG)/(1.6E-19*1E-3/1E-7);



%end
end

%%%%%%%%%%%%%%%%%%%%%%%%%%%%%%%%%%%%%%%%%%%%%%%%%%%%%REORIENTAÇAO%%%%%%%%%%%%%%%%%%%%%%%%%

for theta=0:pi/20:pi/2;
for phi=0:pi/40:pi/4;


% Projectado a coordenada cristalina na coordenada da magnetizaçao 1

Q40=35/8*(sin(theta))^4*O44-35*(sin(theta))^3*cos(theta)*O43+5/2*(sin(theta))^2*(7*(cos↙
(theta))^2-1)*O42-5/2*(sin(2*theta)*(7*(cos(theta))^2-3))*O41+1/8*(35*(cos(theta))^4-30↙
*(cos(theta))^2+3)*O40;
```

```
Q44=1/8*cos(4*phi)*((cos(theta))^4+6*(cos(theta))^2+1)*O44+1/2*sin(2*theta)*cos(4*phi)*↙
((cos(theta))^2+3)*O43+1/2*(sin(theta))^2*cos(4*phi)*((cos(theta))^2+1)*O42+(sin(theta)↙
)^3*cos(4*phi)*cos(theta)*O41+1/8*(sin(theta))^4*cos(4*phi)*O40-(sin(theta))^3*sin(4*ph↙
i)*O4menos1-(sin(theta))^2*sin(4*phi)*cos(theta)*O4menos2-sin(theta)*sin(4*phi)*(3*(cos↙
(theta))^2+1)*O4menos3-1/2*sin(4*phi)*cos(theta)*((cos(theta))^2+1)*O4menos4;

Q60=231/32*(sin(theta))^6*O66-693/8*(sin(theta))^5*cos(theta)*O65+63/16*(sin(theta))^4*↙
(11*(cos(theta))^2-1)*O64-105/8*(sin(theta))^3*cos(theta)*(11*(cos(theta))^2-3)*O63+105↙
/32*(sin(theta))^2*(33*(cos(theta))^4-18*(cos(theta))^2+1)*O62-21/8*sin(2*theta)*(33*(c↙
os(theta))^4-30*(cos(theta))^2+5)*O61+1/16*(231*(cos(theta))^6-315*(cos(theta))^4+105*(↙
cos(theta))^2-5)*O60;

Q64=11/32*(sin(theta))^2*cos(4*phi)*((cos(theta))^4+6*(cos(theta))^2+1)*O66-11/16*sin(2↙
*theta)*cos(4*phi)*(3*(cos(theta))^4+10*(cos(theta))^2-5)*O65+1/16*cos(4*phi)*(33*(cos(↙
theta))^6+35*(cos(theta))^4-65*(cos(theta))^2+13)*O64+5/16*sin(2*theta)*cos(4*phi)*(11*↙
(cos(theta))^4+2*(cos(theta))^2-5)*O63+5/32*(sin(theta))^2*cos(4*phi)*(33*(cos(theta))^↙
4-10*(cos(theta))^2+1)*O62+1/4*(sin(theta))^3*cos(theta)*cos(4*phi)*(33*cos(theta)^2-13↙
)*O61+1/16*(sin(theta))^4*cos(4*phi)*(11*(cos(theta))^2-1)*O60-1/2*(sin(theta))^3*sin(4↙
*phi)*(11*(cos(theta))^2-1)*O6menos1-5/8*(sin(theta))^(2)*cos(theta)*sin(4*phi)*(11*(co↙
s(theta))^2-5)*O6menos2-5/4*sin(theta)*sin(4*phi)*(11*(cos(theta))^4-8*(cos(theta))^2+1↙
)*O6menos3-1/2*cos(theta)*sin(4*phi)*(11*(cos(theta))^4-10*(cos(theta))^2+1)*O6menos4+1↙
1/4*sin(theta)*sin(4*phi)*(5*(cos(theta))^4-1)*O6menos5-11/8*(sin(theta))^2*cos(theta)*↙
sin(4*phi)*((cos(theta))^2+1)*O6menos6;


Vcf=W*(x/F4*(Q40+5*Q44)+((1-abs(x))/F6)*(Q60-21*Q64));


Hani=Hm+Vcf*1.6E-19*1E-3/1E-7;
%HamG=Hm;

[Vectores_proprios2,Valores_proprios2] = eig(Hani);


Valores_Propriosm2=eig(Hani);


Q2=0;


VPexp2=expm(-Valores_proprios2/(k*T));


Jzdiag2=Vectores_proprios2'*Jz*Vectores_proprios2;


Q2=trace(VPexp2);


M2=trace(Jzdiag2*VPexp2)/Q2;


    mag2=g*M2;


%valores=[valores;vectores_pro_teste];

magt=[magt;real(mag2)];

temp=[temp;T];
```

```
concW=[concW;theta*180/pi];

concx=[concx;phi*180/pi];

concJ0=[concJ0;J0];

bmolecular=[bmolecular;b];


end
end
end



if plsv==1

m=[concJ0,concW,concx,temp,magt];
    save c:\teste.dat m /ascii
    disp('')
    disp('Arquivo salvo em c:\teste.dat')

end

if plsv==2
  plot(temp,magt)
hold on
m=[concJ0,concW,concx,temp,magt];
    save c:\teste2.dat m /ascii
    disp('')
    disp('Arquivo salvo em c:\teste.dat')
end

end

end
end
```